Seasonal hydro-and morphodynamics of data-limited bay and coastal inlet systems

Do, Anh

DOI
10.4233/uuid:faa16f1c-524c-4958-b8b0-d9ce4fd7c045

Publication date
2019

Citation (APA)
Do, A. (2019). *Seasonal hydro-and morphodynamics of data-limited bay and coastal inlet systems*. [Dissertation (TU Delft), Delft University of Technology]. https://doi.org/10.4233/uuid:faa16f1c-524c-4958-b8b0-d9ce4fd7c045

SEASONAL HYDRO- AND MORPHODYNAMICS OF DATA-LIMITED BAY AND COASTAL INLET SYSTEMS

Dissertation

for the purpose of obtaining the degree of doctor
at Delft University of Technology,
by the authority of the Rector Magnificus prof.dr. ir. T.H.J.J. van der Hagen
chair of the Board of Doctorates,
to be defended publicly on
Monday 8 April 2019 at 12:30 o'clock

by

Thi Kim Anh DO

Master of Science in Hydraulic and Ocean Engineering
National Cheng Kung University, Tainan, Taiwan,
born in Quang Binh, Vietnam.

This dissertation has been approved by the promotors

Composition of the doctoral committee:

Rector Magnificus,	chairman
Prof. dr. ir. M. J. F. Stive	Delft University of Technology, promotor
Prof. dr. ir. Z. B. Wang	Delft University of Technology, promotor
Dr. ir. S. de Vries	Delft University of Technology, copromotor
Independent members:	
Prof. dr. T. V. Nguyen	ThuyLoi University, Vietnam
Dr. Q. Ye	Deltares
Prof. dr. ir. S. G. J. Aarninkhof	Delft University of Technology
Prof. dr. ir. A. J. H. M. Reniers	Delft University of Technology

This research was funded by the European Commission through the Erasmus Mundus Mobility with Asia 2014 (EMMAsia 2014) for Doctorate Programme, and also partially supported by the Lamminga Fund.

Keywords: Seasonal inlet, data-limited, headland bay beach
Printed by: Anh DO

ISBN 978-94-6366-154-6

An electronic version of this dissertation is available at
http://repository.tudelft.nl/.

To my family

Contents

Summary

The main objective of this study is to unravel the physical processes that control typical coastal systems in Central Vietnam while challenged by the fact that it is a data limited environment. Inlets and bays are the typical coastal system along the central coast of Vietnam. These coastal systems are strongly influenced by tropical monsoon conditions, which are characterised by variations in seasonal wave conditions and seasonal river flow. These systems are even more vulnerable to extreme weather conditions, such as floods and storms, because of the complex topography of a relatively narrow and steep mountain range which is directly connected to a dense river network in the low-lying coastal plains at the downstream end. Economic and ecological values in the coastal area are under pressure as a result of the intensification of natural disasters and human interventions. Notable examples of this are Cua Dai beach and Da Nang bay.
Cua Dai beach lies adjacent to the Cua Dai inlet which is a typical seasonal varying tidal inlet connected to the catchment area of the Vu Gia-Thu Bon River. Cua Dai beach has suffered extreme erosion in the recent decade. Da Nang bay is a complex bay beach headland downstream of the Vu Gia River that discharges into this bay. Also, this system is affected by human interventions. Due to the common downstream basin of the Vu Gia-Thu Bon River system, both being typical coastal systems in Central Vietnam that experience data limitations, this study attempts to combine and understand the hydrodynamics and morphodynamics of Cua Dai inlet and the complex Da Nang embayment.
In order to identify and quantify the main processes governing the evolution of Cua Dai beach to explain the morphological changes and extreme erosion in recent years, a new approach was developed. Historical shoreline positions and sediment budget changes are the two parameters of main importance in the approach to quantify the erosion processes in the Cua Dai coastal inlet. Historical shoreline changes were derived from satellite images and associated sediment budgets were estimated based on shoreline change rates using additional assumptions, such as defining a closure depth and a time invariant beach profile. To gain insight into the sediment transport along the Cua Dai beach, additional numerical models and empirical equations are used to investigate the variation in alongshore sediment transport induced by waves. Further analysis on how seasonal variation in both waves and river discharge impacts the morphodynamics of the ebb tidal delta and its adjacent coasts is performed based on process-based modelling.
The new methodology to extract volume changes from Landsat images combined with process-base modelling have been successfully applied to investigate the main processes that govern morphological changes and extreme erosion at Cua Dai beach during re-

cent decades. The results from shoreline change rates show that the erosion at Cua Dai beach has started since 1995 with the highest rate of erosion appearing in the period between 2000 and 2010. Results of volume change indicate the system has lost a significant sediment volume during this period. The erosion at Cua Dai beach since 1995 was the result of a long-term geomorphological inlet development reflecting a non-periodic cyclic process that took place over several decades. It appears that a channel, shifting from the North to the South, triggered by typhoon Cecil in 1987, dictated the geomorphological development of Cua Dai Beach . The decrease of sediment supply from the river and the squeeze by coastal developments may have contributed to the erosion. The results from alongshore sediment transport gradients, with the existence of a transport divergence point and a transport convergence point induced by waves, has significantly contributed to explain the erosion that occurs at Cua Dai beach.

While developing the proposed methodology of extracting volume changes derived from shoreline changes, we have evaluated it for a data-rich environment (i.e. the North-Holland coast) before applying it to a data limited environment. This important evaluation is presented as an intermezzo in this thesis. The results indicate that the use of Landsat images for deriving shoreline change rates and volume changes have accuracies comparable to observed in-situ measurements when comparing measurements on decadal scales.

To obtain more insight into planform stability of the complex embayed Da Nang Bay, we first employed the simple Parabolic Bay Shape Equation (PBSE) to 26 less complex embayed beaches on the central coast of Vietnam. Shoreline change rates derived from Landsat images were used to evaluate the planform stability of the bay beaches with special attention to difficulties in determining the state of equilibrium due to multiple potential diffraction points. Then the PBSE and shoreline change rates were used to investigate planform stability of the complex headland of Da Nang Bay, also considering the presence of the influence of a seasonal wave climate. Due to the complexity of Da Nang bay beach headland, combining the occurring seasonal river discharges and seasonal climates, the PBSE and shoreline changes do not sufficiently contribute to identify what will result in the stability of this bay beach. Although the PBSE and shoreline change rates analysis have successfully evaluated the planform stability of various less complex headland bay beaches along the central coast Viet Nam, the effect of sediment supply from river may need to be further investigated.

Samenvatting

Het doel van deze studie is de fysieke processen, die zo kenmerkend zijn voor de kust van Centraal -Vietnam, te ontrafelen, en de uitdaging aan te gaan om deze met zeer beperkte gegevens te onderzoeken. Karakteristiek voor het kustsysteem van Centraal -Vietnam zijn de vele inhammen en baaien, met zeer specifieke variaties in seizoensgebonden golfcondities en rivierstromingen en de grote invloed van tropische moessons. Als gevolg van de complexe topografie, met relatief smalle en steile bergketens en een dicht netwerk van rivieren in de laaggelegen stroom-afwaartse kustvlakte, is het kustsysteem kwetsbaarder voor extreme weersomstandigheden, zoals stormen en overstromingen. Economische en ecologische belangen in het kustgebied staan onder druk als gevolg van deze intensivering van menselijke interventies en natuurrampen. Opvallende voorbeelden hiervan zijn het strand van Cua Dai en de baai van Da Nang.
Het strand van Cua Dai grenst aan de Cua Dai-inham, een typische seizoensgebonden getijdeninham, die verbonden is met het stroomgebied van de Vu Gia -Thu Bon Rivier. Het strand van Cua Dai heeft in het afgelopen decennium onder extreme erosie te lijden gehad. De baai van Da Nang is een complexe combinatie van een strand en een baai, waarin de Vu Gia Rivier uitmondt. Bovendien is ook hier de invloed van menselijke interventies merkbaar. Vanwege het gemeenschappelijke stroomgebied van het Vu Gia-Thu Bon Rivier-systeem, waarover weinig wetenschappelijke gegevens beschikbaar zijn, werden in deze studie de hydrodynamica en morfodynamica van de Cua Dai-inlaat en de complexe Da Nang-baai gecombineerd. Om de belangrijkste processen van de ontwikkeling van het Cua Dai-strand te identificeren en te kwantificeren, en om de morfologische veranderingen en extreme erosie van de afgelopen jaren te verklaren, werd een nieuwe aanpak ontwikkeld. De twee belangrijkste variabelen, de ligging van historische oever en de sedimentbudgetveranderingen, zijn van het grootste belang in de aanpak om het proces van erosie in de Cua Dai-kustinham te kwantificeren. De historische veranderingen van de oever, afgeleid vanuit satellietbeelden, en het daarbij horende sedimentbudget werden geschat op basis van de veranderingen met behulp van toegevoegde aannames, zoals het definiëren van een sluitingsdiepte en een tijds-invariant strandprofiel. Om inzicht te krijgen in het sedimenttransport langs het strand van Cua Dai, werden aanvullende numerieke modellen en empirische vergelijkingen gebruikt om de variatie in longitudinaal sedimenttransport, veroorzaakt door golven, te onderzoeken. Analyse van de invloed van seizoensvariatie, in zowel golven als rivierafvoer, op de morfodynamica van de eb-getijde-delta en de aangrenzende kusten, werd uitgevoerd op basis van proces gebaseerde modellering.

De nieuwe methodologie om volumeveranderingen af te leiden uit Landsat-afbeeldingen, in combinatie met procesbasismodellering, is met succes toegepast om de belangrijkste processen van de laatste decennia te onderzoeken, die de morfologische veranderingen en de extreme erosie op het strand van Cua Dai hebben beheerst. De resultaten van de studie van veranderingen in de kustlijn tonen aan dat de erosie op het strand van Cua Dai sinds 1995 is begonnen, met de hoogste mate van erosie in de periode tussen 2000 en 2010. De resultaten van volumeverandering wijzen erop dat het systeem tijdens deze periode een aanzienlijk sedimentvolume heeft verloren. De erosie op het strand van Cua Dai, sinds 1995, was het resultaat van een langlopende geomorfologische ontwikkeling van de inlaat, en een niet-periodiek cyclisch decennialang proces weerspiegelt. Een getijdegeul, zich van het noorden naar het zuiden verplaatsend, en veroorzaakt door de tyfoon Cecil in 1987, heeft de geomorfologische ontwikkeling van het strand van Cua Dai bepaald. De afname van het sedimentaanbod uit de rivier en het estuarium én de druk van kustontwikkelingen hebben mogelijk bijgedragen aan de erosie. De resultaten van het sedimenttransport gradiënt langs de kust, samen met het bestaande transportdivergentiepunt en een transportconvergentiepunt veroorzaakt door golven, hebben aanzienlijk bijgedragen aan een verklaring van de erosie van het strand van Cua Dai.
Bij het ontwikkelen van de voorgestelde methodologie voor het extraheren van volumeveranderingen welke zijn afgeleid van veranderingen in de kustlijn, hebben we de methodologie geëvalueerd voor een datarijke omgeving (d.w.z. de Noord-Hollandse kust), alvorens deze toe te passen op een omgeving met beperkte gegevens. Deze belangrijke evaluatie wordt gepresenteerd als een intermezzo in dit proefschrift. De resultaten geven aan dat het gebruik van Landsat-afbeeldingen voor het afleiden van veranderingen in de kustlijn en in volumeveranderingen zo nauwkeurig zijn dat deze vergelijkbaar zijn met waargenomen in-situ metingen bij het vergelijken van decennia lange metingen.
Om meer inzicht te krijgen in de stabiliteit van de planvorm van de complexe Baai van Da Nang, hebben we eerst de eenvoudige parabolische baai-vormvergelijking (PBSE) gebruikt voor 26 gevallen, minder gecompliceerde, stranden aan de centrale kust van Vietnam. Veranderingen in de kustlijn, afgeleid van Landsat-beelden, werden gebruikt om de stabiliteit van de planvorming van de baaistranden te evalueren, met speciale aandacht voor moeilijkheden bij het bepalen van de evenwichtstoestand als gevolg van meerdere potentiële diffractiepunten. Vervolgens werden de PBSE- en het percentage van verandering in de kustlijn gebruikt om de stabiliteit van de planvorm van de complexe landtong van de Baai van Da Nang te onderzoeken, als ook de invloed van een seizoens-golfklimaat. Vanwege de complexiteit van de landtong, die deel is van het strand van Da Nang, en de seizoensgebonden rivierafvoer en het klimaat van de diverse seizoenen, dragen de PBSE en kustlijnveranderingen onvoldoende bij aan de identificatie van de factoren die bijdragen aan de stabiliteit van deze baai-strand situatie. Hoewel de analyses van de PBSE en de veranderingen in de kustlijn met succes hebben bijgedragen aan de evaluatie van de stabiliteit van de planvorm van verschillende, minder complexe identieke baai-stranden langs de centrale kust van Vietnam, moet het effect van de aanvoer van sediment uit de rivier verder worden onderzocht.

Chapter 1

Introduction

Where there's a will,
there's a way

Angela Merkel

Data limitations are an urgent problem while we approach to understand complex coastal systems such as tidal inlets and bay beaches, especially in tropical monsoon regions. This chapter provides an overview of problem statements, the aim of this study as well as the research methodology and the outline of this dissertation.

1

1.1 Problem statements

THE central coast of Vietnam has suffered from coastal erosion in many places. The central Vietnam coast is characterized by many sandy beaches, seasonal tidal inlets and many headland bay beaches in various shapes. Distinctive geomorphologic features and forcing such as seasonality in wave climate and river flow regime, narrow coastal plains, short steep rivers make the central Vietnam coast one of the most vulnerable coasts to natural disaster such as floods and tropical storms. Next to coastal erosion in the region, coastal threats have been increasing due to human pressure. The pressure of increasing population and economic activities (e.g. fisheries, tourist hotels and associated tourism activities, hydropower plants and land reclamation) have contributed to unwanted changes in the coastal system.

In recent decades, many specific coastal erosion areas have been observed in the central

Figure 1.1: Erosion problem at Cua Dai beach

Vietnam coast. Especially in the cases of river mouths and their adjacent coasts erosion is observed. For example, erosion has been obsereved at Cua Dai beach (Thu Bon river) (Figure 1.1), at Tuy Hoa (Da Rang river) and at Nha Trang (Cai River). Coastal erosion at these areas is problematic for the safety of inhabitants and it needs scientific attention, epsecially because of the limited understanding of such complex coastal systems. It is important to well understand these coastal systems to aid future improved of management of these systems.

Vietnam often lacks the data that are needed for specific coastal studies. The same holds

for many developing countries. The main reason for this is that the coast has long been undervalued as an important societal and economic resource. In recent years, urgent coastal erosion problems have caused coastal monitoring to becoming in high demand. Some data were collected in some projects in Vietnam normally during a short period of time. Although more and more data sources are becoming available on a global scale for assessing the local problems, local observed data is still needed. However, the collected data from unknown sources or different sources may be insufficient and incompatible to realistically elaborate a detailed coastal study. At the same time, obtaining data can be very expensive and time consuming. In this study we focus on the challenges related to data limited environments.

Danang Bay and Cua Dai Inlet (Figure 1.2) are two typical deltaic coastal formations on the central coast of Vietnam. These two coastal systems are associated with the biggest river system in Central Vietnam, The Vu Gia-Thu Bon river system. Downstream of Vu Gia River, the flow discharges into Danang Bay through the Han estuary, while Cua Dai Inlet is the river mouth of Thu Bon River. The Vu Gia-Thu Bon river system is strongly seasonal and floods occur with higher and more frequent discharges in recent years. Moreover, the coastal area of central Vietnam, especially Cua Dai beach, is exposed to typhoons and other natural disasters. Apart from the rainstorms or typhoons it is also highly vulnerable to river floods, flash floods, storm surges, salinity intrusions and tsunamis. During the last ten years, several coastal structures were built in Da Nang Bay and at Cua Dai Beach, such as seawalls, breakwaters, dams and bridges, as well as other human interventions such as land reclamations for the construction of luxurious resorts and hydropower plants at upstream. These human activities along with the effects of climate change potentially pose a threat to the coastal safety of Da Nang Bay and Cua Dai Beach. As a result, at many places along the coast, especially for Cua Dai Beach, extreme erosion has occurred causing immense damage. Figure 1.1 shows results of erosion along Cua Dai beach.

1.2 The Vu Gia-Thu Bon river basin

THE Vu Gia-Thu Bon basin (Figure 1.2) is a large river system in central Vietnam, which originates from the eastern side of the Truong Son mountain range and discharges into the sea via the Han and Cua Dai estuaries. The basin occupies about 10,350 km^2 (roughly 90% of the Quang Nam Province) and includes Da Nang, a very large city with about 876,000 inhabitants. This system has two main rivers, i.e. the Vu Gia and the Thu Bon Rivers.

The Vu Gia River originates from the western region of the Ngoc Linh Mountain Range with a peak elevation of 2600m. It flows through the Quang Nam province and Da Nang City and discharges into the sea through the Han estuary. The distance along the main river from upstream to Ai Nghia is 166 km and to the Han estuary it is 204 km. The catchment area of Vu Gia River to Ai Nghia is 5,180 km^2.

Thu Bon River originates from a mountain 1500 m high in the Kon Tum province then flows through the Quang Nam province and drains to the sea at Cua Dai inlet. The total length of the main river is 198 km. The catchment area of the Thu Bon basin is 4,100

1

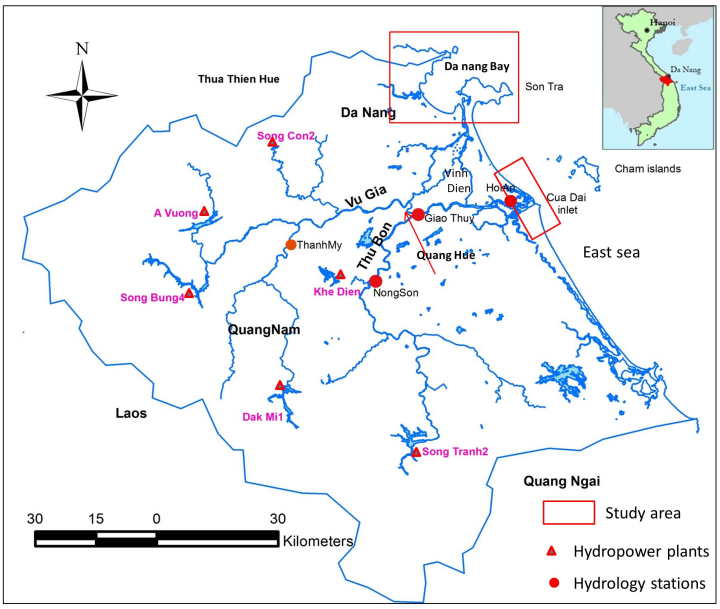

Figure 1.2: The Vu Gia –Thu Bon river basin including Cua Dai inlet and Da Nang Bay

km^2 at the Cua Dai inlet. Between the Vu Gia River and the Thu Bon River, there are two connecting tributaries Quang Hue and Vinh Dien (see Figure 1.2). Due to the mutual exchange of their discharges, these two rivers are considered as one river basin system.
The rivers flow through the many complex topographies of a relative narrow mountain range, which is characteristised by a very steep slope at the upstream and a very flat low-lying coastal zone at the downstream. The average upstream slope of the basin is approximately 25% to 30% (Vo, 2015).
The climate in Central Vietnam is strongly governed by tropical monsoons. Two main seasons can be distinguished, the dry- or summer season and rain- or winter season. Especially due to the influence of the Truong Son mountain range, the hydrological pattern in the Vu Gia-Thu Bon system is highly variable in space and time. The spatial distribution of rainfall shows increasing trends from north to south and from the low area to the high area. The annual average rainfall varies significantly from 2000 mm to 4000 mm. Rainfall usually occurs during the rainy season between September to December, mounting to 65% to 85% of the annual rainfall. The dry season lasts from April to August with a total rainfall only 20% to 35% of the annual amount. Because of the seasonal variation in rainfall distribution, the flow regime in the Vu Gia-Thu Bon also varies significantly over the season. Higher river discharge occurs corresponding to the highest rainfall period. The lower river discharge occurs during the dry season.
Specific topographic features and high seasonal discharge variations lead to vulnerability to floods. The combination of a very high discharge in a very short time during the

rainy season and a very short and steep river, leads to a flood catastrophe in the catchment. Such catastrophe is of high intensity, short period, large amplitude (Vo, 2015).
Downstream coasts of the Vu Gia-Thu Bon river system are not only influenced by the river flow regime but also by tides and waves. The climate of the central coast is dominated by the Asian monsoon regime. The wave climate in this area is also strongly influenced by this monsoon regime. During the NE monsoon regime, the wave directions in the winter season (from September to March) are dominated by both NE and ENE directions. In the summer months (April to August), the waves are characterized by a bi-directional configuration. The waves are clearly influenced by the SE and ENE directional component. The highest wave heights normally occur during winter months due to typhoons or tropical storms and may reach up to $4-7$ m in N, NE, ENE, E and ESE directions. In general, waves during the winter season have higher energy and longer periods than waves in the summer season.
Tides along the central coasts are complex and vary along the coast. Tides at Da Nang and Quang Nam are between mixed, semi-diurnal to mixed and diurnal. The tide range is 0.7 m (Lam, 2009; Tung, 2011).

1.3 Possibilities in data limited environments

In recent years, remote sensing and GIS techniques have been proposed as a relatively low-cost approach to coastal monitoring (Maiti and Bhattacharya, 2009) especially for detecting coastline movement. Monitoring the behavior of shorelines is of considerable social and economic importance in support of setback planning, hazard zoning, erosion-accretion management, regional sediment budgets and the establishment and validation of models for coastal changes (Lawrence, 1994; Sherman and Bauer, 1993 ; Zuzek et al., 2003). Shoreline studies play an important role to understand a variety of components of dynamic beaches. For example shoreline mobility (Dolan et al., 1978), long-term erosion/sedimentation (Guillén et al., 1999), beach rotation and bay beach planform stability (Silvester, 1960) and changes due to human interventions (e.g., Grunnet and Ruessink, 2005). Many applications of remote sensing and GIS on mapping shorelines and inlet dynamics demonstrate that satellite-based remote sensing can be used as a useful tool for mapping shoreline changes and the dynamic behavior of tidal inlets, rivers, and estuaries (Avinash et al., 2012; Avinash et al., 2013; Chen and Chang, 2009; Gilvear et al., 2004; Panda et al., 2013; Pari et al., 2008; Pari et al., 2008; Rajawat et al., 2007; Ryu et al., 2008).
There are some important and generally well known factors that influence coastal erosion. For complex coastal systems, such as tidal inlets further understanding can be obtained from process-based modelling describing the complexity of combined physical processes relevant to waves, tides, river flow and sediment transport processes, Many studies have shown that process-based modelling have been successful applied to study hydrodynamics, morphodynamics and morphological behaviour event in the complex coastal environments of tidal inlet systems (e.g., Bertin et al., 2009; Cayocca, 2001; Chen et al., 2015; Dissanayake et al., 2009; de Vriendº et al., 1993; Herrling and Winter, 2014; Nahon et al., 2012; Ridderinkhof et al., 2016; Van Leeuwen et al., 2003). In the absence of

sufficient observational data, systematic and schematic numerical simulations are assumed to be able to provide insight into medium to long-term coastal evolution (Daly et al., 2011).
The complex feedbacks between system forcing and response of inlet systems influenced by variations in a seasonal wave climate combined with human interventions have received broad scientific interest. Moreover, the common occurrences of seasonal varying tidal inlets are often found in developing countries where data availability is mostly limited. Therefore, it is important to figure out a successful approach to understand the system behavior when dealing with a data limited environment.
A combination between remote sensing data as a resource mapping and process-based modelling provides an approach to understand coastal systems in the cases of data limited environments in this study. Because of the extensive application range and data availability, remote sensing techniques are interesting to apply in data limited coastal areas. Validation of remote sensing techniques is however generally not possible in data limited environments. Data rich coasts could provide the necessary information for validation of remote sensing techniques to be applied in data limited environments.

1.4 Objectives and research questions

THE general objective of this research is to gain understanding of typical coastal systems in the data limited environment of the central Vietnam coast. We have chosen to subdivide this general objective focusing on 2 typical case studies. The first objective is to derive a better understanding of recent and present processes governing the evolution of Cua Dai Beach, while accepting it is a data limited environment. This understanding is expected to explain the reasons behind the morphological changes and extreme erosion at Cua Dai Beach in recent years, to aid in finding possible solutions for protection of the beach and to facilitate future coastal management. The second objective is to assess the stability of the complex bay beach planform of Da Nang Bay. Cua Dai Inlet and Da Nang Bay are two typical coastal river mouth formations of the Vu Gia-Thu Bon basin which are strongly influenced by seasonal river regimes, seasonal wave climates and human interventions.
In order to identify the research questions the following hypotheses are introduced. The primary hypothesis proposed in this thesis is that the variability in seasonal wave climates and in river discharge has an important effect on the bay beach planform stability and on the morphological behavior of a seasonal tidal inlet. A secondary hypotheses is that insight into the effects of and causes behind the morphological changes of a complex coastal system in case of a data limited environment can be gained by reconstructing historical shoreline positions and estimated volume changes from satellite images. In combination with process-based modeling this allows understanding of seasonal longshore sediment transport patterns and associated sediment budget changes. Based on the hypotheses presented above, 4 questions are posed.

- **Research Question 1**: What are the processes that govern morphological changes

and extreme erosion at Cua Dai beach during recent decades?

- **Research Question 2**: What is the estimated combined effect of seasonal varying waves and river discharges on the sediment transport and morphological feedbacks of Cua Dai inlet?
- **Research Question 3**: How can shoreline locations and sediment volumes be evaluated using satellite techniques in data limited and data rich environments?
- **Research Question 4**:Can morphological or planform stability of the complex embayed beach of Danang Bay be explained by seasonal variability in wave conditions?

1.5 Thesis Outline

THROUGHOUT this thesis detailed investigations and approaches to understand the processes controlling the Cua Dai inlet and Da Nang Bay are presented.
The investigation of the complex processes dictating the evolution of Cua Dai inlet and its adjacent coasts are the subjects of two chapters. Chapter 2 presents a comprehensive investigation and quantification of the erosion processes in the Cua Dai coastal inlet and its adjacent beach. The effects of and causes behind existing morphological changes were gained by reconstructing historical shoreline positions in combination with process-based modelling. The modelling aimed at understanding longshore sediment transport patterns and associated sediment budget changes over recent decades under the impact of human interventions. Chapter 3 investigates the effect of the seasonal wave climate and seasonal river discharges by analyzing the effects on resulting hydrodynamics and sediment transports and its morphological feedbacks through the inlet and the adjacent coasts.
Chapter 4 is an intermezzo step that presents the applicability of a method to generate satellite-derived shorelines, shoreline change rates and coastal volume changes. This chapter provides a commonly used method to extract shoreline positions from satellite images and evaluates this for a data-rich region, North-Holland coast, The Netherlands.
In Chapter 5, the planform stability of complex headland bay beach was evaluated by using empirical parabolic bay shape equation and shoreline change rates extracted from Landsat images. Then the effect of a seasonal wave climate on the local bay beach planform Da Nang bay is investigated.
Finally, Chapter 6 summarizes the main findings of this study.
Chapter 2 and Chapter 4 have been published in the Journal of Coastal Research. Chapter 3 and Chapter 5 have been presented in the proceedings of the ICEC 2018 and IAHR 2015 conferences.

References

Avinash, K., Deepika, B., and Jayappa, K. (2013). Evolution of spit morphology: a case study using a remote sensing and statistical based approach. *Journal of coastal conservation*, 17(3):327–337.

Avinash, K., Jayappa, K., and Vethamony, P. (2012). Evolution of swarna estuary and its impact on braided islands and estuarine banks, southwest coast of india. *Environmental Earth Sciences*, 65(3):835–848.

Bertin, X., Fortunato, A. B., and Oliveira, A. (2009). A modeling-based analysis of processes driving wave-dominated inlets. *Continental Shelf Research*, 29(5-6):819–834.

Cayocca, F. (2001). Long-term morphological modeling of a tidal inlet: the arcachon basin, france. *Coastal Engineering*, 42(2):115–142.

Chen, J.-L., Hsu, T.-J., Shi, F., Raubenheimer, B., and Elgar, S. (2015). Hydrodynamic and sediment transport modeling of new river inlet (nc) under the interaction of tides and waves. *Journal of Geophysical Research: Oceans*, 120(6):4028–4047.

Chen, W.-W. and Chang, H.-K. (2009). Estimation of shoreline position and change from satellite images considering tidal variation. *Estuarine, Coastal and Shelf Science*, 84(1):54–60.

Daly, C. J., Bryan, K. R., Roelvink, J. A., Klein, A. H. F., Hebbeln, D., and Winter, C. (2011). Morphodynamics of embayed beaches: The effect of wave conditions. *Journal of Coastal Research SI*, 64(64):1003–1007.

de Vriendº, H., Zyserman, J., Nicholson, J., Roelvinkº, J., and Pechon, P. (1993). Medium-term 2dh coastal area modelling. *Coastal engineering*, 2(1):193–224.

Dissanayake, D., Roelvink, J., and Van der Wegen, M. (2009). Modelled channel patterns in a schematized tidal inlet. *Coastal Engineering*, 56(11-12):1069–1083.

Dolan, R., Hayden, B., and Heywood, J. (1978). A new photogrammetric method for determining shoreline erosion. *Coastal Engineering*, 2:21–39.

Gilvear, D., Tyler, A., and Davids, C. (2004). Detection of estuarine and tidal river hydromorphology using hyper-spectral and lidar data: Forth estuary, scotland. *Estuarine, Coastal and Shelf Science*, 61(3):379–392.

Grunnet, N. M. and Ruessink, B. (2005). Morphodynamic response of nearshore bars to a shoreface nourishment. *Coastal Engineering*, 52(2):119–137.

Guillén, J., Stive, M., and Capobianco, M. (1999). Shoreline evolution of the holland coast on a decadal scale. *Earth Surface Processes and Landforms: The Journal of the British Geomorphological Research Group*, 24(6):517–536.

Herrling, G. and Winter, C. (2014). Morphological and sedimentological response of a mixed-energy barrier island tidal inlet to storm and fair-weather conditions. *Earth Surface Dynamics*, 2(1):363–382.

Lam, N. (2009). *Hydrodynamics and Morphodynamics of a Seasonally Forced Tidal Inlet System*. PhD thesis, Delft University of Technology.

Lawrence, P. L. (1994). Natural hazards of shoreline bluff erosion: a case study of horizon view, lake huron. In *Geomorphology and Natural Hazards*, pages 65–81. Elsevier.

Maiti, S. and Bhattacharya, A. K. (2009). Shoreline change analysis and its application to prediction: a remote sensing and statistics based approach. *Marine Geology*, 257(1-4):11–23.

Nahon, A., Bertin, X., Fortunato, A. B., and Oliveira, A. (2012). Process-based 2dh morphodynamic modeling of tidal inlets: A comparison with empirical classifications and theories. *Marine Geology*, 291:1–11.

Panda, U., Mohanty, P., and Samal, R. (2013). Impact of tidal inlet and its geomorphological changes on lagoon environment: A numerical model study. *Estuarine, Coastal and Shelf Science*, 116:29–40.

Pari, Y., Murthy, M. R., Subramanian, B., Ramachandran, S., et al. (2008). Morphological changes at vellar estuary, india—impact of the december 2004 tsunami. *Journal of Environmental Management*, 89(1):45–57.

Rajawat, A., Gupta, M., Acharya, B., and Nayak, S. (2007). Impact of new mouth opening on morphology and water quality of the chilika lagoon–a study based on resourcesat-1 liss-iii and awifs and irs-1d liss-iii data. *International Journal of Remote Sensing*, 28(5):905–923.

Ridderinkhof, W., Swart, H., Vegt, M., and Hoekstra, P. (2016). Modeling the growth and migration of sandy shoals on ebb-tidal deltas. *Journal of Geophysical Research: Earth Surface*, 121(7):1351–1372.

Ryu, J.-H., Kim, C.-H., Lee, Y.-K., Won, J.-S., Chun, S.-S., and Lee, S. (2008). Detecting the intertidal morphologic change using satellite data. *Estuarine, Coastal and Shelf Science*, 78(4):623–632.

Sherman, D. J. and Bauer, B. O. (1993). Coastal geomorphology through the looking glass. *Geomorphology*, 7:225–249.

Silvester, R. (1960). Stabilization of sedimentary coastlines. *Nature*, 188(4749):467.

Tung, T. T. (2011). *Morphodynamics of seasonally Closed Coastal IInlet at the Central coast of Vietnam*. PhD thesis, Delft University of Technology.

Van Leeuwen, S., Van der Vegt, M., and De Swart, H. (2003). Morphodynamics of ebb-tidal deltas: a model approach. *Estuarine, Coastal and Shelf Science*, 57(5-6):899–907.

Vo, N. D. (2015). *Deterministic hydrological modelling for flood risk assessment and climate change in large catchment. Application to Vu Gia Thu Bon catchment, Vietnam*. PhD thesis, University of Nice Sophia Antipolis.

Zuzek, P. J., Nairn, R. B., and Thieme, S. J. (2003). Spatial and temporal considerations for calculating shoreline change rates in the great lakes basin. *Journal of Coastal Research*, pages 125–146.

Chapter 2

Beach Evolution adjacent to a seasonally varying tidal inlet

Kites rise highest against the wind,
not with it

Winston S. Churchill

Cua Dai Inlet is a typical, seasonally varying tidal inlet in central Vietnam. Since 1995 the northern adjacent coast, known as Cua Dai Beach, has experienced serious erosion. The decadal scale behavior of this inlet appears to reflect a nonperiodic cyclic process. Inlet channel shifting from north to south has welded the abandoned ebb-tidal delta with Cua Dai Beach, leading to accretion but subsequently triggering erosion. Although erosion of Cua Dai Beach was exacerbated by decrease of sediment supply from the estuary and ebb-tidal delta and by coastal developments, the channel shifting to the south, and the ebb shoal development were important primary controlling mechanisms. This study aims to quantify the main erosional processes in and near the Cua Dai coastal inlet and adjacent beaches since 1995. First, satellite data were used to detect shoreline change trends and to estimate volume changes. Second, alongshore, wave-driven sediment transports were estimated using numerical models. Observed shoreline changes indicate that, during the period from 2000 to 2010, erosion rates at the northern side of the inlet were on average 12 m/y. Close to the inlet, erosion rates were larger, up to 19 m/y. At the same time, the southern coast of the inlet was found to accrete with a mean rate of 11 m/y. Calculated alongshore sediment transport rates explain the observed erosion and accretion patterns. The overall system lost a significant sediment volume, which is estimated to amount to 243,000–310,000 m^3/y. A logical conclusion is that the effects of the shifting of the inlet channel to the south caused erosion of the northern adjacent coast, whereas human interventions in the river catchment, the estuary, and along the coast contributed importantly to the overall sediment deficit of the inlet system and its beaches and to the shifting erosion pattern toward the north.

This chapter has been published in Journal of Coastal Research Do et al. (2017).

2

2.1 Introduction

TIDAL inlets connecting an estuary, lagoon or river to the coast are commonly found throughout the world (Elias and van der Spek, 2006; Kragtwijk et al., 2004; Oertel, 1988; Stive and Wang, 2003). Tidal inlets showing seasonal behavior are found at many locations in Southeast Asia and Australia due to variability in monsoon wind directions and/or dry and wet periods (Duong et al., 2016; Stive et al., 2012). Coastal features near inlets are generally amongst the most dynamic regions (Stive et al., 2009). They are not only affected by ocean processes (tides, waves, and mean sea level), but also by fluvial and estuarine processes (Duong et al., 2016; Lam, 2009; Ranasinghe et al., 2013; Tung, 2011). Furthermore, they are increasingly influenced by human interventions such as dredging, coastal structures and land reclamation in the tidal basins. The complex feedbacks between the forcing and response of inlet systems influenced by variations in a seasonal wave climate combined with human interventions have received a broad scientific interest (Dissanayake et al., 2012; Lam, 2009; Ranasinghe et al., 1999; Tung, 2011). In Central Vietnam, one finds many seasonally varying tidal inlets. These inlets are in a microtidal, wave dominated, coastal environment and experience a strong seasonal variation in river discharge and wave climate (Ranasinghe and Pattiaratchi, 1999; Tung, 2011). The climate in Central Vietnam is strongly governed by tropical monsoons. Two main seasons can be distinguished, the dry- or summer season and rain- or winter season.

Cua Dai estuary in central Vietnam is a typical, seasonally varying inlet connected to

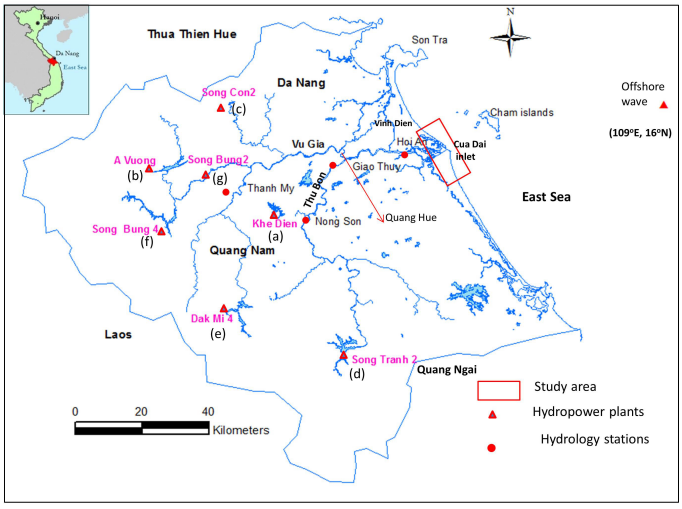

Figure 2.1: Location of Cua Dai inlet and the Vu Gia-Thu Bon river system

the catchment area of the Vu Gia and Thu Bon Rivers. The total catchment area is approximately 10,350 km^2 and includes roughly 90% of the Quang Nam province and 10% of Danang city. The catchment area of the Thu Bon basin is 4,100 km2 at the Cua Dai inlet. The total length of the main river is 152 km. Between the Vu Gia River and the Thu

Bon River, there are two connecting tributaries Quang Hue and Vinh Dien (see Figure 2.1). Due to the exchange of their discharges, these two rivers need to be considered as one river basin system. Figure 2.1 shows a map of the river network and of the location of hydro-meteorological stations as well as of hydropower plants. Another distinctive feature in this system is the Cham islands group, which is comprised of a group of 8 islands, located about 16 km in Northeast direction from the Cua Dai inlet. Besides natural processes, this system has been influenced by human activity. The human activities are the construction of hydropower plants in the upstream of the Vu Gia-Thu Bon basin, the construction of resorts near and on the beach, land reclamations and sand mining for building and infrastructure in the estuary.
Since 1995, Cua Dai Beach, located on the north side of Cua Dai Inlet, has experienced severe erosion. The long-term geomorphological development of this inlet appears to reflect a nonperiodic cyclic process that takes place over several decades. In addition, coastal developments leading to squeeze and decrease of sediment supply from the river and the estuary took place. These factors have created changes in sediment budgets and have put Cua Dai Beach under stress by causing the shoreline to erode. This study aims to quantify the erosion processes in the Cua Dai coastal inlet and adjacent beach system since 1995. To aid future management of this system, it is necessary to understand the factors that influence the existing morphology and that cause coastal retreat of the system. Insight into the effects and causes of these changes can be gained by reconstructing historical shoreline positions in combination with process-based modelling to understand longshore sediment transport patterns and associated sediment budget changes over recent decades under the impact of human interventions.

2.2 Environmental Conditions

BOTH the river flow regimes and coastal processes such as waves and tides influence Cua Dai inlet and its adjacent coasts. The tide range is 0.7 m (Lam, 2009 and Tung, 2011) and the wave height ranges from 0 to 2 m. Therefore, Cua Dai is classified as a microtidal, mixed energy/wave-dominated inlet according to Hayes (1979) tidal classification diagram.
The monsoon influences both the wave conditions and the river flow. During the NE monsoon regime, waves in the winter season (from September to March) are mainly from ENE direction. In the summer months (from April to August) when the SW monsoon is active waves come from SE and ENE. In terms of river discharge, previous studies (Ho et al., 2010; Lam, 2009; Tung, 2011) show that there are two distinctive seasons, a flood season lasting from September to December and a dry season lasting from January to August.
When combining both the hydrology and the wave climate, we may conclude that three seasons exist, an ENE monsoon with a flood season from September to December, an ENE monsoon with a dry season from January to March and a dry bidirectional SE/ENE monsoon from April to August. The winter/flood season lasts for 4 months, from September to December, with an average discharge of 625 m^3/s. The average discharge during the winter/dry season, from January to March, is 160 m^3/s while the average discharge

during the summer/dry season is only 88 m^3/s. Figure 2.2 also indicates that the high values of monthly discharge at the Nong Son station often occur in three months: October, November and December. During the relatively long dry period the flow is quite low, with an average lowest of 71 m^3/s in July. The average annual discharge from 1977 to 2011 at the Nong Son station is 285 m^3/s.

In recent years, floods occur more frequently and with higher peak discharges. The

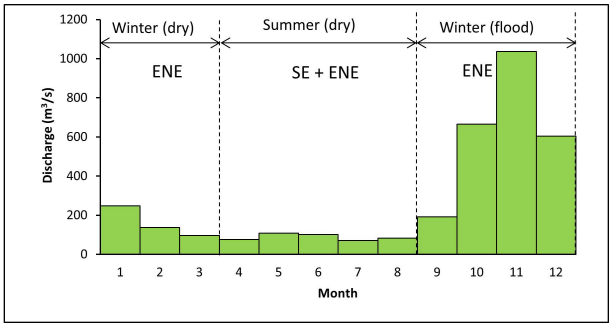

Figure 2.2: Seasonal variation of the average monthly discharge at Nong Son station, upstream the Thu Bon River (1977-2011). ENE and SE are the dominant wave directions in each season.

highest discharge that occurred every year from 1977 to 2011 is displayed in Figure 2.3. The red points indicate the average of the yearly highest discharges over the preceding 10-year period. The trends indicate an increase in the 10-year mean highest discharges. The reason behind this is unknown. Extreme floods occurred in 1986, 1998, 1999, 2007, 2009, and 2011. The floods were often induced by intense meteorological phenomena (heavy rain, storm, typhoon or tropical depression). These events caused severe damage in terms of loss of life and infrastructure. The green bars in Figure 4 present the number of floods that occurred every year from 1989 to 2010 (Bank (2014)). For the number of floods in recent years from 2011 to 2015 we lack this information. This figure indicates that during recent years, from 2005 to 2010, floods occur more frequently. In 2005, six floods occurred. In 2007 nine floods occurred of which one was an extreme flood with a peak discharge of 10,600 m^3/s. In general, the average number of floods that occurred during 2005 to 2010 is 5.6 floods per year, whereas the average number of floods during the period from 1989 to 2004 is only 2.7 floods per year. These data indicate that also the number of floods has increased in recent years at the Vu Gia-Thu Bon basin.

Besides the increasing frequency and increasing magnitude of river floods, the Quang Nam Province experiences storms, typhoons, tropical depressions and human interventions. An overview of the most important events and human interventions is shown in the time line in Figure 2.4. The data of storms, typhoons and tropical depressions were extracted from the National Weather Service (United States) by using individual storm tracking records at location 15°N, and 110°E in the Western Pacific. The classification of hurricanes based on the Saffir/Simpson hurricane scale is used which defines a tropical depression with wind speed less than 34 knots, a tropical storm with wind speed from 34 to 63 knots and a hurricane or typhoon with wind speeds greater than 64 knots. In general, 68 tropical cyclones and depressions occurred that affected or directly hit the

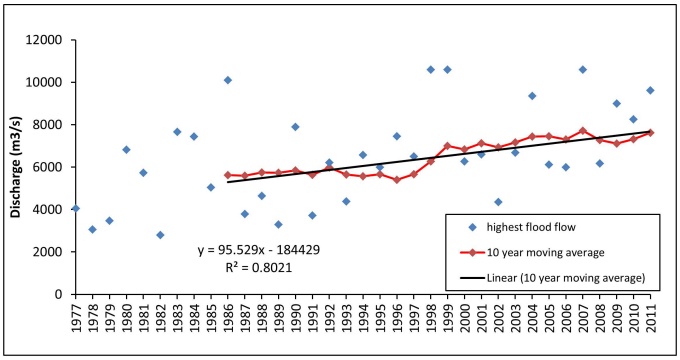

Figure 2.3: Yearly highest flood discharge at Nong Son Station (1977-2011). The black line indicates the mean of the yearly highest flood discharge over the preceding 10-year period

coastline of the Quang Nam Province during the period from 1988 to 2014 with an average of 2.5 cyclones per year. This includes 27 typhoons, 24 tropical storms and 17 tropical depressions. There were four big typhoons that hit directly, causing heavy rain and subsequent flooding. These were Typhoon Cecil (May 1989), Typhoon Xangsane (October 2006), Typhoon Ketsana (September 2009) and Typhoon Nari (October 2013).

Since 2000 there have been many human activities such as the building of resorts at

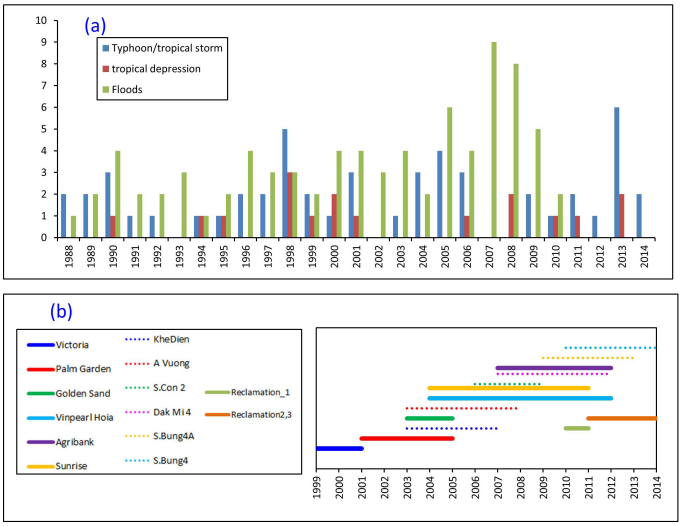

Figure 2.4: Time line of events and human interventions at the Vu Gia-Thu Bon river basin. (a) The number of typhoons/tropical storms, tropical depressions and floods (note that from 2011 to 2014 no data on floods are available); (b) Construction period of resorts, hydropower plants and reclamations (solid lines indicate the name of resorts, whereas dotted lines indicate the name of hydropower plants).

Cua Dai Beach, the construction of hydropower plants upstream and land reclamations inside the estuary for urbanization purposes. The date of the construction of the resorts

and hydropower plants as well as land reclamations were derived from observations based on a series of Landsat images and local papers (A Vuong Joint Stock Hydropower Company, 2011; Song Ba Joint Stock Company, 2015; Song Bung 4 hydropower project management, 2015). The location of the hydropower plants is indicated in Figure 4.1 and the location of the resorts and land reclamations in Figure 2.5. Starting from Cua Dai inlet and going along the beach toward the North, the first resort is Vinpearl Hoi An. The construction started around 2004. After the construction, the shoreline has significantly retreated so that the investors choose to protect their resort by construction of a seawall in front of the resort. The second resort is Fusion Alya, which was constructed during the period 2010 to 2012. This resort also has used a seawall to protect itself from severe erosion. A 700-m stretch between Fusion Alya and Sunrise resort has been protected by a heavy embankment along this stretch funded by the Ministry of Construction, which presently suffers from toe erosion. Groynes made of large geo-bags defend the third resort Sunrise, constructed in the period of 2006 to 2011. The fourth resort, Golden Sand constructed from 2002 to 2005, has been protected by a rip-rap stone embankment. The last one in this row of five is Victoria resort, the first resort that was constructed at Cua Dai beach in 1999. Presently, it also uses a stone riprap embankment to protect against erosion. Further to the North there are two more resorts, Agribank and Palm Garden. These were less impacted by shoreline retreat but very recently in October 2016 erosion has reached this location as well. (M.J.F. Stive, personal observation).

Figure 2.5: Location of resorts and land reclamations and the ebb tidal delta of Cua Dai Beach

2.3 Methods

To investigate the erosion at Cua Dai Beach, the present work collected the available data concerning its past evolution. Satellite data and GIS techniques were used to estimate the trends in shoreline evolution and volume changes during recent decades. The numerical model SWAN combined with an empirical equation was applied to calculate the local longshore sediment transport rate (LSTR) and the gradients in LSTR. Based on the results of the LSTR and shoreline change rate as well as the background information of Cua Dai beach, this study aims to explain the prevailing transport mechanisms and especially those causing erosion problems in this system.

2.3.1 Rates of change in shoreline location

Recent progress in remote sensing and GIS techniques has been proposed as a relatively low-cost approach to coastal monitoring (Maiti and Bhattacharya, 2009). Many applications of remote sensing and GIS on mapping shorelines and inlet dynamics demonstrate that satellite-based remote sensing can be used as a useful tool for mapping shoreline changes and the dynamic behavior of tidal inlets, rivers, and estuaries (Avinash et al., 2013; Avinash et al., 2012; Chen and Chang, 2009; Gilvear et al., 2004; Panda et al., 2013; Pari et al., 2008; Rajawat et al., 2007; Ryu et al., 2008).

To detect the shoreline location in Cua Dai beach during the last decades, a total of six multispectral satellite images acquired on different dates were selected based on the lowest cloud cover (Table 2.1). The six orthorectified satellite images of the study area from the sensors Landsat-5TM, Landsat-7 ETM+ and Landsat-8 OLI-TIRS in the years, 1988, 1995, 2000, 2005, 2010, and 2015 were downloaded from U.S Geological Survey (USGS) Earth Explorer web tool. The images in the years between 1990 and 1995 were not selected because of the poor quality. Although the image of 2005 was selected to extract the shoreline position, it was eventually not used to present our shoreline change results, since the trends from 2000 to 2005 and from 2005 to 2010 are very similar.

The methodology to extract the shoreline includes three steps: (1) conversion of the digital number (DN) to spectral radiance and to the top of atmospheric (TOA) reflectance for radiometric calibration according to Chander et al. (2009); (2) application of the normalized difference water index (NDWI) (McFeeters, 1996) to enhance the TOA reflectance; (3) delineation of the land-sea boundary was achieved using iso cluster unsupervised classification and the enhanced NDWI images. Then, the boundary between land and sea in the classified image is converted into a vector file for shorelines in ArcGIS software.

The shoreline change rates are estimated for four zones around Cua Dai inlet: Zone A (northern coast), Zone B (southern coast) and Zone C (river bank) and Zone D (extent of spit due to welding of tidal bar). Transects were chosen at simple right angles from the baseline at 50m intervals (Figure 2.6). Zone A includes 74 transects (3650m) from transect A1 to transect A74 starting from the north. Zone B also includes 74 transects from transect B1 to transect B74 (3650m). The river bank, zone C, includes 49 transects (2400m) from C1 to C48, starting from the river towards the sea.

Shoreline change rates are calculated following the End Point Rate (EPR) method using

the Digital Shoreline Analysis System (DSAS) software version 4.3, an ArcGIS extension for calculating shoreline change developed by the USGS (Thieler et al., 2009). The EPR is calculated by dividing the distance of shoreline movement by the time elapsed between the earliest and latest measurements at each transect (Thieler et al., 2009). A baseline is constructed to serve as a starting point for all transects derived by the DSAS application. Using the EPR method shoreline change rates in each period 1988 and 1995; 1995 and 2000; and 2000 and 2010, and between 2010 and 2015 are calculated. Shoreline change rate at every transect location is calculated by subtracting two derived shoreline locations at the beginning and the end of each period.

Table 2.1: Characteristics of images analyzed

Name	Acquisition Date	Path/Row	Resolution (m)	Type	Used Bands
Landsat 5 TM	3 September 1988	124/049	30	Geo Tiff	2 and 4
Landsat 5 TM	19 June 1995	124/049	30	Geo Tiff	2 and 4
Landsat 7 ETM+	5 July 2000	124/049	30	Geo Tiff	2 and 4
Landsat 5 TM	16 July 2005	124/049	30	Geo Tiff	2 and 4
Landsat 5 TM	12 June 2010	124/049	30	Geo Tiff	2 and 4
Landsat 8 OLI-TIRS	10 June 2015	124/049	30	Geo Tiff	3 and 4

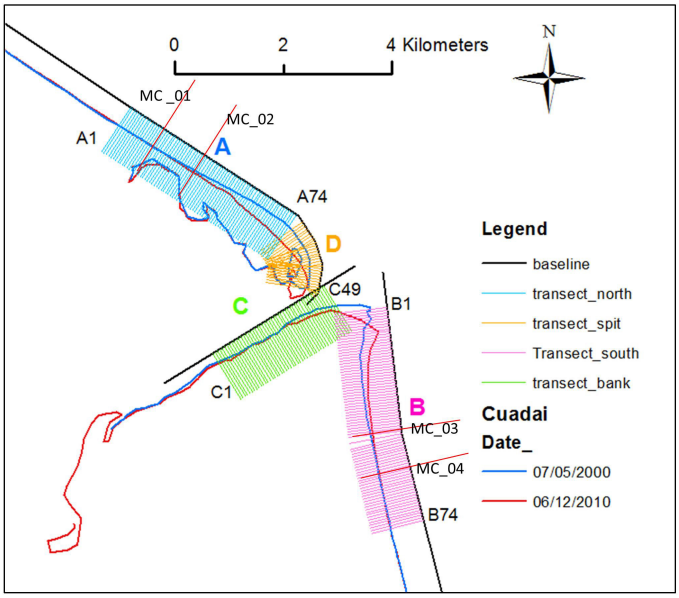

Figure 2.6: Transects at the northern side, the southern side, the riverbank and the spit created with a 50-m interval to extract shoreline changes around Cua Dai inlet.

2.3.2 Calculation of volume changes

To understand sediment sources, sinks and transport pathways in a coastal system, the concept of estimating a sediment budget is commonly used (Hapke et al., 2010; Rodriguez and Dean, 2005; Rosati, 2005). This study uses the satellite-derived shoreline change rates to calculate the volume changes (m^3y) for each zone A, B, C and D. The cell volume changes (m^3/y) were estimated by using Equation 4.1 (Rosati, 2005; Rosati and Kraus, 1999).

$$\Delta V = A_D \sum_{i=1}^{n} \left(\Delta_y \Delta_x\right) \tag{2.1}$$

where Δ_y is the shoreline change rate for the each transect (m/y), A_D is the average active depth for the cell (m), Δ_x represents the transect spacing (m), and n is the total transects of each zones. The active depth represents the vertical extent of the beach profile that is eroding or accreting during the period of consideration, and is typically defined as the absolute sum of the berm crest or dune elevation, B, and depth of closure, D_c (Equation 2.2). However, in the absence of dune elevation data, it was assumed that the closure depth was representative for the active depth:

$$A_D = B + D_c \tag{2.2}$$

in which B is assumed zero.

The depth of closure indicates the seaward limit of appreciable depth change or limit of long-shore and cross-shore sediment movement (Hallermeier, 1978; Nicholls et al., 1997; Rodriguez and Dean, 2005). In cases with no available data, an analytical approach is commonly used to estimate an annual depth of closure. Since no systematic measurements of the active beach profiles are available, this study used the method proposed by Hallermeier (1980) to estimated closure depth according to:

$$d_{l,t} = 2.28 H_{e,t} - 68.5\left(H_{e,t}^2 / g T_{e,t}^2\right) \tag{2.3}$$

where $d_{l,t}$ is the predicted depth of closure over t years, related to mean low water; $H_{e,t}$ is the non-breaking significant wave height that is exceeded 12 hours per t years; $T_{e,t}$ is the associated wave period; g is the acceleration due to gravity. The computed closure depth ($d_{l,t}$) by Equation 2.3 is verified to some extent by using two available bathymetric maps of the area from 2009 and 2010.

The wave characteristics used to compute closure depth were derived using nearshore wave models. Because the contour bathymetry is only available for two years (2009 and 2010), this study used wave conditions during this period to estimate the closure depth. Firstly, the offshore wave conditions during 2009 and 2010 were extracted from the National Oceanic and Atmospheric Administration (NOAA) Wave Watch III archives at grid point (16.0°N, 109.0°E) (Figure 2.1), approximately 65 km offshore of Cua Dai inlet. Then, SWAN transformed the extreme wave height that exceeds 12 hours in two years to the nearshore. The significant wave height and wave period in the nearshore were used into Equation 2.3 to estimate the annual closure depth. The results of this estimated closure depth are compared with the depth profiles available for 2009 and 2010. The results of estimated closure depth by Hallermeier (1980) are 5.2 m to 6.3 m corresponding to the

nearshore significant wave height around Cua Dai inlet of 2.8 m to 3.3 m. The four profiles, MC-01, MC-02, MC-03 and MC-04 (Figure 2.6), in which two profiles located 4 km and 3.2 km north of Cua Dai inlet and the other two profiles located 3.3 km and 2.6 km south of Cua Dai inlet, indicate the closure depth is around 6 to 7 m. To capture both ranges in values, the depth of closure for the study area is assumed from 5.5 to 7 m in order to estimate the shoreline volume changes.

2.3.3 Longshore sediment transport capacity

The LSTR is estimated on the basic of the widely used Coastal Engineering Research Center (CERC) (Engineers (1984)) formulae. The CERC formulation can be summarized as wave driven alongshore sediment transport (S [m^3/s]) being proportional to the longshore wave energy flux (Bosboom and Stive, 2012).

$$S = \frac{K}{16\left(\frac{\rho_s}{\rho} - 1\right)(1-p)} \sqrt{\frac{g}{\gamma}} \sin(2\phi_b) H_b^{2.5} \tag{2.4}$$

where ρ is the density of water [kg/m^3]; ρ_s is the density of sediment [kg/m^3]; p is the porosity; g is the gravitational acceleration [m/s^2]; H_b is the significant wave height at the breaker line [m]; γ is the breaker index; ϕ_b is the wave angle at the breaker line between wave propagation direction and shore normal direction (°); K is an empirical coefficient. Engineers (1984) recommends a value of K of 0.39 when the significant wave height Hs is used. However, a value of 0.2 has been used on sandy beaches (Bayram et al., 2007; Schoonees and Theron, 1997) and 0.054 for a gravel beach (de Alegria-Arzaburu and Masselink, 2010). K = 0.2 is used in this study since Cua Dai is a sandy beach.
To obtain first-order longshore sediment transport estimates, the offshore wave climate is transformed to a nearshore wave climate at the location of initial wave breaking and used as input to the CERC formulation (Equation 2.4). Seasonal representative offshore wave directions are selected as input for the wave generation and propagation model, SWAN. Then the nearshore breaking wave height was derived from the offshore to nearshore wave transformation by the SWAN model. The shoreline orientation was read from satellite imagery. The breaking wave heights and their direction relative to the shoreline orientation were used to estimate LSTRs for the summer and the winter season and for the year average.
The wave characteristics required for the calculation of wave-induced longshore sediment transport have been estimated using the offshore wave climate in combination with a numerical model. The only continuous series of wave data available is measured at the Con Co station, approximately 188 km northward of our study zone. Close to Cua Dai beach, visual observations are available but the record is short in time and not continuous. Since observations are so limited, this study uses offshore wave conditions extracted from the NOAA Wave Watch III archives at grid point (16.0°N, 109.0°E) (Figure 2.1), which is approximately 65km offshore of Cua Dai inlet.

2.4 Results

THIS section first presents the results of the offshore wave climate. Second, this section presents and discusses the results of shoreline changes and volume changes during the period 1988 to 2015. Third, the results of longshore sediment transport are presented and discussed. The longshore sediment transport is separately derived for the winter and the summer period before aggregating these results into a net, yearly averaged result.

2.4.1 Wave climate

The offshore wave data in the period 2005-2013 indicate that the wave climate in this area is strongly influenced by the monsoon regime. Figure 2.7 shows strong variations in height, period and directional distribution of the waves. Because of the NE monsoon regimes, the wave direction in the winter season (from September to March) is dominated by the NE (7.1%) and ENE (79.5%) directions. Considering the incoming waves between 60° and 75°, most wave heights range between 1.0 and 3.0 m and periods between 8 and 10 s. In the summer months (April to August), the waves are characterized by a bi-directional configuration. The waves are clearly influenced by the SE and ENE directional component. The first dominant direction is from SE (44.7%) including waves coming from between 135° and 150° with wave heights of 0-1.0 m and periods of 4-6 s. The second dominant wave direction is ENE (34.9%) with typical wave heights of 0.5-1.0 m and periods of 6-10 s. The highest wave heights normally occur during winter months because of typhoons or tropical storms and may reach up to 4-7 m in N, NE, ENE, E and ESE directions. In general, waves during the winter season have higher energy and longer periods than waves in the summer season.

2.4.2 Derived shoreline changes and changes in sediment volume

Shoreline changes and changes in sediment volume were estimated in each of four selected periods, i.e. 1988 to 1995; 1995 to 2000; 2000 to 2010; and 2010 to 2015. The selection was based on comparability of the change pattern. The extracted shoreline positions are shown in Figure 2.8. These results indicate that in 1988 an ebb-tidal bar of the inlet existed. This suggests that the system was rich in sediment. Because of a big tropical storm that made landfall in May 1989 (Typhoon Cecil), the ebb tidal bar merged with Cua Dai beach, north of the inlet. Since 1995, after the welding of the ebb-tidal bar, this beach has been eroding.

Period 1988-1995

The long-term geomorphological development of the inlet reflects a nonperiodic cyclic process that takes place over several decades. Channel shifting from North to South dictates the geomorphological development of Cua Dai Beach, and much less so for the reverse situation for the southern beach. The channel shifting to the south in 1989 that created the new ebb shoal development was an important controlling mechanism. The

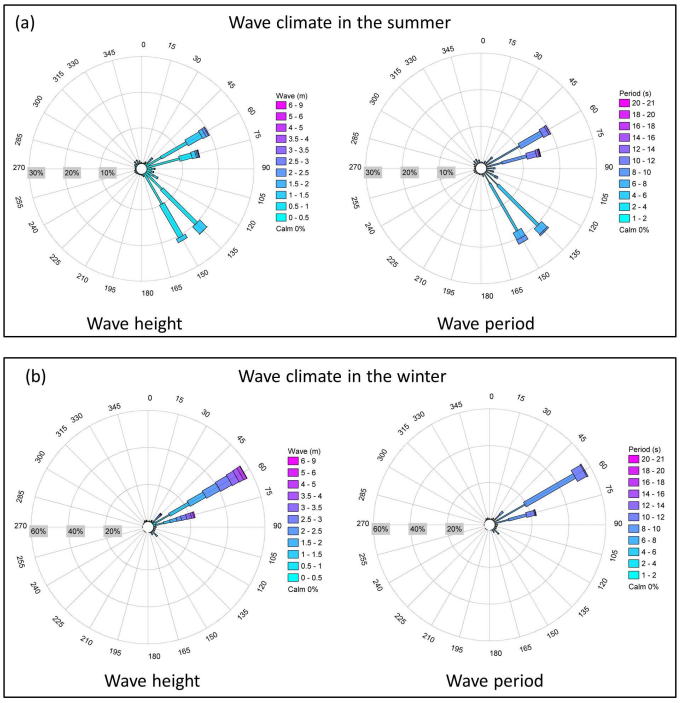

Figure 2.7: Occurrence frequencies for directional wave height and wave period; (a) Wave climate in the summer; (b) Wave climate in the winter

welding of this ebb-tidal bar over this 7-year period (1989-1995) with Cua Dai beach explains the large accretion that the northern coast has experienced. Landsat 5TM data taken from 1988 to 1995 (Figure 2.9) illustrate how the tidal bar welded to the northern coast and formed a new sand spit that developed seaward and extended southward. For this reason, the northern coast experienced much accretion in this period. The accretion of the shoreline of the southern coast can probably be explained by having benefitted from the bypassing of sediments due to waves, tide and floods, and the southern directed longshore transports.

The shorelines change rates in three zones (A, B, and C) for the period from 1988 to 1995 are shown in Figure 2.10. The shoreline change rate results show the welding of the subareal beach barrier being part of the ebb-tidal delta of Cua Dai inlet. Figure 2.10 also shows accretion on both sides of the inlet. An average increase in the shoreline of 25 m/y is observed for this 7-year period over the 2.6 km north of Cua Dai inlet. The first 2.5 km south of the inlet, the shoreline accreted with an average of 11 m/y, followed by a stable trend without any significant changes. The results of the riverbank show a relatively stable trend.

The derived volume changes for the 7-year period from 1988 to 1995 are shown in Table 2.2, where overall accretion is strongly evident. In general, north of the inlet (zone A) the volume increased by approximately 378,000 m^3/y to 481,000 m^3/y corresponding to an

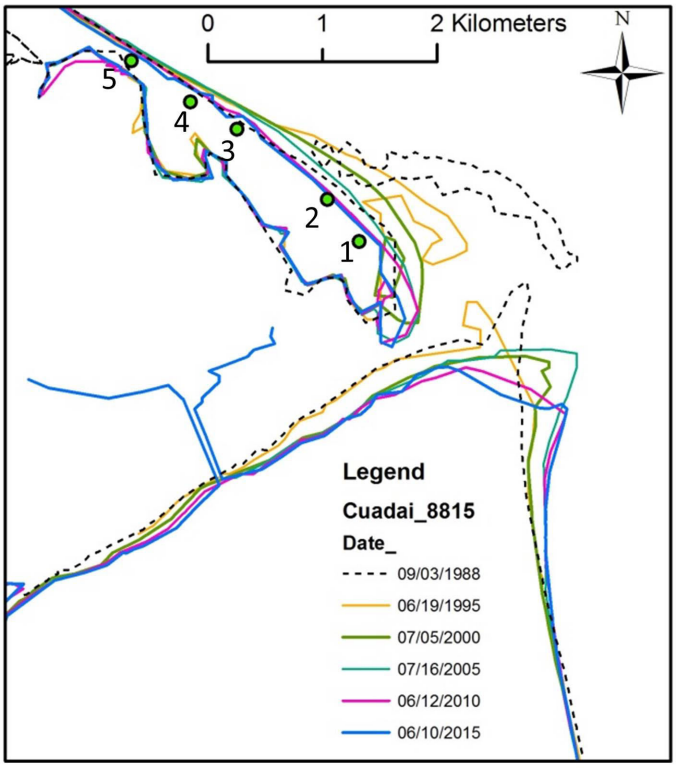

Figure 2.8: Shoreline positions including the ebb tidal bar welding at Cua Dai Beach from 1988 to 2015 (labels indicate the date of observation, and green dots indicate the location of the first five resorts).

active depth A_D of 5.5 m and 7 m respectively. The southern segment is characterized by a total accumulation of 114,000 m^3/y to 145,000 m^3/y. The river bank shows an average reduction in the volume of -10,000 m^3/y to -13,000 m^3/y. Overall, the system indicated to be rich in sediment with a total gain in zone A, zone B and zone C of 481,000 m^3/y (corresponding to 5.5m Dc) of which 378,000 m^3/y was due to the welding.

Period 1995 -2000

The shoreline change rates from 1995 to 2000 are presented in Figure 2.11. For the 2550-m segment north of zone A, there is an average positive trend of 3 m/y. Then, from transect A53 to transect A74 (1100 m) the shoreline has eroded with a mean rate of erosion of 18 m/y. The beach immediately south of the inlet showed accretion with mean of 0.7 m/y from 1.0 km to 2.4 km, followed by an erosional segment of 2.6 m/y over a 1.9-km stretch of beach. It seems that no bypassing occurred during this period. The riverbank segment experienced strong erosion of its estuarine shoreline with a mean rate of 25m/y. The significant retreat of all three zones is possibly related to the completion of the welding of the beach barrier and due to extreme flood events in 1998 and 1999 (Figure 2.3).

The derived volume changes for the period of 1995 to 2000 are summarized in Table 2.2. A total of 60,000 m^3/y to 77,000 m^3/y has been lost at the north and 22,000 m^3/y to 29,000

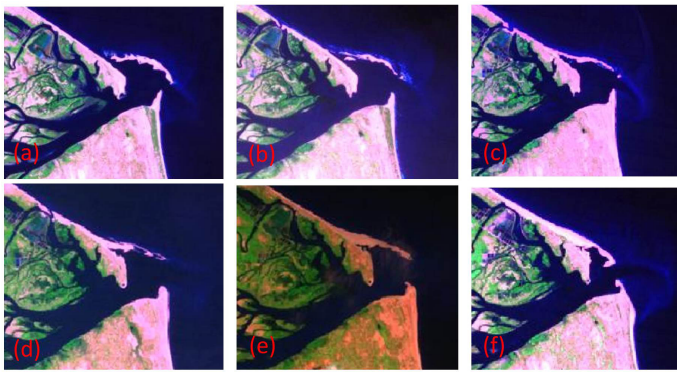

Figure 2.9: Observed welding of the ebb-tidal delta bar. (a) 3 September 1988; (b) 17 May 1989; (c) 7 July 1990; (d) 10 July 1991; (e) 25 May 1992; and (f) 19 June 1995

m^3/y at the south. There was a large loss in sediment of the riverbank with an average of 335,000 m^3/y to 426,000 m^3/y. The whole system lost 418,000 m^3/y of which the riverbank lost 335,000 m^3/y. The big erosion that occurred at the riverbank might be related to the two extreme floods in 1998 and 1999 (Figure 2.3). These floods may have scoured the riverbank and flushed sediment into the ebb tidal delta and later feeding Zone B. These floods could also have caused the shift of the tip of the south coast in seaward and southern direction (Figure 2.8).

Period 2000-2010

The shoreline change rates for each zone for the period from 2000 to 2010 are shown in Figure 2.12. The shoreline of the northern coast has continued to erode with a mean rate of erosion of 12 m/y from 1.5 km to 4.3 km. The erosion has extended to the end of the spit (the yellow color bar in Figure 2.6) with an average rate of 19 m/y from 0.3 km to 1.4 km. In contrast, the southern coast has shown strong accretion. The most accretion at the southern coast is observed from 0.9 km to 3.2 km with a mean rate of 11 m/y, followed by a gradual decrease in change rates. At the riverbank, an average shoreline retreat of 4.5 m/y is observed over 2.4 km of the shoreline.

The derived volume changes in this period are presented in Table 2.2. For a closure depth of 5.5 and 7 m respectively, the total sediment loss at the north coast is 323,000 m^3/y to 411,000 m^3/y including zone A and zone D, whereas the southern coast experienced a total gain of 139,000 m^3/y to 177,000 m^3/y. Over this period, the riverbank has experienced a slight erosional pattern of approximately 59,000 m^3/y to 76,000 m^3/y. In terms of total loss, the three zones A, B and C have lost approximately from 104,000 m3/y to 132,000 m^3/y. The total loss has increased to approximately 243,000 m^3/y to 310,000 m^3/y including the loss at the spit. Compared with the period 1995-2000 the total loss is less but of the same order of magnitude.

Period 2010-2015

Shoreline change rates of the northern coast, the southern coast and the riverbank from 2010 to 2015 are shown in Figure 2.13. The shoreline north of Cua Dai inlet shows retreat in the order of 6m/y between 3.2 km and 5.2 km and of 5 m/y between 1.5 km to

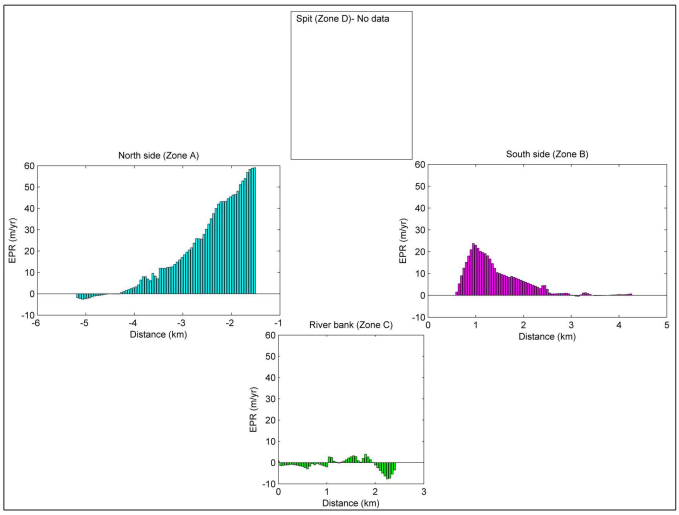

Figure 2.10: Shoreline change rates from 1988 to 1995. Distance (km) from the inlet measured from the centerline of the inlet, with negative values to the north, and positive values to the south of the inlet. For the riverbank, distance (km) is positive from the river to sea. During this period the northern spit did not form; hence, data are absent for this zone. Note that the definition of parameters is given in Figure 2.6

.

3.1 km. A short stretch of shoreline advancement of 4 m/y between 3.1 km to 3.2 km is observed near the location of the Sunrise Resort. The highest erosion is observed over 750 m of the spit with a rate of 31 m/y. The shoreline south of Cua Dai inlet indicates accretion. Within the first 850 m south of the inlet, the shoreline advanced an average of 5 m/y. Then the shoreline was stable with an average of accretion 0.1m/y over a 2300 m stretch of beach. Erosion and accretion are observed in the riverbank segment, i.e. a 1500 m region of retreat with a mean rate of 2.0 m/y and a 750 m region of accretion with average rate of 8.6 m/y.

The volume changes for this 5-year period are presented in Table 2.2. In general, the northern coast of Cua Dai inlet shows a negative volume change of approximately 247,000 m^3/y to 315,000 m^3/y for zones A and D. The southern portion is characterized by a positive volume change. The annual volume change in this segment is approximately 25,000 m^3 to 32,000 m^3. The shorelines at the riverbank are characterized by the alternation of erosion and accretion in shoreline change rate but in general the cumulative average volume change shows a positive value of approximately 19,000 m^3/y to 24,000 m^3/y. The whole system lost from 203,000 m^3/y to 259,000 m^3/y of which major losses have occurred at the northern coast and the spit. In general, the total loss in this period is similar in magnitude to the previous period of 2000 to 2010.

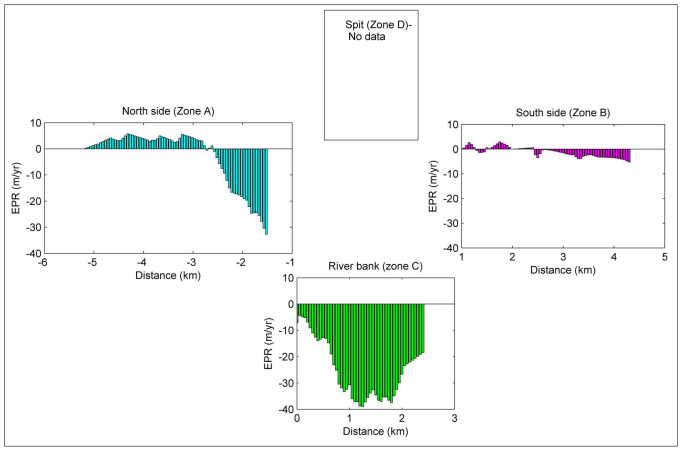

Figure 2.11: Shoreline change rates from 1995 to 2000

2.4.3 Derived longshore sediment transports

Evaluations of the seasonal and annual longshore transport quantities, S (m^3/y), are carried out based on the CERC formula. The total considered number of days per year is 365 days. The main offshore wave propagation directions and their associated occurring seasons along the year are NE in the winter; ENE in the winter and summer; and SE in the summer. The approximate total considered number of days for each season is summarized in Table 2.3. The LSTR (m^3/s) in Equation 2.4 was converted into m^3/y corresponding to the occurrence probability of each wave direction. In order to reduce the number of model runs, the average wave periods corresponding to each wave height class have been used to simulate each of the dominant wave directions. The cumulative LSTR corresponding to the summer, the winter and the annual average are estimated by summary of all LSTR from the waves occurring as in Table 2.3. In the following both the results of the wave nearshore transformation and LSTR are presented.

Figure 2.14 presents examples of the derived nearshore patterns of significant wave heights that are representative for the winter and the summer season. For the ENE direction of incident waves, the nearshore wave directions around Cua Dai inlet show significant influence of diffraction caused by Son Tra mountain and the Cham islands group. The significant wave heights behind Cham islands and in front of the inlet are significantly smaller than for the rest of Cua Dai beach. In general, the significant wave heights reduce gradually from a deep-water value of 2.3 m to around 0.8 m to 1.2 m in front of the inlet. For the SE direction of incident waves (Figure 2.14b), the wave direction of the whole southern coast area is almost SE, except the area behind the Cham islands and the northern coast of the inlet where the wave direction turns slightly to ESE. These areas are in the wave shadow region of Cham islands and of the shoal of Cua Dai inlet. The results of the nearshore wave transformation during the winter and summer season indicate that the northern and southern shoreline of Cua Dai inlet experience sheltering effects of the Cham islands in the case of ENE offshore waves. In contrast, only the northern

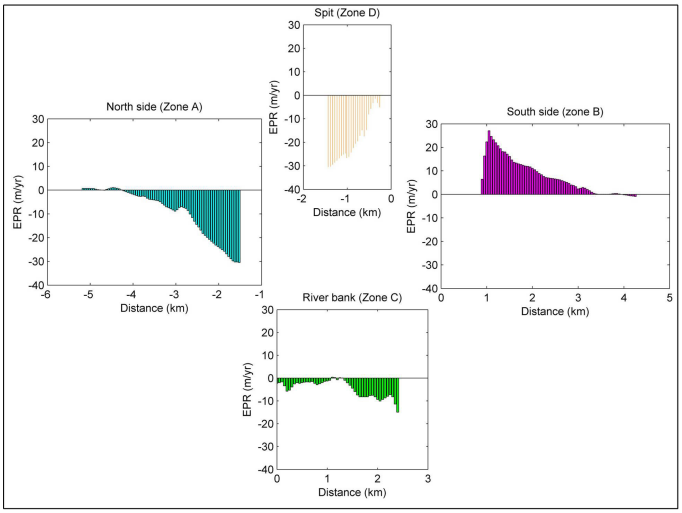

Figure 2.12: Shoreline change rates from 2000 to 2010

shoreline experiences the impact of the shadow zone caused by waves from the SE.
The LSTR estimated for each wave direction during the summer months and the winter months are indicated in Figure 2.15 and Figure 2.16. For the offshore waves from the SE, the LSTR is toward the North on both sides of the inlet (Figure 2.15c and 2.15d). At the northern coast, the LSTR slightly increases from the inlet to the north while at the southern coast the LSTR decreases significantly from the south in the direction of the inlet. The magnitude of LSTR at the southern adjacent coast is larger than at the northern adjacent coast, most likely because the northern adjacent coast is shielded from the SE wave direction by the ebb tidal delta, reducing the breaking wave height due to diffraction. For the offshore waves from the NE (45° to north), the LSTR is generally toward the southern direction. Whereas for the NE waves (60° to north), Figure 2.16b shows a reversal in the direction of LSTR. Near the inlet, the LSTR is directed to the south while, the LSTR is directed to the North further from the inlet. The LSTR caused by the ENE waves are typical for winter conditions and form the dominant component of the annual longshore transport.

The cumulative LSTR corresponding to the summer season, the winter season and the annual average are shown in Figure 2.17. During the summer months, despite the bidirectional occurrence of ENE and SE, the net LSTR is directed towards the North (Figure 2.17a). At the northern coast, the LSTR increases from the inlet to the north. At the southern coast, the LSTR decreases from the south in the direction of the inlet. The first 3 km from the inlet toward the North, the LSTR increases from 55,000 m^3/y to approximately 180,000 m^3/y. This positive gradient in LSTR induced by the SE wave would imply erosion of the spit. At the southern coast, the LSTR decreases in the direction of the alongshore transport near the inlet, over a distance ranging from 1.4 km to 4.6 km. This decreasing gradient in LSTR would imply accretion of the first 3 km from the inlet toward south. Based on these derived LSTR, the longshore sediment transport in the

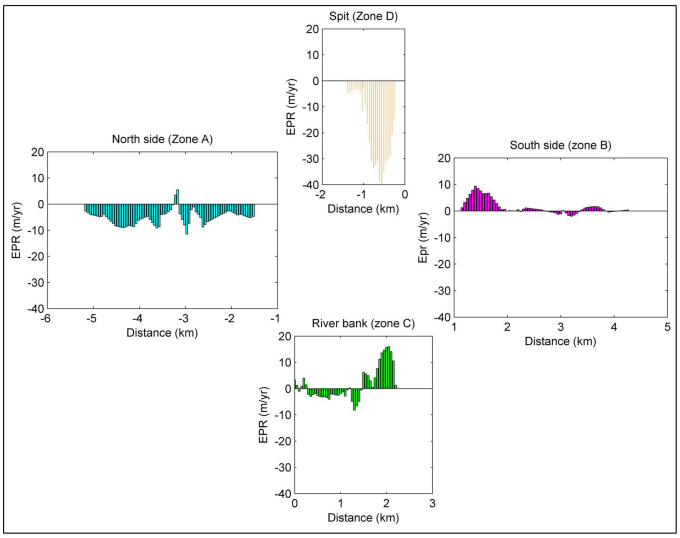

Figure 2.13: Shoreline change rates from 2010 to 2015

summer would create erosion at the first 3 km at the northern coast and accretion at the southern coast.

During the winter, when ENE events dominate, the LSTR close to the inlet is generally directed to the South. However, there is a transport divergence point at approximately 3 km to the north. A transport convergence point exists at approximately 4 km to the south where the direction of LSTR is toward the North. At the part of the northern shoreline between 3 km to approximately 8 km, the LSTR is toward the north with an average rate of 283.10^3 m^3/y, while near the inlet the LSTR is toward the South with an average rate of 87.10^3 m^3/y. There is a strong gradient from -275.10^3 m^3/y to 111.10^3 m^3/y of LSTR at approximately three kilometers from the Cua Dai inlet. This point is near the location of Golden Sand and Sunrise resorts where the shoreline changes orientation. The existence of the transport convergence and divergence locations suggests that local accretion is expected at the southern coast due to a decrease in LSTR while erosion is expected due to an increase in northward transport. Supporting evidence of this is presented in Figure 2.11 and Figure 2.12 because the results of volume change during period 1995 to 2000 and from 2000 to 2010 indicate very strong erosion at the northern and strong accretion at the southern shore. Near the inlet to the north, the longshore sediment transport potential shows a clear decrease, which would result in sand accumulation. However, the results of shoreline change rates and volume change show rapid erosion of the spit. This cannot be explained by the results of gradient in LSTR. This is most likely caused by the presence of resorts and coastal structures and the complex interaction between river regime and tidal regime, which are not taken into account for in LSTR estimation.

The net annual LSTR are shown in Figure 2.17c. Generally, the direction of net LSTR is similar to the direction of alongshore transport induced by the waves during the winter. Waves from the SE contribute to reducing the magnitude of LSTR to the South while en-

Table 2.2: Volume changes around Cua Dai inlet during period 1988 to 2015

Coastal zone	$A_D(m)$	1988-1995 (ΔV(x10^3; m^3/y)	1995-2000 (ΔV(x10^3; m^3/y)	2000-2010 (ΔV(x10^3; m^3/y)	2010-2015 (ΔV(x10^3; m^3/y)
Zone A	5.5	378	-60	-183	-103
	7	381	-77	-233	-131
Zone B	5.5	114	-22	139	25
	7	145	-29	177	32
Zone C	5.5	-10	-335	-59	19
	7	-13	-426	-76	24
Zone D	5.5			-140	-144
	7			-178	-184
Sum (A+D)	5.5			-323	-247
	7			-411	-315
Sum (B+C)	5.5	104	-357	80	44
	7	132	-455	101	56
Sum(A+B+C)	5.5	481	-418	-104	-59
	7	613	-531	-132	-75
Sum(A+B+C+D)	5.5			-243	-203
	7			-310	-259

Table 2.3: Wave direction schematizations for the seasonal wind directions used in the LSTR calculations.

Offshore wave propagation direction	Wave angle to North (°)	Summer season (d)	Winter season (d)
Coming from NE	45		17
Coming from ENE	60	38	139
	75	29	56
Coming from SE	135	44	
	150	42	
Total days		153	212

hancing the magnitude of LSTR to the North. At the northern coast the divergence point is still at the same location as present for ENE waves. Approximately 3 km to the north the net transport is oriented towards the north with an average rate of 466.10^3 m^3/y. From this point southwards, the alongshore transport is increasing with a steep gradient from 466.10^3 m^3/y to almost zero, this suggests intense erosion. Near to the inlet, the LSTR is more or less southward oriented with a relatively low LSTR magnitude. Because from this location the shoreline orientation is changing southward, the sediment transport is found to decrease near the inlet. Especially at the spit the ENE waves compensate the influence of the SE waves leading to lower magnitudes of the net sediment transport in this area. Close to the inlet at the Southside, the waves that come from the ENE are reoriented to the E direction (Figure 2.14a) due to the impact of shoals of the ebb tidal delta leading the net LSTR towards the inlet. From this sector the sediment transport is found to decrease toward to the convergence point of sediment movement with an average rate of 56.10^3 m^3/y. From the south segment to the convergence point, the net LSTR is oriented towards the north with an average rate of 526.10^3 m^3/y. The pattern of net LSTR explains the accretion of the southern coast and erosion of the northern coast.

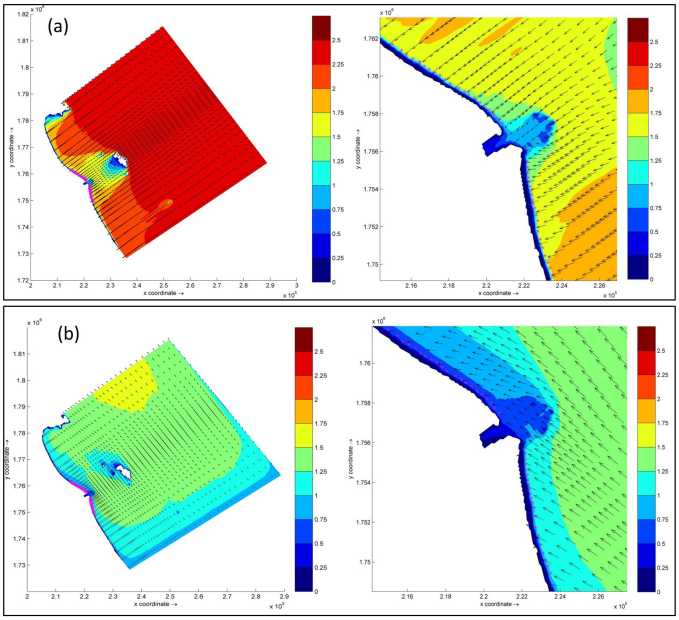

Figure 2.14: Derived wave fields (winter and summer). (a) winter season: direction ENE (60°), Hs =2.25m, Tp = 7.64s; (b) summer season: direction SE (135°), Hs =0.75m, Tp = 6.4s. The black arrows show the mean wave direction and the colored contour patches indicate the significant wave height. X and Y coordinates indicate the longitude and latitude that convert into the UTM zone 48N coordination. The pink points indicate the location to extract breaking wave heights.

2.5 Discussion

CUA Dai Inlet and its adjacent coasts form a complex system comprising interactions between the ebb-tidal delta, the rivers, their estuaries, and tidal and wave-driven sediment transports. In this section the main mechanisms regarding the extreme erosion problem in this system will be discussed on the basic of the results of observed and calculated shoreline change rate, volume changes and associated events and human interventions. Even though the erosion problem at Cua Dai receives much attention since 2000, the erosion has been present since 1995 already (Vnexpress, 2014, 2015,).
The erosive mode since 1995 was triggered by a long-term geomorphological development of this inlet reflecting a nonperiodic cyclic process that takes place over several decades (Figure 2.18). It appears that channel shifting from north to south, triggered by Typhoon Cecil in 1987, caused significant geomorphological changes from 1988 to 2015 to the northern adjacent coast (Cua Dai beach) of Cua Dai inlet. During the first 7-year period, 1988-1995, the beach accreted significantly because of the welding of a sub-areal beach barrier being part of the ebb-tidal delta of Cua Dai inlet (Figure 2.9). In general, during this time the system did not experience any impact of human activities but only experienced natural processes. It is our hypothesis that the river system provided a large amount of sediment to the inlet gorge or to the ebb-tidal delta, depending on the dry or wet season respectively. Hence, the wave-driven alongshore sediment transport on the

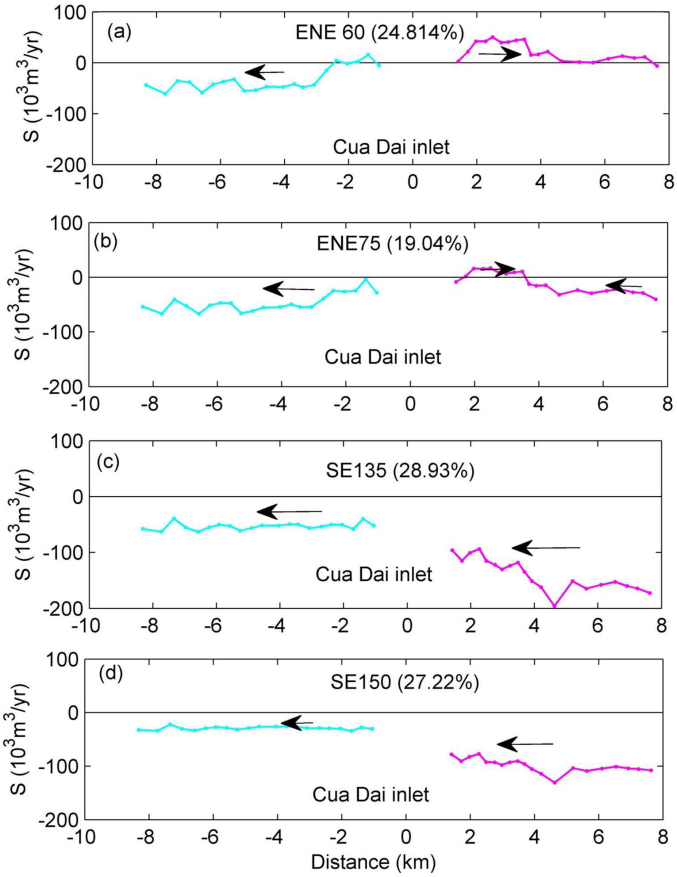

Figure 2.15: Longshore sediment transport quantities for ENE and SE propagation during the summer. The blue lines indicate LSTR at the northern adjacent coast while the pink lines indicate LSTR at the southern adjacent coast. (Negative indicates northward transport; Positive indicates southward transport). The arrow indicates the direction of LSTR.

northern beaches caused by the ENE waves was available to not only build a shoal such as present in 1988, preventing erosion of the Cua Dai near inlet shore, but also to feed the more northern shore, annihilating the effect of divergence in transport. Since 1995, after the welding of the ebb-tidal beach barrier, Cua Dai Beach has retreated. The most severe period of erosion is from 2000 to 2010. The average shoreline change rate at the spit was 19 m/y and a mean rate of 12 m/y at Cua Dai beach. The increasing and northward-shifting erosion rates during that period might be attributed to human causes. At least five resorts and six hydropower dams (Figure 2.4) were constructed and started to operate and three reclamations were carried out during this period. We hypothesize that the dams and the reclamations have decreased the feeding of the ebb-tidal delta with sediments from the river and its estuary. The impact of the presence of the resorts might be reflected in the results of shoreline change during the next period, 2010-2015 (Fig-

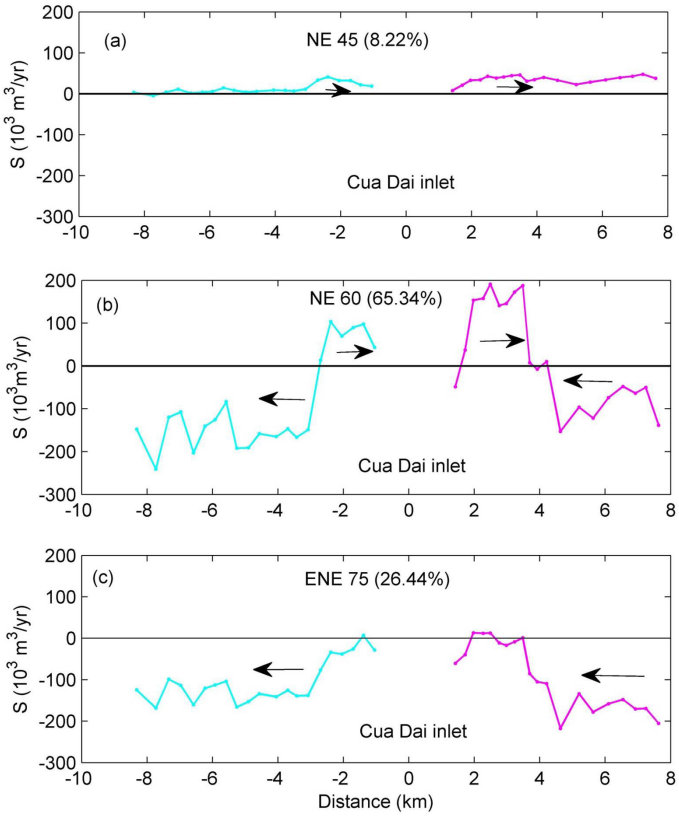

Figure 2.16: Longshore sediment transport quantities for NE and ENE propagation during the winter. The arrow indicates the direction of LSTR.

ure 2.13). Normally, the LSTR induced by the ENE waves creates a divergence point in the LSRT as indicated in Figure 2.17b. It means that the sediment source must originate from this coast and the presence of erosion and accretion at the northern coast is expected to be due to the gradients in longshore sediment transport. In the period 2010 to 2015, however, the erosion has been extended further to the north side of this coast. This is most likely due to the resorts and coastal structures interrupting the wave-driven transport to the north.

The erosion of Cua Dai Beach close to the inlet where the resorts are located is likely also influenced by what is known in literature as coastal squeeze (Doody, 2004; Gilman et al., 2007; Torio and Chmura, 2013) i.e. occupying the natural dune area preventing the natural restoration of a beach and dune area after a storm promoting erosion. Because the beaches and dunes where originally pristine (no permanent structures) the beach and dune habitats could maintain their integrity by managed retreat (e.g. using tree planting), but with the presence of the resorts and other coastal defense structures this is seriously disturbed. These resorts have caused coastal squeeze in addition to sediment transport blockage toward the up drift side of Cua Dai Beach.

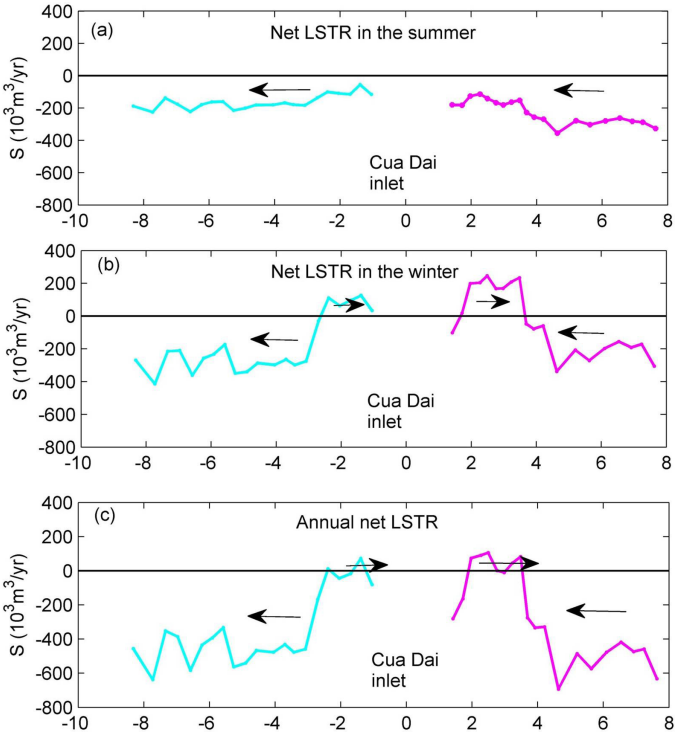

Figure 2.17: Net longshore sediment transport during the summer (a), the winter (b) and the whole year (c). The arrows indicate the direction of LSTR.

The southern adjacent coast shows signs of a typical downdrift coast that has historically benefited from the bypassing of sediment because of tidal and wave action. During the first period, 1988 to 1995, Zone B gained from 114,000 m^3/y to 145,000 m^3/y. From 1995 to 2000 virtually no sediment was gained, whereas it increased again to reach 139,000 m^3/y to 177,000 m^3/y during the next period from 2000 to 2010. It is hypothesized that the sediment input from zone A and C during the flood period (1995-2000) was deposited in the ebb-tidal delta to feed the later accretion of the southern adjacent coast. The amount of sediment receiving at the southern coast has been reduced to 25,000 m^3/y to 32,000 m^3/y during the period 2010 to 2015.

The sediment budgets constructed in accordance with volume changes of the four zones (Table 4.2) show clear variations. In general, zone A has experienced erosion since 1995 with a total loss of 60,000 m^3/y to 183,000 m^3/y in the period 1995 to 2010 corresponding to 5.5 m of closure depth. The period from 1988 to 1995 is an exception. Because of the occurrence of a welding ebb-tidal bar, zone A accreted with a high amount of 378,000 m^3/y. Since 2000 the northern shoreline has significantly retreated near the inlet (zone D), with a total loss of 140,000 m^3/y to 178,000 m^3/y corresponding to a closure depth of 5.5 and 7 m, respectively. The adjacent coast to the south of the inlet (zone B) shows historical accretion over the whole 27-year period. Normally sediment gain from bypassing

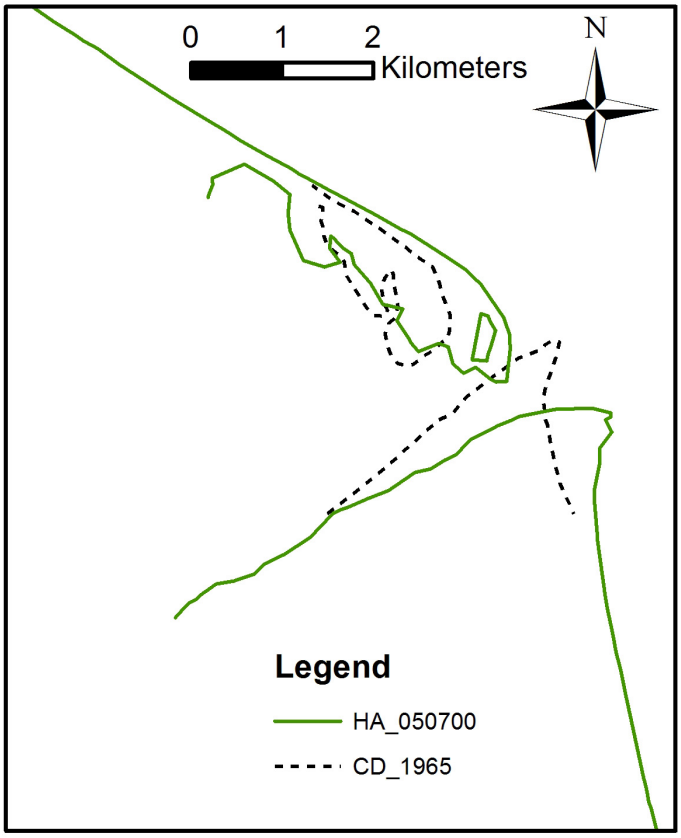

Figure 2.18: Observed inlet and channel shifting to the south triggered by typhoon Cecil in 1989. Shoreline in 1965 was taken from Mau, 2006.

at the southern adjacent coast is approximately from 114,000 m^3/y to 145,000 m^3/y as in the period 1988-1995. However, in recent years this amount has been decreased because of reduced sediment availability. In total the system indicates a loss of sediment since 2000 with exception of the first period 1988-1995; the system misses some 203,000 m^3/y to 310,000 m^3/y since 2000. The construction of dams in the river system and sediment mining in the estuaries has likely decreased the sediment supply. It is hypothesized that the decrease of the river and estuarine sediment source has triggered erosion along Cua Dai Beach to feed the ebb-tidal delta and the estuarine gorge by wave-driven transport. Instead of being a historical sediment source the gorge and the ebb-tidal delta developed into an important sediment sink that triggered the Cua Dai erosion.
The remaining existence of a bypassing transport system is significantly affected by the seasonal climate, including seasonal waves and seasonal river discharges. A long dry season combines a lower wave energy condition with a lower river discharge whereas higher wave energy is associated with a higher flood discharge during the winter season. In the winter/ dry season with waves coming from ENE the inlet shoals because of wave-

driven sediment transport (Figure 2.16b) and the lack of significant freshwater discharge to maintain the larger cross-section that was created in the flood season. In the beginning of the rainy typhoon season, flash floods flush out the relatively shallow inlet and the sediment that was deposited in the inlet mouth during the dry period. The flushed sediment is deposited in the ebb-tidal delta. During the winter, waves also induce the alongshore transport and bypass sand to the southern shores. Therefore the amount of sediment bypassing to the south mostly depends on the volume of ebb-tidal delta. The disappearance of the ebb-tidal bar present in 1988 and the huge sediment loss during period 2000 to 2010 indicate that the system lacks sediment at present.
Compared with the observed shoreline change rate, the trends of the alongshore sediment transport show a similar qualitative pattern. Quantitatively, the calculated LSTRs are approximately two times the observed LSTRs, which is quite common in LSTR studies (Bosboom and Stive, 2012). Along approximately 3 km of the northern coast (including zone C and apart from zone A), the net LSTR is increasing with a steep alongshore gradient of 466,000 m3/y corresponding to a rate of shoreline change from 24 m/y to 28 m/y with 5.5 m and 7 m of closure depth respectively. At the same time the observed shoreline change rate at Zone A and Zone D indicates a rate of 12 m/y and 19 m/y (period 2000 to 2010). Along approximately 4 km of the southern coast, the net LSTR shows a strong decrease from 526,000 m^3/y to almost 56,000 m^3/y. This negative gradient corresponds to approximately 20 m/y to 26 m/y of shoreline change rate with 5.5 m and 7 m of closure depth respectively. At the same time, the observed shoreline change rate was 11 m/y during the period 2000 to 2010. The probable explanation for these differences lies in the limitations of the CERC formula, both regarding the longshore transport estimation and the neglect of other effects than wave heights and directions alone and of the assumed closure depth.

2.6 Conclusions

SEASONAL variations in river discharge and wave climate, human interventions, and the presence of Cham Islands make Cua Dai Inlet a very complex and unique seasonal varying tidal inlet. This study focused on trying to understand the dynamics and evolution of the adjacent coasts of the inlet by a comprehensive investigation of historical shoreline change rates and prevailing wave-driven LSTRs. To investigate the reasons that caused extreme erosion at Cua Dai Beach, this study used remote sensing and GIS techniques to evaluate the shoreline evolution during the period from 1988 to 2015. An empirical approach was applied to estimate the volume changes over four main zones, Cua Dai northern beach (Zone A), southern beach (Zone B), riverbank (zone C), and spit (Zone D, an extended part of Cua Dai Beach). Additionally, the nearshore wave transformation model SWAN was combined with an empirical equation CERC Engineers (1984)) to estimate the LSTR from the dominant offshore wave directions occurring during the summer and the winter season and over 1 year.
Our analysis indicates that Cua Dai Beach has been eroding since 1995. During the period 1988 to 1995 Cua Dai Inlet was a rich sediment system with a subareal beach barrier being part of the ebb-tidal delta in 1988. During this period, large accretion occurred be-

cause of the process of the welding of this barrier to Cua Dai Beach. From 1995 to 2000, Cua Dai Beach eroded at both adjacent coasts of the inlet. Significant erosion occurred during the period from 2000 to 2010 with an average rate of erosion of 12 m/y at Cua Dai beach and 19 m/y at its southern spit. The southern coast of the inlet experienced strong accretion with a mean rate of 11 m/y. If we would assume that no sediment is stored in the estuary or ebb-tidal delta, our sediment balance between the northern side, southern side and river bank indicates that the system has lost a considerable sediment volume. This loss is approximately 243,000 m^3/y to 310,000 m^3/y during the period from 2000 to 2010. At the same time, there are at least seven resorts built close to or even on Cua Dai Beach and seven hydropower plants were constructed upstream of the Vu Gia-Thu Bon River. Besides these activities, illegal sand mining and land reclamation could have contributed to reducing the sediment supply from the river into the CuaDai Inlet system. These human activities might have created a negative impact on the system in terms of reducing sediment availability contributing to the erosion during this period.

The results from the nearshore wave field modelling indicate that the Cham Islands have an important impact on the offshore wave propagation to the nearshore, increasing the complexity of the seasonal wave climate of Cua Dai Beach. Especially the area around Cua Dai Inlet, waves from the SE direction induces alongshore sediment transport to the north, whereas the waves from ENE create LSTR to the south. At Cua Dai Beach, the direction of LSTR shows strong alongshore gradients. At the northern part, predicted transports are directed northwards. At the area near the inlet, predicted transport is to the south. There is a large variation in alongshore gradients in LSTR at the northern coast and southern coast, with dominant offshore waves during the winter and the summer seasons. These results contribute to explaining the erosion that occurs at the northern side and the accretion that occurs at the southern coast adjacent to Cua Dai Inlet. The southern coast shows behavior of a typical downdrift-to-an-inlet coast, which has benefited from the bypassing of sediment after the channel switch to the south.

The erosive mode of Cua Dai Beach since 1995 was the result of a long-term geomorphological inlet development reflecting a nonperiodic cyclic process that takes place over several decades. It appears that channel shifting from north to south, triggered by Typhoon Cecil in 1987, dictated the geomorphological development of Cua Dai Beach. The decrease of sediment supply from the river, estuary and squeeze by coastal developments may have contributed to the erosion. Understanding the role of the ebb-tidal delta as a consequence of channel shifting and its seasonality due to river discharge and wave climate is a remaining challenge.

References

Avinash, K., Deepika, B., and Jayappa, K. (2013). Evolution of spit morphology: a case study using a remote sensing and statistical based approach. *Journal of coastal conservation*, 17(3):327–337.

Avinash, K., Jayappa, K., and Vethamony, P. (2012). Evolution of swarna estuary and its impact on braided islands and estuarine banks, southwest coast of india. *Environmental Earth Sciences*, 65(3):835–848.

Bank, A. D. (2014). Vie: Urban environment and climate change adaption project. Technical report, Manila, Phillipines:Asian Development Bank, Document No.IE 131001410-06- RP- 103, 134p.

Bayram, A., Larson, M., and Hanson, H. (2007). A new formula for the total longshore sediment transport rate. *Coastal Engineering*, 54(9):700–710.

Bosboom, J. and Stive, M. J. (2012). *Coastal Dynamics I: Lectures Notes CIE4305*. VSSD.

Chander, G., Markham, B. L., and Helder, D. L. (2009). Summary of current radiometric calibration coefficients for landsat mss, tm, etm+, and eo-1 ali sensors. *Remote sensing of environment*, 113(5):893–903.

Chen, W.-W. and Chang, H.-K. (2009). Estimation of shoreline position and change from satellite images considering tidal variation. *Estuarine, Coastal and Shelf Science*, 84(1):54–60.

de Alegria-Arzaburu, A. R. and Masselink, G. (2010). Storm response and beach rotation on a gravel beach, slapton sands, uk. *Marine Geology*, 278(1-4):77–99.

Dissanayake, D., Ranasinghe, R., and Roelvink, J. (2012). The morphological response of large tidal inlet/basin systems to relative sea level rise. *Climatic change*, 113(2):253–276.

Do, A. T., de Vries, S., and Stive, M. J. (2017). Beach evolution adjacent to a seasonally varying tidal inlet in central vietnam. *Journal of Coastal Research*, 34(1):6–25.

Doody, J. P. (2004). 'coastal squeeze'–an historical perspective. *Journal of Coastal Conservation*, 10(1):129–138.

Duong, T. M., Ranasinghe, R., Walstra, D., and Roelvink, D. (2016). Assessing climate change impacts on the stability of small tidal inlet systems: Why and how? *Earth-science reviews*, 154:369–380.

Elias, E. P. and van der Spek, A. J. (2006). Long-term morphodynamic evolution of texel inlet and its ebb-tidal delta (the netherlands). *Marine Geology*, 225(1-4):5–21.

Engineers, U. A. C. O. (1984). Shore protection manual. *Army Engineer Waterways Experiment Station, Vicksburg, MS. 2v*, pages 37–53.

Gilman, E., Ellison, J., and Coleman, R. (2007). Assessment of mangrove response to projected relative sea-level rise and recent historical reconstruction of shoreline position. *Environmental monitoring and assessment*, 124(1-3):105–130.

Gilvear, D., Tyler, A., and Davids, C. (2004). Detection of estuarine and tidal river hydromorphology using hyper-spectral and lidar data: Forth estuary, scotland. *Estuarine, Coastal and Shelf Science*, 61(3):379–392.

Hallermeier, R. J. (1978). Uses for a calculated limit depth to beach erosion. In *Coastal Engineering 1978*, pages 1493–1512.

Hallermeier, R. J. (1980). A profile zonation for seasonal sand beaches from wave climate. *Coastal engineering*, 4:253–277.

Hapke, C. J., Lentz, E. E., Gayes, P. T., McCoy, C. A., Hehre, R., Schwab, W. C., and Williams, S. J. (2010). A review of sediment budget imbalances along fire island, new york: can nearshore geologic framework and patterns of shoreline change explain the deficit? *Journal of Coastal Research*, pages 510–522.

Hayes, M. (1979). Barrier island morphology as a function of tidal and wave regime, in, leatherman, sp (ed.), barrier islands from the gulf of st. *Lawrence to the Gulf of Mexico: Academic Press, New York, New York*, page 28.

Ho, L., Umitsu, M., and Yamaguchi, Y. (2010). Flood hazard mapping by satellite images and srtm dem in the vu gia–thu bon alluvial plain, central vietnam. *International archives of the photogrammetry, remote sensing and spatial information science*, 38(Part 8):275–280.

Kragtwijk, N., Zitman, T., Stive, M., and Wang, Z. (2004). Morphological response of tidal basins to human interventions. *Coastal engineering*, 51(3):207–221.

Lam, N. (2009). *Hydrodynamics and Morphodynamics of a Seasonally Forced Tidal Inlet System*. PhD thesis, Delft University of Technology.

Maiti, S. and Bhattacharya, A. K. (2009). Shoreline change analysis and its application to prediction: a remote sensing and statistics based approach. *Marine Geology*, 257(1-4):11–23.

McFeeters, S. K. (1996). The use of the normalized difference water index (ndwi) in the delineation of open water features. *International journal of remote sensing*, 17(7):1425–1432.

Nicholls, R. J., Birkemeier, W. A., and Hallermeier, R. J. (1997). Application of the depth of closure concept. In *Coastal Engineering 1996*, pages 3874–3887.

Oertel, G. (1988). Processes of sediment exchange between tidal inlets, ebb deltas and barrier islands. In *Hydrodynamics and sediment dynamics of tidal inlets*, pages 297–318. Springer.

Panda, U., Mohanty, P., and Samal, R. (2013). Impact of tidal inlet and its geomorphological changes on lagoon environment: A numerical model study. *Estuarine, Coastal and Shelf Science*, 116:29–40.

Pari, Y., Murthy, M. R., Subramanian, B., Ramachandran, S., et al. (2008). Morphological changes at vellar estuary, india—impact of the december 2004 tsunami. *Journal of Environmental Management*, 89(1):45–57.

Rajawat, A., Gupta, M., Acharya, B., and Nayak, S. (2007). Impact of new mouth opening on morphology and water quality of the chilika lagoon–a study based on resourcesat-1 liss-iii and awifs and irs-1d liss-iii data. *International Journal of Remote Sensing*, 28(5):905–923.

Ranasinghe, R., Duong, T. M., Uhlenbrook, S., Roelvink, D., and Stive, M. (2013). Climate-change impact assessment for inlet-interrupted coastlines. *Nature Climate Change*, 3(1):83.

Ranasinghe, R. and Pattiaratchi, C. (1999). The seasonal closure of tidal inlets: Wilson inlet—a case study. *Coastal Engineering*, 37(1):37–56.

Ranasinghe, R., Pattiaratchi, C., and Masselink, G. (1999). A morphodynamic model to simulate the seasonal closure of tidal inlets. *Coastal Engineering*, 37(1):1–36.

Rodriguez, E. and Dean, R. G. (2005). *Sediment Budget Analysis and Management Strategy for Fort Pierce Inlet, Florida*. Coastal and Oceanographic Engineering Program, Department of Civil and Coastal Engineering, University of Florida.

Rosati, J. D. (2005). Concepts in sediment budgets. *Journal of Coastal Research*, pages 307–322.

Rosati, J. D. and Kraus, N. C. (1999). Formulation of sediment budgets at inlets. Technical report, ENGINEER RESEARCH AND DEVELOPMENT CENTER VICKSBURG MS COASTAL AND HYDRAULICS LAB.

Ryu, J.-H., Kim, C.-H., Lee, Y.-K., Won, J.-S., Chun, S.-S., and Lee, S. (2008). Detecting the intertidal morphologic change using satellite data. *Estuarine, Coastal and Shelf Science*, 78(4):623–632.

Schoonees, J. and Theron, A. (1997). Improvement of the most accurate longshore transport formula. In *Coastal Engineering 1996*, pages 3652–3665.

Stive, M., Tran, T., and Nghiem, T. (2012). Stable and unstable coastal inlet cross-sectional behaviour. In *International Conference on Estuaries and Coasts, Water Resources University, Vietnam*.

Stive, M. J., Van de Kreeke, J., Lam, N. T., Tung, T. T., and Ranasinghe, R. (2009). Empirical relationships between inlet cross-section and tidal prism: A review. In *Proceedings Of Coastal Dynamics 2009: Impacts of Human Activities on Dynamic Coastal Processes (With CD-ROM)*, pages 1–10. World Scientific.

Stive, M. J. and Wang, Z. (2003). Morphodynamic modeling of tidal basins and coastal inlets. In *Elsevier oceanography series*, volume 67, pages 367–392. Elsevier.

Thieler, E. R., Himmelstoss, E. A., Zichichi, J. L., and Ergul, A. (2009). The digital shoreline analysis system (dsas) version 4.0-an arcgis extension for calculating shoreline change. Technical report, US Geological Survey.

Torio, D. D. and Chmura, G. L. (2013). Assessing coastal squeeze of tidal wetlands. *Journal of Coastal Research*, 29(5):1049–1061.

Tung, T. T. (2011). *Morphodynamics of seasonally Closed Coastal IInlet at the Central coast of Vietnam*. PhD thesis, Delft University of Technology.

Chapter 3

Detailed Hydrodynamics and Sediment Transport at a Seasonal Inlet and its Adjacent Beach

Experience does for the soul
what education does for the mind

Casey Neistat

Cua Dai inlet is a typical microtidal, mixed energy-wave dominated inlet in a tropical monsoon regime in central Vietnam. Both the river flow regime and coastal processes such as induced by waves and tides influence Cua Dai Inlet and its adjacent coasts. Cua Dai Beach, the northern adjacent coast of Cua Dai inlet, has experienced severe erosion since 1995 due to an apparent non-periodic cyclic process, a decrease of sediment supply from the river, estuary and squeeze by coastal developments (previous chapter 2). The inlet channel has shifted from North to South which served as an important controlling mechanism for the creation of a new ebb shoal. However, the role of the ebb-tidal delta in relation to the channel shifting and seasonal varying hydrodynamic conditions (river discharge and wave climate) remains poorly understood. Most studies have only considered the impact of waves and tides on the development of the ebb tidal delta. No study has included the impact of a varying river discharge on ebb shoal development and inlet migration. This paper investigates the seasonal varying hydrodynamics and sediment transport of the inlet and adjacent coasts due to the seasonal varying river discharge and wave climate. There exists an East North East monsoon with a flood season from September to December, an East North East monsoon with a wet season from January to March, and a dry bidirectional South East/East North East monsoon from April to August. We investigate the effect of the seasonal wave climate and seasonal river discharges at Cua Dai inlet by exploring the effects on the resulting hydrodynamics, sediment transports

This chapter has been published in in 6th ICEC 2018 Do et al. (2018).

and potential morphological changes through the inlet and at the adjacent coasts. The 2DH process-based morphodynamic numerical model (Delft3D) is applied using schematized wave conditions and river discharge. Six simulations with varying dominant wave conditions for the winter and for the summer are executed in combination with varying river discharge classes that corresponding to the dry, wet and flood seasons. Primary results indicate that the seasonal variation in the wave climate has a strong influence on the sediment transport patterns in the adjacent coasts. The variation in the river flow has significantly influenced the magnitude of sediment transport through the inlet. The results of the simulations reveal that the inlet generally imports sediment into the estuary except in the case of the flood event. Interestingly, the wave direction that varies during summer also influences the magnitude of sediment import into the estuary. Waves coming from the ENE contributes to larger sediment import than waves coming from the SE.

3.1 Introduction

Cua Dai inlet is a typical microtidal, mixed energy- wave dominated inlet in a tropical monsoon regime and is strongly influenced by both river discharge and waves. Cua Dai Beach, the adjacent coast of Cua Dai inlet, located on the north side of Cua Dai Inlet, is experiencing severe erosion since 1995. To aid future management of this system, it is necessary to understand the factors that influence the existing morphology and that cause coastal retreat of the system. Chapter 2 reconstructed historical shoreline positions in combination with crude assumptions with respect to longshore sediment transport patterns and associated changes in sediment budgets over recent decades. In the study of chapter 2, it is found that the long-term geomorphological development and the decrease in sediment supply from the river and the estuary have put Cua Dai Beach under stress by causing the shoreline to erode.

The long-term geomorphological development of Cua Dai inlet appears to reflect a non-periodic cyclic process that takes place over several decades. It appears that the inlet channel shifted from North to South. Welding of the initial ebb shoal to the abandoned ebb-tidal delta and the development of a new ebb shoal were important primary controlling mechanisms. We propose two conceptual theories that represent the geomorphological development of the Cua Dai inlet. The first theory (A; Figure 3.1a) is derived based on Landsat images in 1988 that depict the system in the past. The existing ebb shoal such as present in 1988 suggests that the system was rich in sediment. It is my hypothesis that the river flow was normally directed to the North and provided a large amount of sediment to the inlet gorge and to the ebb tidal delta, depending on the dry or wet season respectively. Hence, the wave driven alongshore sediment transport on the northern beaches caused by the waves from ENE direction caused two important mechanisms. It builds a shoal such as present in 1988, preventing erosion of the Cua Dai near inlet shore and it also feds the more northern shore, annihilating the effect of divergence in transport. The second theory (B; Figure 3.1b) derived based on Landsat images in 2015 depicts a more recent image. Due to storm Cecil (1989), the existing ebb shoal in 1988 was abandoned and it migrated landward until it attached to the beach due to bar welding process resulting in accretion at both adjacent coasts during the period 1988-1995 (chapter 2). After the bar welding, a new ebb shoal started to develop further to the south than the previous ebb shoal. This process created a major sediment sink since formation of the new ebb shoal requires sediment to reach equilibrium. The new ebb shoal is also orientated more to the South. The northern beach is now not protected by the shoal and erosion continues due to the local divergence in longshore sediment transport, whereas the southern coast starts to accrete due to sand supply from bypassing.

Understanding the role of the ebb-tidal delta that interacts with the shifting channel and its associated seasonal behavior due to river discharge and wave climate is a remaining challenge. Inlets probably represent the most extreme level of difficulty in evaluating quantities of sediment transport related to the variety of acting physical forces (Komar, 1996). The complexity of the interaction of tides, waves, and freshwater discharge, lead to very complex morphodynamic behavior observed in many inlets (Oertel, 1988, 1972; Robinson, 1975; Hubbard et al., 1979;Ping, 1989; Komar, 1996; Fitzgerald, 1984;

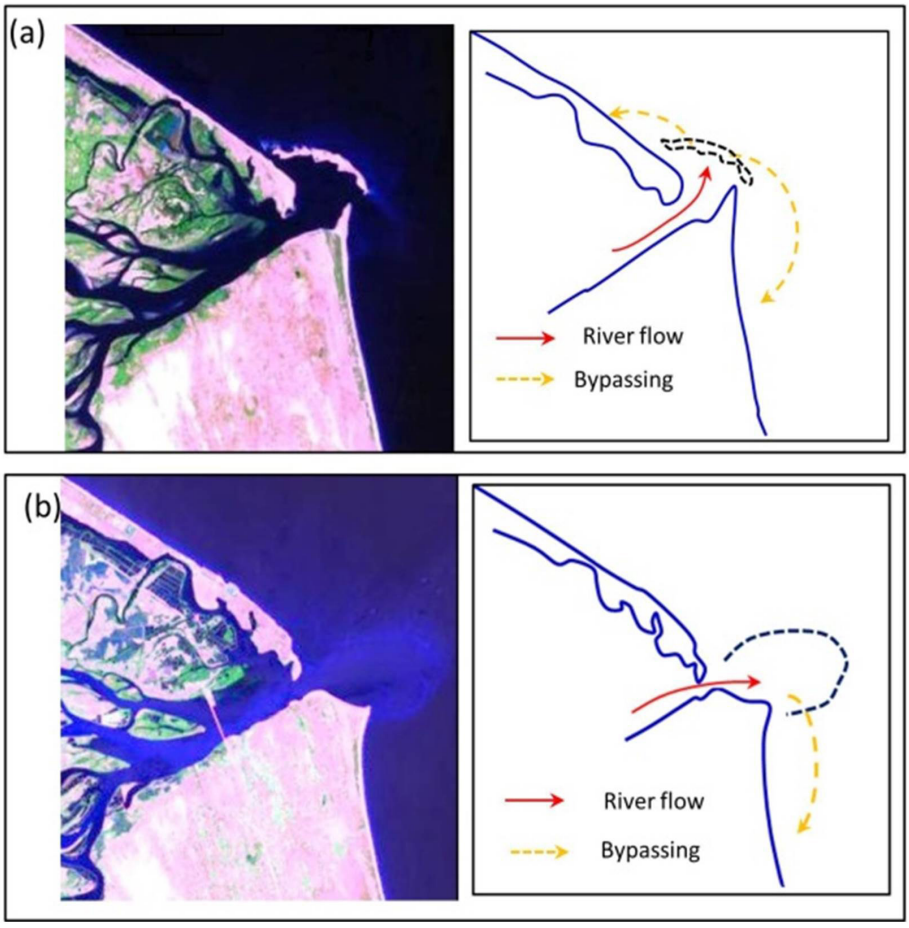

Figure 3.1: Conceptual model description for the non-periodic cyclic process of Cua Dai inlet. (a) Scenario in the past, 1989 and (b) Scenario at present, 2015.

and FitzGerald et al., 2000).

Recently, numerical modeling has been widely used and has been proved to be useful to study morphological behavior of complex coastal environments, including tidal inlets (e.g. Bertin et al., 2009; Cayocca, 2001; Chen et al., 2015; Dissanayake et al., 2009; de Vriendº et al., 1993; Herrling and Winter, 2014; Nahon et al., 2012; Ridderinkhof et al., 2016; Van Leeuwen et al., 2003). Today, medium to long-term coastal behavior can be investigated using process-based morphodynamic models (de Vriendº et al., 1993; Roelvink, 2011; Van der Wegen et al., 2010; Winter, 2006). Such model simulates the non-linear interaction between currents; sediment transport and bed level changes at real world scales and may therefore overcome limitations of coastline models and flume experiments. Recent advances in numerical morphodynamics models allow simulations over very large spatial and temporal scales (Roelvink, 2006; Dissanayake et al., 2009;

Van der Wegen et al., 2010). In the absence of sufficient observational data, systematic and schematic numerical simulations are assumed to be able to provide insight into medium to long-term coastal evolution (Daly et al., 2011).
Most studies have considered the impact of waves and tides to the development of ebb tidal deltas. Fewer studies have considered the impact of river discharge on the development of ebb shoals and inlet migration. This paper investigates the seasonal varying hydrodynamics and sediment transport of the inlet and adjacent coasts due to a seasonal varying river discharge and wave climate. This study uses a 2DH process-based morphodynamic numerical model (Delft3D) and schematized wave conditions and river discharge.

3.2 Methodology

THE investigation of the seasonal varying hydrodynamics and sediment transport of the inlet and adjacent coasts due to a seasonal varying river discharge and wave climate requires a comprehensive model. A 2DH process-based numerical morphodynamic model (Delft3D), which consists of Delft3D-WAVE and Delft3D-FLOW, is used to simulate hydrodynamics of river flows, tides, sediment transport at the inlet and its adjacent coasts simultaneously. In this section, the numerical model will first be introduced and then the details of the model setup and hydrodynamic settings will be discussed. An overview of the simulations is finally provided.

3.2.1 The numerical model

The modeling system Delft3D (Hydraulics (2014)) solves the shallow water equations. The systems of equations consist of the equations of horizontal motion, with turbulence models to close the system of mean flow, the continuity equation, and the sediment transport equations. The details of the model have been described in e.g., Lesser et al. (2004) and Van der Wegen and Roelvink (2008). The spectral wave model SWAN in Delft3D-WAVE (Booij et al., 1999, and Ris et al., 1999) may run in stationary mode to simulate the wave propagation and deformation from offshore to nearshore. The hydrodynamics module (Delft3D-FLOW) is coupled to Delft3d-WAVE through the exchange of relevant parameters. The wave parameters and the forcing terms associated with the wave radiation stresses computed by Delft3D-WAVE module are used as input for the Delft3D-FLOW module to compute wave-driven currents, enhanced turbulence, bed-shear stress and sediment stirring by wave breaking. Then at each interval of one hour has been reached by FLOW, the water level, current velocities and bottom elevation from the Delft3D-FLOW are used as input to computation in Delft3D-WAVE.
The sediment transport formulation of van Van Rijn et al. (1993) is used. The total sediment transport is calculated as the sum of both bed load and suspended load transport. Suspended sediment transport is treated above a reference height and calculated by a depth-average advection-diffusion equation, whereas the bed load is treated below that

reference height.

3.2.2 Model Setup of Cua Dai inlet

The computational domain of the model has been developed to represent the Cua Dai inlet which includes the open sea, the inlet and part of the river (Figure 3.2). Three nested grids are used that range from a large regional model to Cua Dai inlet with decreasing spatial dimensions and increasing grid resolutions. The largest model with grid cell resolutions of 1500m covers almost the entire central coast of Vietnam with 125km in width and 190km in length. This model was used to generate water level time series at the boundaries of the flow model. The wave model grid extends about 30km in both northward (up to Son Tra mountain) and southward direction from the Cua Dai inlet to allow the proper development of waves in the domain of interest. The finest flow model extends to Nong Son hydrology station where the observed river discharge is available. Detailed bathymetry at the river area is derived from Vo (2015). Bathymetric data near the coast and inlet areas are collected in 2014 from measurement. The extended bathymetry at the open sea is derived from GEBCO.

The boundary conditions of the regional model are extracted from the global ocean tide

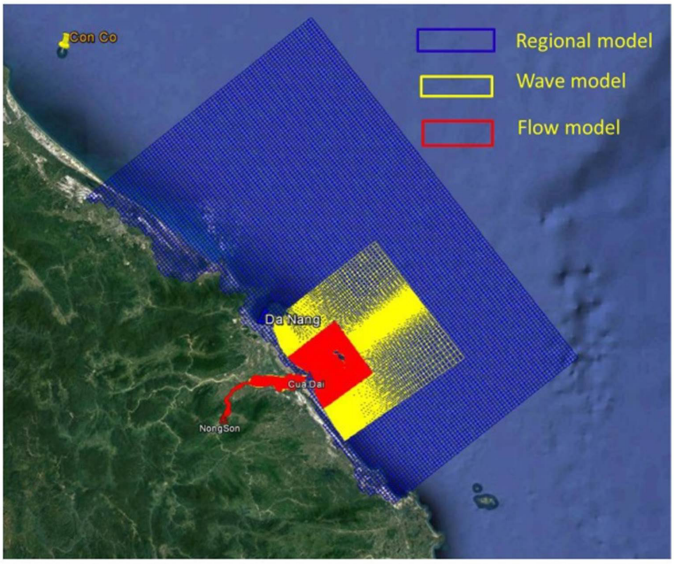

Figure 3.2: Model domain including wave model domain and flow model domain

model TPXO8.0. Thirteen tidal constituents (M2, S2, N2, K2, K1, O1, P1, Q1, MF, MN, M4, MS4 and MN4) are applied to generate tidal conditions at the boundaries of the regional model. This model is calibrated using the measured tide time series measured from the station at Da Nang near to Son Tra mountain. Then the regional model is nested to generate the boundary conditions for the flow model. The results of the flow model are

validated with water level and velocity measured at Cua Dai inlet.
Wave forcing at the sea boundary in the wave model was extracted from the National Oceanic and Atmospheric Administration (NOAA) Wave Watch III archives at grid point (16.0°N, 109.0°E) in the period 2005-2013. Fresh water from Thu Bon River that flows into Cua Dai inlet was implemented at the river upstream boundary using the monthly average discharge during the period from 1977 to 2008. Measured discharge time series were obtained at the Nong Son station.
The sediment transport formulation of van Van Rijn et al. (1993)) is used for computing sediment transport by waves and currents. The simulations were performed with a median sediment diameter (D50) of 0.2 mm, a sediment density of non-cohesive sand of 2650 kg/m^3. A uniform value of 5m of initial sediment layer thickness at the bed is used as default in Delft3D.
The regional model is calibrated with measurements of the water level at Da Nang station. Then the flow model is validated with observed data of water level and velocity that were measured in Cua Dai inlet. Figure 3.3 shows water levels computed by the model and measured data extracted from global tides at Da Nang station during a one month period.

Figure 3.3, 3.4 and 3.5 show the comparison of observed and simulated water levels

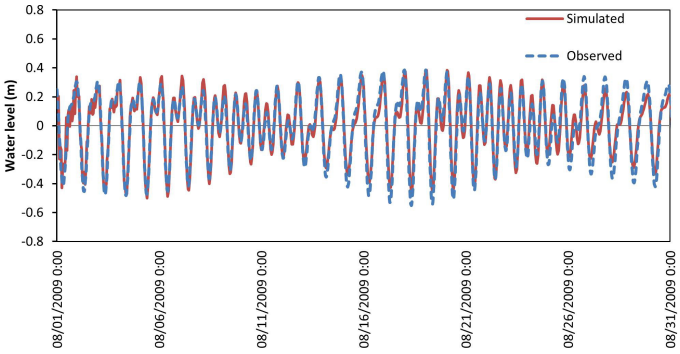

Figure 3.3: Observed and simulated water level at Da Nang station

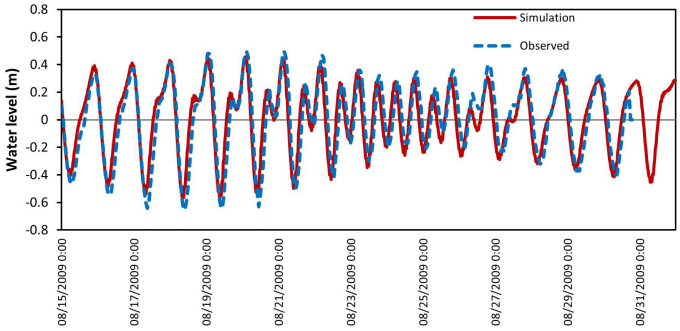

Figure 3.4: Observed and simulated water level at Cua Dai inlet

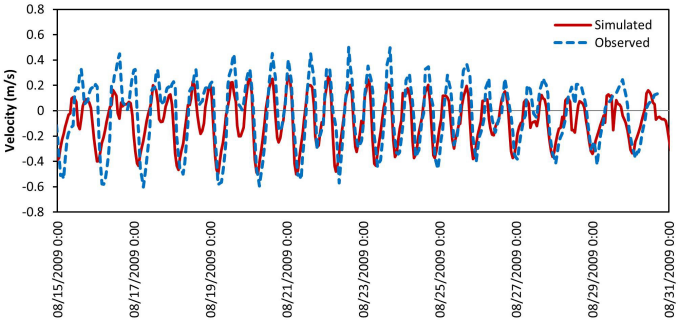

Figure 3.5: Observed and simulated depth average velocity at Cua Dai inlet

and velocities at Cua Dai inlet. Although the observed velocities are higher than compared to simulated data, the computed water level agrees well with observed data. These plots show that in general the level of agreement between observed and simulated data is good. Therefore the model is used to analyze the sediment transport pattern.

3.2.3 Model simulations

To test the influence of seasonal waves and seasonal river flow on hydrodynamics and sediment transport at the inlet and its adjacent coasts. In this study 6 different conditions that represent winter and summer and one extreme flood event are simulated. Details can be found in Table 3.1. This selection is based on the integrated analysis based on both hydrology and wave climate from chapter 2. When combining both the hydrology and the wave climate, three seasons exist. An ENE monsoon with a flood season from September to December, an ENE monsoon with a dry season from January to March, and a dry bidirectional SE/ENE monsoon from April to August.

The representative river discharge of each season was selected based on average river

Table 3.1: Overview of structure of the morphodynamic simulation considering seasonal waves and seasonal river discharges.

Case		River discharge, Q(m^3/s)	Wave height, Hs (m)	Wave period, Tp(s)	Wave direction, θ (°)
Winter season	Run1	168	1.25	7.9	60 (ENE)
	Run2	634	1.25	7.9	60 (ENE)
	Run3	1037	1.25	7.9	60 (ENE)
Summer season	Run4	88	0.75	6.42	60 (ENE)
	Run4	88	0.75	6.40	135 (SE)
Extreme flood event	Run6	10600	1.25	7.9	60 (ENE)

discharge at Nong Son station measured from 1977 to 2011. The winter season when the ENE waves dominant, three discharge classes were chosen, a maximum value of 1037 m^3/s as a representative discharge during flood season, an average river discharge from September to December of 634 m^3/s as representative during normal and a lower

river discharge during January to March of 168 m^3/s as representative for the dry season. During the summer season the bidirectional waves SE/ENE dominant, the average river discharge from April to August is 88m^3/s is chosen as a representative flow during this season.
The representative wave heights for each season were selected based on the significant induced longshore sediment transport rate (LSTR). In the previous chapter, the LSTR induced by waves were calculated for each wave height class. Then the accumulated LSTR for the season was estimated by summing the LSTR of all the classes using the percentage of occurrence of each wave conditions. In this chapter, only one wave height was derived as representative wave dominant for each season by comparing the sediment transport pattern of each wave condition to the net sediment transport graph of the season. The selection is based on associated magnitude of longshore sediment transport for each season and the frequency of occurrence.
For each condition the residual sediment transport patterns and alongshore sediment transport at the adjacent coasts were computed and compared. The first five cases are simulated with the same duration of one month and the extreme flood event is simulated in 4 days representing the average time of flood in this area. The longshore sediment transports (LST) computed over one month for each condition, during the summer months and the winter months, are computed by defining 39 transects in which 20 transects are at the north coast and the other 19 transects are at the south coast. These transects are chosen as the same positions that were used to estimate LST induced by waves in chapter 2. Positive values indicate southward transport whereas negative values indicate northward transport.

3.3 Results and discussion

THIS section firstly presents the results of the sediment transport pattern around the ebb tidal delta. Secondly, the results of the alongshore sediment transport at the adjacent coasts are presented and discussed. Thirdly, the results of sediment transport through the mouth are presented and discussed. Finally, the morphological feedback around the ebb tidal delta and adjacent coast is presented and discussed.

3.3.1 Sediment patterns

The estimated spatial distribution of sediment transport patterns in the estuary and at the ebb tidal delta during different cases in the winter and the summer are shown in Figure 3.6. The pattern of sediment transport is complex because the flow responds to the combined forcing of tides, river flow, waves, and estuarine circulation. The influence of waves is particularly noticeable in the seaward side of the ebb tidal delta and at the northern coast near the inlet. For the waves coming from the ENE during the winter (Figure 3.6a, b, and c), high sediment transport in landward direction can be found around the seaward side of the ebb tidal delta especially at the southward side. At the northward

side of ebb tidal delta, the direction of sediment transport is toward the north. However, the magnitude depends on the river discharge. The higher sediment transport to the north corresponds to the larger river discharge (Figure 3.6c). For the lower river discharge during the summer season (Figure 3.6d) the sediment transport is less compared to other cases. At the landward side of ebb tidal delta there is an interaction between sediment import and sediment export due to river flow, tide and current induced by waves. At the northern side of the coast near the inlet, the sediment transport induced by waves

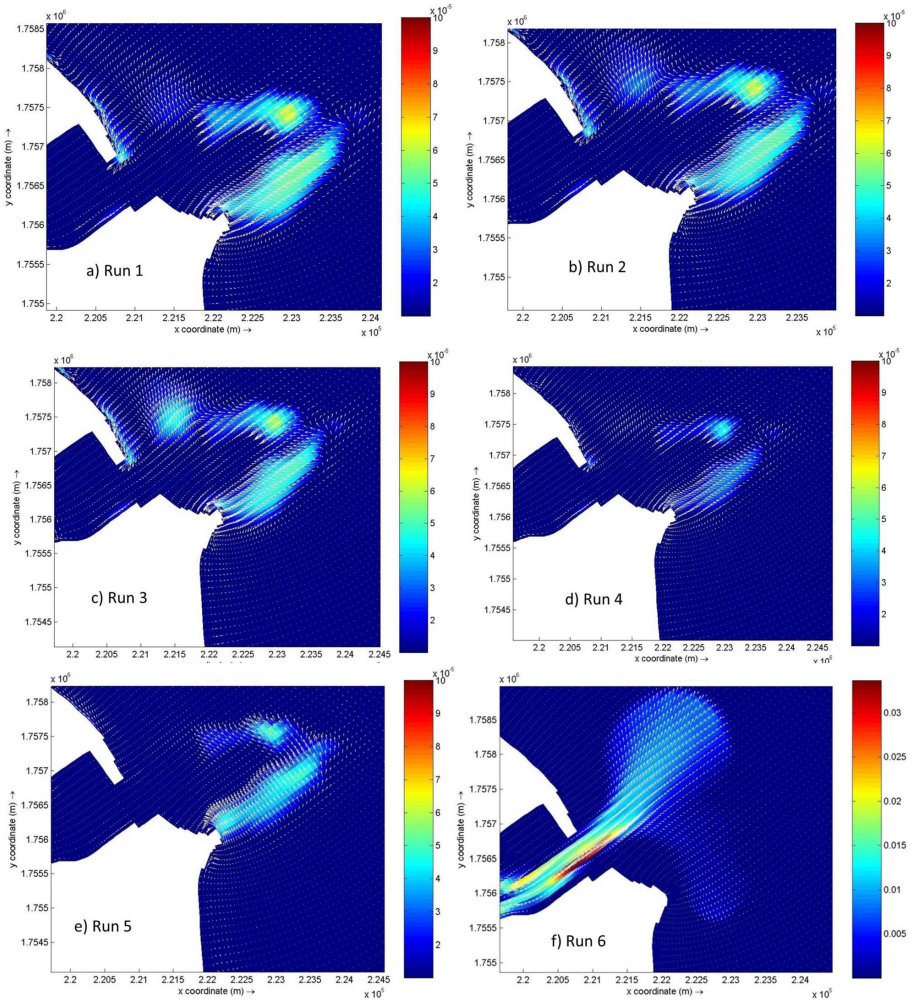

Figure 3.6: Mean total sediment transport during one month for all the cases (vectors indicate direction and color map indicate the magnitude, scale on the right).

and tides is generally towards the inlet throat in the case of waves from ENE. The magnitude of this sediment transport depends on wave height. Higher wave height in the winter induces larger sediment transport than the lower wave height in the summer (Figure

3.6d).
Sediment transport patterns in the estuary and ebb tidal delta during different cases in the summer are shown in Figure 3.6d and e. When waves come from the southeast direction (Figure 3.6e); sediment transport around the ebb tidal delta is tending towards the North, especially at the southern side of the ebb tidal delta. This result supports the results of LST induced by SE waves in the northern direction at the southern coast as shown in the previous chapter.
The flush of sediment through the inlet and even ebb shoal is clearly visible in the case of an extreme flood event (Figure 3.6f). During the extreme flood event, a large amount of sediment flushes out from estuary which is mainly transported directly to the north and a small part is transported towards the south. In this case, the sediment transport in the system indicates a dominant influence of the flood discharge.

3.3.2 Longshore sediment at adjacent coasts

The resulting sediment transports within one month are shown at the cross-sections for the different cases in Figure 3.7 and 3.8. In the case of ENE waves (60° to north) during the winter (Figure 3.7) and the summer (Figure 3.8a) the LST at the northern coast, close to the inlet is generally directed to the south, whereas the LST is directed to the north further from the inlet. There is a transport diversion point at approximately 3km to the north. Generally, at the northern coast the LST increases from the inlet to north, whereas at the southern coast the LST decreases from the inlet in the south direction.
For the offshore waves from the SE (135° to the north), the LST is generally towards the north on both sides of the inlet (Figure 3.8b). At the northern coast, the LST slightly increases from the inlet to the north, whereas at the southern coast the LST decreases significantly from the south in direction of the inlet. At around kilometer 6 at the northern coast, the LST significantly increase in the northern direction.
In general, the LST pattern induced by waves, tides and river discharge are similar when compared with the results calculated by chapter 2, it considered LST induced by waves only. The model results show that tides and river discharge have no significant impact on LST at the adjacent coasts.

The extreme flood event has strong impact on the sediment transport pattern at both southern and northern coast. At the northern coast there is a transport divergent point at approximately 3km from the inlet to the north. This phenomenon is similar to the results of LST during the winter season when the ENE waves dominate (chapter 2).

3.3.3 Sediment transport through the mouth

Sediment transport capacities through the inlet were investigated by comparing the cumulative sediment transport. Figure 3.10 shows the influence of different waves and river discharges on the sediment transport through the inlet during a one month period. Negative values indicate export of sediment whereas positive values indicate import of sediment. Generally, the inlet experiences sediment import into the estuary, except in

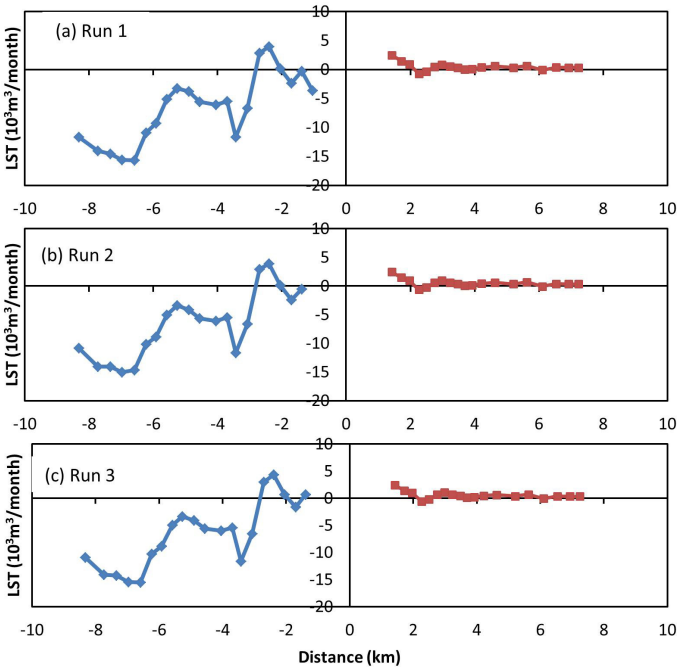

Figure 3.7: Longshore sediment transport during the winter with different cases (Run1, Run2, and Run 3 as in Table 3.1).

the case of the extreme flood event when the river discharge is extremely large. Run 1, 2 and 3 shows clearly the impact of the river discharge on sediment transport through the inlet. The increasing river discharge leads to less sediment import into the estuary. This can be explained by the wave induced sediment supply to the inlet in contrast to the sediment transport away from the inlet due to the ebb flow capacity by the tides and river discharges. When the exported sediment induced by tide and river is higher than the imported sediment induced by waves, the inlet is generally exporting sediment.

Figure 3.10 also shows that waves approaching from both SE and ENE directions cause different magnitudes of sediment import into the estuary. Simulations show that waves coming from the ENE (run 4) contribute to larger sediment import than waves coming from the SE (run 5). Because the sediment patterns induced by the ENE waves present the sediment transport in landward direction whereas the SE waves induce sediment transport in northern direction. This result also explains why the sediment import into the estuary induced by SE waves is smaller (or nearly no import) than the import of sediment induced by ENE waves.

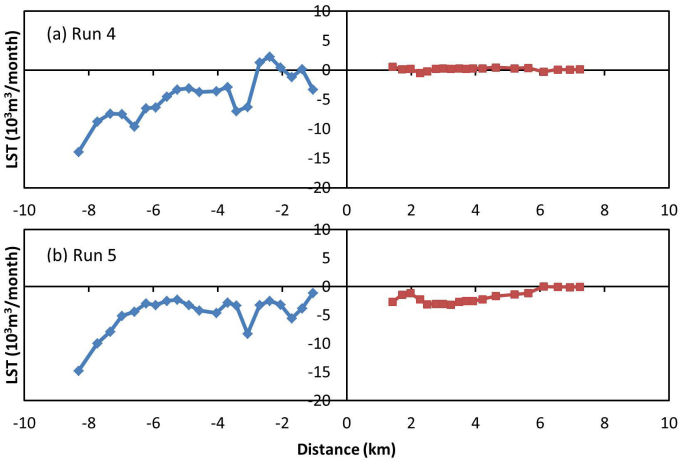

Figure 3.8: Longshore sediment transport during the summer with different wave conditions (Run 4 and Run 5 as in Table 5.1).

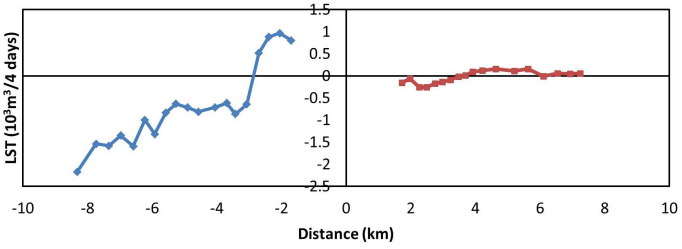

Figure 3.9: Longshore sediment transport during the extreme flood event (Run 6 in Table 3.1).

3.3.4 Pattern of erosion and deposition

Figure 3.11 shows the erosion/sedimentation pattern for the one month simulation period for all cases. The first three cases during the winter exhibit similar erosion/sedimentation patterns. Outside of the ebb tidal delta, erosion is shown whereas inside sedimentation is shown. The outside of the ebb tidal delta is affected by wave induced onshore sediment transport. At the inside of the ebb tidal delta, wave induced sediment transport diminishes and consequently erosion appears outside and deposition appear inside the ebb tidal delta. The sedimentation inside of the ebb tidal delta may originate from the outside of the ebb tidal delta or from river supply. At the north of the ebb tidal delta, sedimentation occurs in all cases considering the winter season. The larger sedimentation corresponds to the larger river flood (Figure 3.11c). During the summer, especially when waves are coming from SE and the river discharge is very small, this area experiences no sedimentation.
The morphology change of the inlet throat is less effected by variability in wave conditions because wave energy is dissipated at the shallow ebb –tidal shoals. There is only large sedimentation at the northern side of the inlet throat. The littoral drift induced by

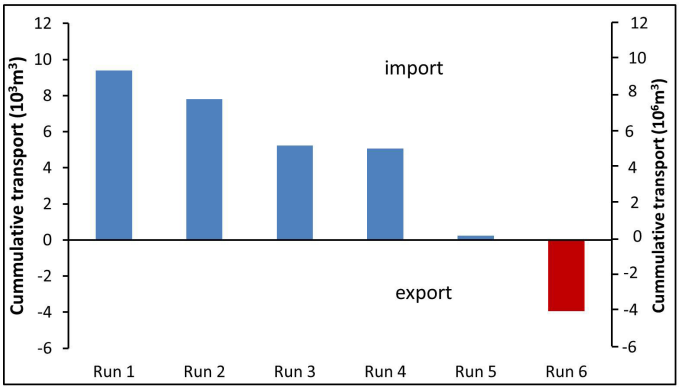

Figure 3.10: Cumulative sediment transport through the inlet for varying waves conditions and river discharges (left coordinator indicate cumulative sediment transport for first five run ($10^3 m^3$) and right coordinator indicate cumulative sediment transport in flood event (run 6, $10^6 m^3$).

waves and tides along the northern coast supplies sediment to the inlet throat leading to the sedimentation at the northern side to the inlet throat. This can explain the results of sediment import through the inlet in almost all cases in Figure 3.10. In the deep part of the channel inlet, the river flow is strong enough to carry out and supply sediment to the ebb tidal delta. The results of the model simulations reveal that the morphological changes on the ebb tidal delta mainly occur during normal conditions in the winter and the summer. Only the extreme flood event has large influences on channel inlet morphology when the river discharge is dominant the inlet channel and ebb –tidal delta are scoured and the wave driven longshore sediment transport is interrupted.

3.4 Conclusions

SEASONAL variations in river flow and wave climate combined with long-term geomorphological developments make Cua Dai inlet a very complex seasonal varying tidal inlet. This study focused on understanding the effect of seasonal variations in wave conditions and seasonal river discharge. The effects of those on the resulting hydrodynamics, sediment transports and potential morphological feedback through the inlet and at the adjacent coasts are investigated. Hydrodynamics and sediment transport at Cua Dai inlet and its adjacent coasts were simulated using Delft3D. Six scenarios with varying dominant wave conditions in the winter and the summer are executed in combination with various river discharge classes that correspond to the dry, wet and flood seasons.

The results from the validation of the simulated hydrodynamics (water levels and velocities) using observations indicate that the hydrodynamic model performs well.

The results from the alongshore sediment transports at adjacent coasts indicate that the seasonal variation in wave climate has a strong influence on the sediment transport pattern. Waves from the SE during the summer time generally induce alongshore sediment

transport (LST) to the north, whereas the waves from the ENE create LST to the south. At the northern coast, the LST increases from the inlet to the north. At the southern coast, the LST decreases from the south in the direction of the inlet. The model shows that the patterns of LST are agree well with the LST induced only by waves from chapter 2.
The simulated sediment transports through the mouth show clear variations due to seasonal variability of the river discharge and wave climate. Waves coming from the ENE at the northern coast induce longshore sediment transport toward the inlet and supply sediment to the inlet. The river flow helps to carry out and supplies sediment to the ebb tidal delta. When the river becomes dominant during an (extreme flood event) this leads to export of sediment. The results also indicate the influence of wave directions that influence the magnitude of sediment that is imported into the estuary. Waves coming from the ENE contribute to larger sediment import than waves coming from the SE.
The results from sediment patterns and morphological changes around the ebb tidal delta indicate that the influence of waves are particularly noticeable on the seaward side of the inlet and less in the landward side of the inlet due to the interaction between the tides and river flow. Waves generally induce landward sediment transport. When the river flow is large during the flood season, river processes are dominant leading to the system to flush out sediment through the estuary and even ebb tidal delta. Especially during the simulated flood event, sediment fluxes are large at the estuary and inner ebb tidal delta.
In a quantitative sense the simulation results are still insufficient to fully explain the channel shifting from north to south. In a qualitative sense however, the model results of this study show a large impact on the seasonal variation in waves and river discharge on sediment transports at Cua Dai inlet and its adjacent coasts. Especially the extreme flood event creates a large sediment export through the inlet and ebb tidal delta.

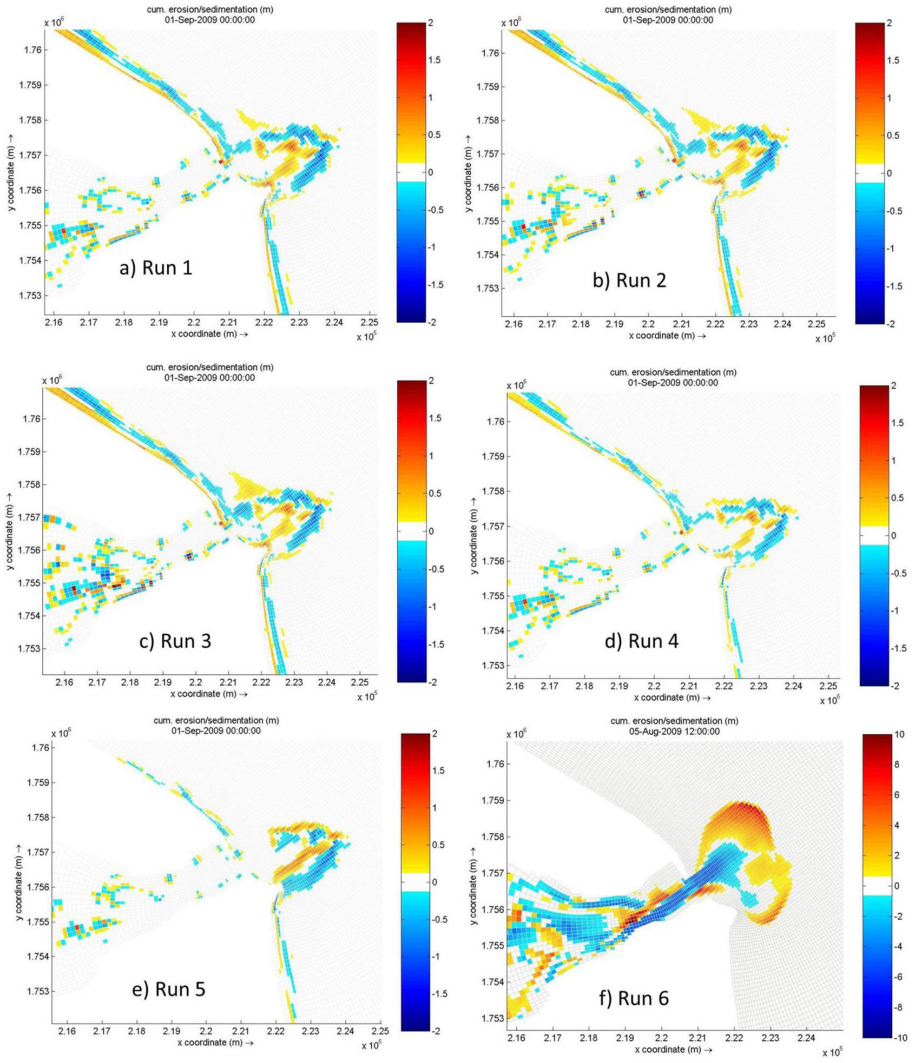

Figure 3.11: Modelled erosion/deposition of ebb tidal delta and adjacent coast (negative values indicate erosion and positive values indicate sedimentation)

References

Bertin, X., Fortunato, A. B., and Oliveira, A. (2009). A modeling-based analysis of processes driving wave-dominated inlets. *Continental Shelf Research*, 29(5-6):819–834.

Booij, N., Ris, R., and Holthuijsen, L. H. (1999). A third-generation wave model for coastal regions: 1. model description and validation. *Journal of geophysical research: Oceans*, 104(C4):7649–7666.

Cayocca, F. (2001). Long-term morphological modeling of a tidal inlet: the arcachon basin, france. *Coastal Engineering*, 42(2):115–142.

Chen, J.-L., Hsu, T.-J., Shi, F., Raubenheimer, B., and Elgar, S. (2015). Hydrodynamic and sediment transport modeling of new river inlet (nc) under the interaction of tides and waves. *Journal of Geophysical Research: Oceans*, 120(6):4028–4047.

Daly, C. J., Bryan, K. R., Roelvink, J. A., Klein, A. H. F., Hebbeln, D., and Winter, C. (2011). Morphodynamics of embayed beaches: The effect of wave conditions. *Journal of Coastal Research SI*, 64(64):1003–1007.

de Vriendº, H., Zyserman, J., Nicholson, J., Roelvinkº, J., and Pechon, P. (1993). Medium-term 2dh coastal area modelling. *Coastal engineering*, 2(1):193–224.

Dissanayake, D., Roelvink, J., and Van der Wegen, M. (2009). Modelled channel patterns in a schematized tidal inlet. *Coastal Engineering*, 56(11-12):1069–1083.

Do, A. T., de Vries, S., Ye, Q., Stive, M. J., and Nguyen, T. V. (2018). Hydrodynamics and sediment transport at a seasonal inlet and its adjacent beach: Cua dai, vietnam. In *Sixth International Conference on Estuaries and Coasts (ICEC-2018)*.

FitzGerald, D., Buynevich, I., Fenster, M., and McKinlay, P. (2000). Sand dynamics at the mouth of a rock-bound, tide-dominated estuary. *Sedimentary Geology*, 131(1-2):25–49.

Fitzgerald, D. M. (1984). Interactions between the ebb-tidal delta and landward shoreline; price inlet, south carolina. *Journal of Sedimentary Research*, 54(4):1303–1318.

Herrling, G. and Winter, C. (2014). Morphological and sedimentological response of a mixed-energy barrier island tidal inlet to storm and fair-weather conditions. *Earth Surface Dynamics*, 2(1):363–382.

Hubbard, D. K., Oertel, G., and Nummedal, D. (1979). The role of waves and tidal currents in the development of tidal-inlet sedimentary structures and sand body geometry; examples from north carolina, south carolina, and georgia. *Journal of Sedimentary Research*, 49(4):1073–1091.

Hydraulics, D. (2014). Delft3d-flow user manual: Simulation of multi-dimensional hydrodynamic flows and transport phenomena. Technical report, including sediments. Technical report.

Komar, P. D. (1996). Tidal-inlet processes and morphology related to the transport of sediments. *Journal of Coastal Research*, pages 23–45.

Lesser, G., Roelvink, J. v., Van Kester, J., and Stelling, G. (2004). Development and validation of a three-dimensional morphological model. *Coastal engineering*, 51(8-9):883–915.

Nahon, A., Bertin, X., Fortunato, A. B., and Oliveira, A. (2012). Process-based 2dh morphodynamic modeling of tidal inlets: A comparison with empirical classifications and theories. *Marine Geology*, 291:1–11.

Oertel, G. (1988). Processes of sediment exchange between tidal inlets, ebb deltas and barrier islands. In *Hydrodynamics and sediment dynamics of tidal inlets*, pages 297–318. Springer.

Oertel, G. F. (1972). Sediment transport of estuary entrance shoals and the formation of swash platforms. *Journal of Sedimentary Research*, 42(4):858–863.

Ping, S. L. (1989). Cyclic morphologic changes of the ebb-tidal delta, texel inlet, the netherlands. In *Coastal Lowlands*, pages 35–48. Springer.

Ridderinkhof, W., Swart, H., Vegt, M., and Hoekstra, P. (2016). Modeling the growth and migration of sandy shoals on ebb-tidal deltas. *Journal of Geophysical Research: Earth Surface*, 121(7):1351–1372.

Ris, R., Holthuijsen, L., and Booij, N. (1999). A third-generation wave model for coastal regions: 2. verification. *Journal of Geophysical Research: Oceans*, 104(C4):7667–7681.

Robinson, A. (1975). Cyclical changes in shoreline development at the entrance to teignmouth harbour, devon, england. *Nearshore Sediment Dynamics and Sedimentation. John Wiley, London*, pages 181–198.

Roelvink, D. (2011). *A guide to modeling coastal morphology*, volume 12. world scientific.

Roelvink, J. (2006). Coastal morphodynamic evolution techniques. *Coastal Engineering*, 53(2-3):277–287.

Van der Wegen, M., Dastgheib, A., and Roelvink, J. (2010). Morphodynamic modeling of tidal channel evolution in comparison to empirical pa relationship. *Coastal Engineering*, 57(9):827–837.

Van der Wegen, M. and Roelvink, J. (2008). Long-term morphodynamic evolution of a tidal embayment using a two-dimensional, process-based model. *Journal of Geophysical Research: Oceans*, 113(C3).

Van Leeuwen, S., Van der Vegt, M., and De Swart, H. (2003). Morphodynamics of ebb-tidal deltas: a model approach. *Estuarine, Coastal and Shelf Science*, 57(5-6):899–907.

Van Rijn, L. C. et al. (1993). *Principles of sediment transport in rivers, estuaries and coastal seas*, volume 1006. Aqua publications Amsterdam.

Vo, N. D. (2015). *Deterministic hydrological modelling for flood risk assessment and climate change in large catchment. Application to Vu Gia Thu Bon catchment, Vietnam.* PhD thesis, University of Nice Sophia Antipolis.

Winter, C. (2006). Meso-scale morphodynamics of the eider estuary: analysis and numerical modelling. *Journal of Coastal Research*, pages 498–503.

Chapter 4

Estimation and Evaluation of Shoreline Locations, Shoreline Change Rates and Coastal Volume Changes derived from Landsat Images

You can't go back and change the beginning,
but you can start where you are and change the ending.

C. S. Lewis

Shoreline change data are of primary importance for understanding coastal erosion and deposition as well as for studying coastal morphodynamics. Shoreline extraction from satellite images has been used as a low cost alternative and as an addition to traditional methods. In this work, satellite derived shorelines and corresponding shoreline change rates and changes in volumes of coastal sediments have been estimated and evaluated for the case of the data-rich North-Holland coast. This coast is globally unique for its long in-situ monitoring record and provides a perfect case to evaluate the potential of shoreline mapping techniques. A total of 13 Landsat images and 233 observed cross-shore profiles (from the JAaRlijkse KUStmeting [JARKUS] database) between 1985 and 2010 have been used in this study. Satellite derived shorelines are found to be biased in seaward direction relative to the JARKUS derived shorelines, with an average ranging 8m to 9m over 25 years. Shoreline change rates have been estimated using time series of satellite derived shorelines and applying linear regression. The satellite derived shoreline change rates show

This chapter has been published in Journal of Coastal Reseach Do et al. (2019).

a high correlation coefficient (R^2>0.78) when compared with the JARKUS derived shoreline change rates over a period of 20 and 25 years. Volume changes were calculated from the satellite derived shoreline change rates using assumptions defining a closure depth. Satellite derived volume changes also show a good agreement with JARKUS based values. Satellite derived shorelines compare better with in situ data on beaches that have intertidal zone widths ranging from one to two pixel sizes (30m-60m). The results show that the use of Landsat images for deriving shorelines, shoreline change rates and volume changes have accuracies comparable to observed JARKUS based values when considering decadal scales of measurements. This shows the potential of applying Landsat images to monitor shoreline change and coastal volume change over decades.

4.1 Introduction

MONITORING the behavior of shorelines is of considerable social and economic importance in support of setback planning, hazard zoning, erosion-accretion management, regional sediment budgets and the establishment and validation of models for coastline changes (Lawrence, 1994; Sherman and Bauer, 1993; Zuzek et al., 2003). Shorelines are inherently dynamic features that mark the transition zone between land and sea. The inherent dynamics of the shoreline span over a range of spatial and temporal scales (Gens, 2010; Pajak and Leatherman, 2002) which makes shoreline change assessment very challenging. The zone around the shoreline is highly dynamic and undergoes frequent changes caused by the impact of both natural and human activities. Furthermore, shoreline erosion and coastal flooding are highlighted as among the largest effects of climate change (IPCC, 2001).

Traditional techniques for shoreline change studies include analyzing historic maps, in situ beach profiling, LIDAR surveys and aerial photography and video imgagery (Chen and Chang, 2009; Kumar and Jayappa, 2009; L.Miller and H.Flectcher, 2003; Pianca et al., 2015; Ruggiero et al., 2005). These techniques are inherently limited in temporal coverage, typically being either too short to identify long term trends or too widely spaced in time to distinguish short term, seasonal changes. Also, traditional techniques are both costly and labor-intensive. For developing countries, budgets for coastal monitoring and shoreline change are scarce. Therefore, a cost-effective approach is required, particularly for those places where there is concern about shoreline erosion. This is where satellite imagery based on freely available high quality images such as Landsat might offer a good alternative. Moreover, it is possible to assess coastline changes over longer periods of time since Landsat missions have been collecting spectral satellite imagery for over forty year now (Maiti and Bhattacharya, 2009; Guariglia et al., 2006).

Satellite Derived Shorelines (SDS) are based on extracting shorelines from collected satellite images based on grouping pixels by their different spectral properties in different wavebands (e.g. Lu and Weng, 2007; W.Muttitanon and N.K.Tripathi, 2005; Phinn et al., 2000). These methods have been widely used in recent decades for automatic and semi-automatic shoreline detection and mapping. Some studies use a single band image (Frazier et al., 2000) while other studies use a band ratio (Guariglia et al., 2006) or a combination of different reflective bands to improve surface water detection (Du et al., 2012). For instance, the Normalized Difference Water Index (McFeeters, 1996) was used to enhance the difference in pixel resolution between land and water in shoreline extraction (Bouchahma and Yan, 2012; Grigio et al., 2005; Noernberg and Marone, 2003). Also, the Normalized Difference Moisture Index (Wilson and Sader, 2002), the Modified Normalized Difference Water Index (Xu, 2006), the Water Ratio Index (Shen and Li, 2010), the Normalized Difference Vegetation Index (Rouse Jr et al., 1974) and the Automated Water Extraction Index (Feyisa et al., 2014) also found wide application. Rokni et al. (2014) applied and compared the different satellite-derived indexes above to extract surface water of Lake Urmia. Their results demonstrated that the Normalized Difference Water Index (NDWI) is superior to other indexes with the highest accuracy results. Consequently, NDWI was selected as the method to extract shoreline positions in our study. More recently, new approaches for shoreline extraction have been investigated. Foody et al.

(2003); Muslim et al. (2006) and Pardo-Pascual et al., 2012 explore sub-pixel shoreline extraction in which individual pixels could be assigned to partly land and partly water.
Many previous studies have investigated the potential of optical satellite images for coastal monitoring (Blodget et al., 1991; Chen and Chang, 2009; Kumar et al., 2007; Ekercin, 2007; Foody et al., 2003; Gutierres et al., 2016; Kingston, 2003; Kuleli et al., 2011; Liu and Jezek, 2004; Mason et al., 1997; Ojeda, 2008; Plant et al., 2007; Teodoro, 2016; Teodoro et al., 2018; Wang et al., 2010; White and Asmar, 1999). However, few of these studies have fully explored the accuracy of the derived shorelines through comparison with simultaneous and independent in situ observations because of limitations in the availability of satellite images and in-situ data.
A literature search resulted in only five recent studies related to SDS accuracy. First, Pardo-Pascual et al., 2012 used 45 images (28 TM and 17 ETM) to assess accuracy in shoreline position extraction applying the sub-pixel method with two shoreline segments consisting of seawalls in the Spanish Mediterranean Sea. This case just applies to artificially stabilized coastal segments that have a constant shoreline position. Moreover, the accuracy was derived by using only one reference image. However, on natural beaches the shoreline positions are variable due to seasonal and episodic events. For this reason, the accuracy assessment for seawalls is not the same as for natural beaches. Second, García-Rubio et al. (2015) used in situ shoreline measurements to compare with SDS from multispectral images (SPOT) with 8 shoreline segments including a beach and a man-made structure at Progreso, Yucatá, México. Again, their research only used one image to evaluate accuracy. Third, Almonacid-Caballer et al. (2016) used the annual mean shoreline positions (the average shoreline position over a year) extracted from Landsat images to quantify the mid-term beach trend during the period of 2000-2014. In their work, the annual mean Landsat shorelines were compared with the mean annual shorelines obtained from more accurate sources RTK-GPS and LiDAR. The test was applied on a 9 km stretch of beach at EI Saler (Valencia, Spain) located on the beach barrier. It is shown that the use of annual mean shorelines indicates that the same rate of change is obtained as when using the whole set of shorelines. Both instantaneous and mean annual shorelines appear to show a seaward bias of about 4 or 5 m compared to those obtained using Lidar and RTK-GPS. Similarity, Sánchez-García et al. (2015) also used the same method for extraction shoreline position, as described in Pardo-Pascual et al. (2012) to compare an annual mean shoreline obtained from Landsat TM /ETM+ and from high precision data, RTK-GPS. The comparison was applied on a 9 km stretch of beach at EI Saler (Valencia, Spain) for two short periods (2006-2007 and 2009-2010). Several statistical tests peformed to compare the grade of similarity between Landsat and high-precision data, which indicates that both source of data provide similar information regarding annual mean shoreline. Finally, Hagenaars et al. (2018) have evaluated different drivers of inaccuracy of SDS using very detailed measurements of morphology. Their results contain a near perfect comparison of SDS and in-situ data that were collected simultaneously during cloud free conditions showing an average accuracy of about 1 m.
No previous studies have explored the potential of deriving changes in coastal volumes using satellite data. Only Rosati et al. (1999) used 10 historical shoreline data sets from survey maps, aerial photography and digital rectified scanned aerial photography to es-

timate volumetric change rates to derive a regional sediment budget for Fire Island to Montauk Point. These authors focused on the time period from 1979 to 1995 (a 16-year time period). Their research considered only general uncertainties in their regional sediment budget estimation based on the potential longshore sediment transport (LST). The uncertainty was derived following Rosati and Kraus (1999) who divided the standard deviation in the net LST by the square root of the number of yearly averages. This evaluation did not use any observed data for validation.
The aim of the present study is to explore the potential of satellite images in monitoring shoreline change rates and changes in volumes of coastal sediments which can be applied to beach locations where data are lacking or scarce. Specific objectives are to provide a straightforward, quantitative and objective method that builds on existing methods that have proven to be easy and widely applicable for extracting shoreline locations using satellite images. The estimation of shoreline change rates follows this derivation of shoreline position and eventually changes in coastal sediment volumes. These process were applied and evaluated at the Dutch coast which provides a data-rich site to evaluate the methodology.

4.2 Test site and imagery

4.2.1 Study site

The selected study area is located at the North-Holland coast and stretches from Wijk aan Zee to Den Helder, over a length of approximately 60 km 4.1. It is bounded in the North by a tidal inlet (the Marsdiep) and in the South by the 2.5km long jetties of IJmuiden. The North-Holland coast is a sandy, microtidal, wave-dominated coast. The plan shape of the coast is slightly concave, except near the Petten Seawall that protrudes into the sea, giving the shoreline a local convex curvature. The coastline orientation in the North is about 2º with respect to the North, and increases up to 22º at IJmuiden. The average beach slope is in the order of 1:60. The near shore zone has an average slope of 1:60 – 1:150 (Knoester, 1990). The slopes can vary significantly in longshore direction. Near Den Helder, the influence of the channels of the Marsdiep inlet cause steeper slopes. Near IJmuiden, the dry beach and the near shore zone have a larger width.
Most of the winds along the Holland coast come from the North Sea. The prevailing wind direction is southwest (23%), followed by west (16%), east (13%) and northwest (12%) (Stolk, 1989). Storms that cause the largest wind set-up along the coast are coming from northwest (van Rijn et al., 2002). Tides are semidiurnal with a mean tidal range between 1.4 m in the north and 1.6 m in the south. Waves mainly approach the coast from southwesterly and north northwesterly directions. The wave climate is quite homogeneous along the whole stretch of coast (Wijnberg, 2002), with a mean annual significant wave height of about 1.3 m.

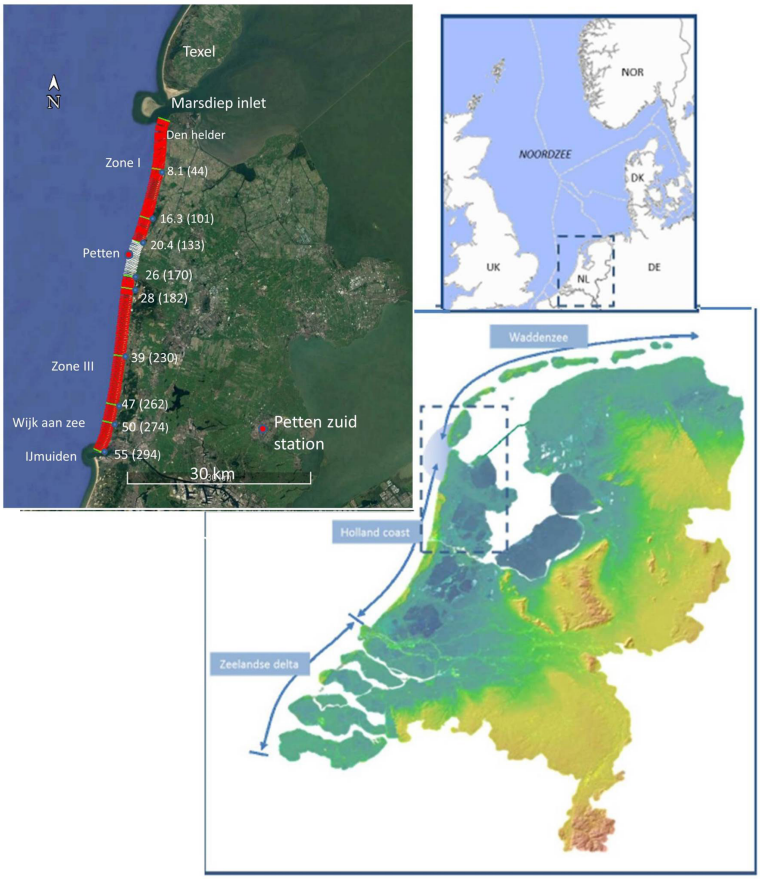

Figure 4.1: Overview of The Netherlands, its three coastal systems and the study area (Modified from Actueel Hoogtebestand Nederland, 2010)

4.2.2 Landsat Images

To detect SDS of the North-Holland coast, a total of 13 Landsat images were selected with the lowest cloud coverage. All the used images are free of clouds, except Landsat TM, 2nd October 1988 (10% cloud coverage) and Landsat TM, 2nd June 2010 (8% cloud coverage). The availability of cloud free images did not allow a subset of images at regular intervals. Thirty scenes of the Thematic Mapper (Landsat 5 TM) and Enhanced Thematic Mapper (Landsat 7 ETM+) sensor data were acquired during the period from 1985 to 2010. Those were downloaded from the U.S. Geological Survey (USGS) Earth Explorer Web Tool. All the obtained Landsat data (Level 1 Terrain Corrected (L1T) product) were pre-georeferenced to UTM zone 31 North projection using WGS -84 datum. Landsat 5 TM consists of seven spectral bands with a spatial resolution of 30 meters for bands 1 to 5 and 7, and one thermal band (band 6) is 120 meters that is resampled to 30m pixels. Landsat 7 ETM+ consists of eight spectral bands with a spatial resolution of 30m for

bands 1 to 7. The resolution of band 8 (panchromatic) is 15m. As reported by NASA, all the Landsat TM/ETM+ are georeferenced with a level of precision better than 0.44 pixels (meaning 13.4m). (Pardo-Pascual et al., 2012).
For the interpretation of the satellite dataset, it is important to take the instantaneous water level into account. The observed location of the waterline is influenced by the instantaneous water level where a change of water level by 1 meter will cause the waterline to shift 50 meters over a 1:50 beach slope when other factors are assumed constant. Instantaneous water levels are measured at several locations in the study area. Along the study area there are three tidal stations; Den Helder, Petten Zuid and IJmuiden. The tide station of Den Helder is located in the tidal inlet and is thus not necessarily representative for tide level along the coast (Wijnberg, 2002). TThe tide station of IJmuiden is located near the IJmuiden harbor. Figure 4.2 indicates one tidal cycle in January, 1985 at the three tidal stations. There is a slight difference in phase and tidal ranges between the stations. The tidal range indicates a slight increase from Den Helder to I IJmuiden. In order to identify how tides influence the SDS a numerical model is needed to apply to simulate the tidal wave propagation along the coast, but this falls beyond the scope of this study. The Petten Zuid station is located near the Petten seawall, in middle of Noord Holland. The tide measured at the Petten Zuid station was therefore selected as representative for the study area since it is the closest to the study area. The tidal conditions at the time of image acquisition were estimated by the tide data at Petten Zuid station (http://live.waterbase.nl/waterbase_wns.cfm?taal=en). The tide level corresponding to the moment of the Landsat image collection is presented in Table 4.1 alongside the details of the satellite data.

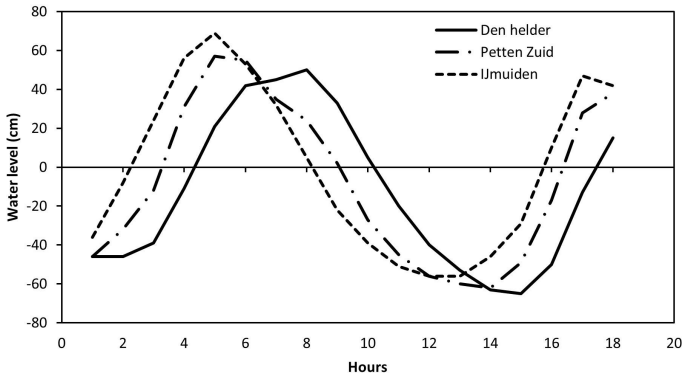

Figure 4.2: The difference in the tide between the stations, Den Helder, Petten Zuid and IJmuiden

4.2.3 JARKUS Data

To assess the accuracy of SDS, shoreline positions were derived from the JAaRlijkse KUStmeting (JARKUS) database available for this study (Minneboo, 1995). A yearly survey program for the Dutch coastal area collects the JARKUS profile data since 1963. Long

Table 4.1: Details of the satellite dataset used in this study

No	Path/Row	Acq.Date	Acq.Time	Sensor	Tidal height (cm)
1	199/23	12/02/1985	10:10:04	TM	34
2	198/23	16/06/1986	9:57:10	TM	65
3	198/23	05/07/1987	9:58:26	TM	67
4	199/23	02/10/1988	10:10:16	TM	47
5	199/23	23/05/1989	10:01:51	TM	12
6	199/23	30/03/1990	9:59:43	TM	6
7	198/23	16/05/1998	10:10:54	TM	29
8	198/23	30/07/1999	10:26:20	ETM	7
9	198/23	13/05/2000	10:25:34	ETM	-24
10	198/23	28/09/2005	10:21:34	TM	50
11	198/23	11/09/2006	10:27:11	TM	69
12	198/23	19/09/2009	10:23:16	TM	-31
13	198/23	02/06/2010	10:24:09	TM	58

fixed transects at a longshore distance of 200m-250m, depths and heights of coastal profiles are measured each year, called JARKUS profiles. These data are primarily used to inspect and provide the position of the momentary coastline, to record volumes of beach profiles and to plan nourishments. Because of the size of the JARKUS data, they are grouped into 16 regions covering the Dutch North Sea coast from North to South. This study used the data of region 7 (Noord-Holland) which includes 294 transects (corresponding to the name of profile in JARKUS data, 7000000 to 7005500) locations in total covering the coast from Den Helder to Wijk aan Zee.
Due to its geography, the North-Holland coast was divided into three segments for the analysis. The first segment, termed Zone I, is located immediately south of the Marsdiep inlet starting from transect 2 to transect 133. The second segment, termed zone II, includes 31 transects from transect 134 to transect 170. This segment is located at the Petten seawall, where JARKUS profile data are only available since 1990. The third segment is Zone III, starting from transect 171 to transect 294 at the jetties of IJmuiden. Landsat derived shorelines along seawalls are not necessarily the same as along natural shorelines (Almonacid-Caballer et al., 2016). On a seawall stretch the water depth close to the shoreline increases sharply whereas on natural beaches the depth drops more gradually. As a result the shoreline definition is different and therefore, this study only focuses on the accuracy assessment for natural beaches, Zone I and Zone III.

4.3 Methods

To assess the accuracy of using satellite images in monitoring shoreline change rates and changes in coastal volume changes, the present work used the most common

and easy to apply method as the basic method to derive shoreline position (SDS). Then SDS change rates (SDSCR) are calculated based on the SDS and the volume changes (SDVC) are estimated based on the SDSCR. Additionally, shoreline positions, shoreline change rates and volume changes derived from JARKUS data are used to access accuracy by using statistical parameters.

4.3.1 Extracting SDSs from Landsat Images

The SDS is defined as the position of the boundary between water and land at the time of satellite imagery acquisition. To detect the shoreline position and calculate the shoreline change rate, this study applied an algorithm as shown in the flow chart in Figure 4.3 consisting of three main steps: (1) conversion of the digital number (DN) to spectral radiance (L_λ) and to the top of atmospheric (TOA) reflectance (ρ_λ) for radiometric calibration according to Chander et al. (2009); this step is applied for two bands; the green and near infrared bands. (2) Extracting satellite derived shorelines base on classification of the normalized difference water index (NDWI) values by using unsupervised classification techniques; (3) All shoreline positions were used to derive shoreline change rates. Step 1 consists of radiometric calibration and atmospheric correction. Data records of different remote sensors are not directly comparable because there are time differences in image acquisition, signal variations of exoatmostpheric solar irradiance arising from spectral band distinctions, and atmospheric effects of aerosol scattering under various weather conditions on the image acquisition date (Kuleli et al., 2011). Therefore it is necessary to conduct radiometric calibration and apply atmospheric correction before extracting the shoreline position (Chander et al., 2009; Tyagi and Bhosle, 2011). The digital numbers recorded by the Landsat TM and ETM+ were transformed to TOA reflectance (ρ_λ) using the method developed by **?**. During radiance calibration, the digital numbers (DN) recorded by Landsat images were converted to radiance values (L_λ) using the bias and gain values following Equation 4.1 . Then these radiance values were converted to reflectance values using Equation 4.2.

$$L_\lambda = G_{Rescale} \times Q_{cal} + B_{Rescale} \tag{4.1}$$

and

$$\rho_\lambda = \frac{\pi . L_\lambda . d^2}{ESUN_\lambda . sin\theta_{SE}} \tag{4.2}$$

where
L_λ = Spectral radiance at the sensor's aperture [W/(m^2 sr μm)]
Qcal = Quantized calibrated pixel value [DN]
$G_{rescale}$ = Band-specific rescaling gain factor [(W/(m^2 sr μm))/DN]
B$_{rescale}$ = Band-specific rescaling bias factor [(W/(m^2 sr μm))/DN]
ρ_λ = Planetary TOA reflectance [dimensionless]
d =Earth-sun distance [astronomical units]
$ESUN_\lambda$ = Mean exoatmospheric solar irradiance [W/(m^2 μm)]
θ_{SE} = Local sun elevation angle

Step 2 involves extracting the SDS based on the classification of the NDWI index values.

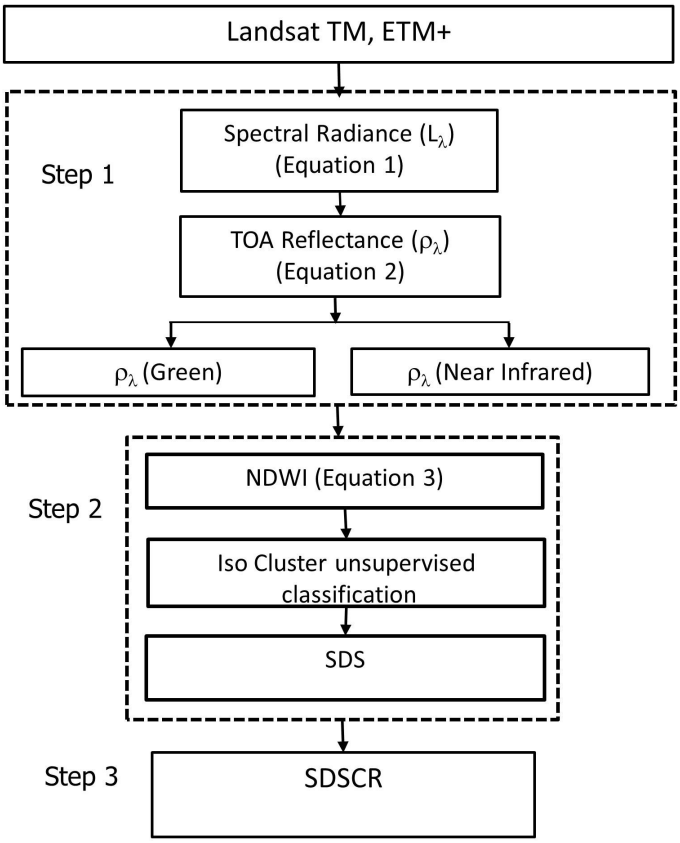

Figure 4.3: Flow chart of shoreline change analysis methodology

In order to enhance maximum distinction between land and sea, the NDWI (Normalized Difference Water Index) was used according to Equation 4.3 (McFeeters, 1996).

$$NDWI = (\rho_\lambda(Green) - \rho_\lambda(NIR))/(\rho_\lambda(Green) + \rho_\lambda(NIR)) \tag{4.3}$$

where Green is the green band (Land sat TM/ETM+ band 2), and NIR is the near infrared band (Landsat TM/ETM+ band 4). The NDWI is designed to (1) maximize reflectance of water using green wave-lengths, (2) minimize the low reflectance of NIR by water features and (3) take advantage of the high reflectance of NIR by vegetation and soil features. As a result, water features have positive and enhanced values, while vegetation and soil usually have zero or negative values and are therefore suppressed (McFeeters, 1996). Moreover, the NDWI technology can avoid the influence of the water content of leaves of vegetation and the influence of floating leaved vegetation and extract the pure standing water content (Karsli et al., 2011). The unsupervised classification by the Iterative Self-Organizing Data Analysis Technique Algorithm (ISODATA) method was applied

to identify pixels as sea and land. This method does not require information about the image while classification and is therefore especially useful in data limited cases compared to other algorithms. The ISODATA method requires the user to set thresholds for different classification parameters. Liu et al. (2011) advise consideration of higher numbers of classes for coastal areas of many different land covers, and lower classes for areas consisting of only few types of land cover. Since our study zone is a long stretch of coast and the images' region covers different types of land cover, 20 classes were needed to define land and water surface appropriately. A lower and a higher number of classes resulted in either a poor description of land and water surface or a poor distinction because some classes can be merged or removed. The process of the classification from the NDWI images is including the intermediate steps mentioned illustrated in Figure 4.4. The shoreline identification is based on grouping all classified pixels from the NDWI image, from 20 classes, into two contrasting classes, water and land. The output from the classification process is an image with pixels grouped either as sea or land. The boundary between land and sea in the classified image is converted into a vector. The resulting vector requires a manual edit whereby inland features not related to the shoreline are removed. The process of extracting the shoreline position is performed using the ArcGIS 10.2 software suite.

Step 3 involves the derivation of the Satellite Derived Shoreline Change Rates (SDSCR)

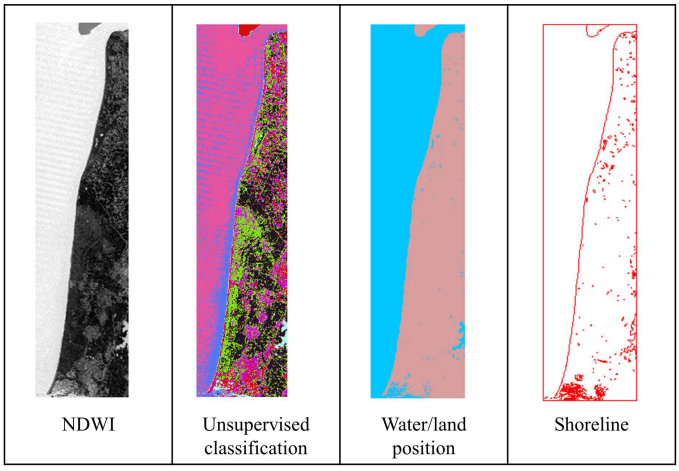

Figure 4.4: Processing to extract shoreline position from Landsat (example data of 2005)

by using linear regression. This method is available in the Digital Shoreline Analysis System (DSAS) software version 4.3, an ArcGIS extension for calculating shoreline change developed by the USGS (Thieler et al., 2009). A baseline is constructed to serve as a starting point for all transects derived by the DSAS application. The transects used are at the same locations as the JARKUS data to allow for comparison. A least-squares regression line is fitted to all shoreline points for a particular transect (Thieler et al., 2009). The evaluation of SDSCR are performed over a 5-year period(1985-1990), a 10-year period (1990-2000, 2000-2010), a 20-year period (1990-2010), and a 25-year period (1985-2010).

4.3.2 Observed Shoreline Position from JARKUS Profiles

In order to extract shorelines from JARKUS profiles, the measured water level at Petten Zuid tidal station was used to find the intersection point between the water level and the cross-shore profiles corresponding to the time appearances of the Landsat images. The water level corresponding to each Landsat image was derived using the exact date and time of image collection. The location of the observed shoreline position from JARKUS is derived as the intersection between each of the 294 cross-shore profiles and the water level at the time of Landsat image collection.

4.3.3 Calculation of profile volumes from satellite and JARKUS data

The satellite derived volume change for each transect, ΔV_{SDS} (m^3/y), was calculated from the shoreline change rates by assuming that the shoreline is translated horizontally without changing shape over an active depth (A_D) as shown in Figure 4.5. This is summarized in Equation 4.4 (Rosati and Kraus, 1999 and Rosati, 2005).

$$\Delta V_{SDS} = A_D \Delta_y \Delta_x \tag{4.4}$$

where Δy is the shoreline change rate for the each transect (m/y), A_D is the active depth for each transect (m) and represents the transect spacing (m). The active depth represents the vertical extent of the beach profile that is eroding or accreting during the period of consideration. It is typically defined as the absolute sum of the berm crest or dune elevation, D_B, and depth of closure, D_c (Equation 4.5).

$$A_D = D_B + D_c \tag{4.5}$$

The volume change for each transect derived from the JARKUS profiles, $\Delta V_{profile}$ (m^3/y), was estimated using linear regression. First, the volume of each transect of each year, $\Delta V_{profile}$ (m^3/m), was derived based on the JARKUS profile. The dune elevation (D_B) was used as landward boundary and the closure depth, Dc as the seaward limit for this volume calculation Figure 4.6. Then the volume change in (m^3/m) was estimated by multiplying with the transect distance, (m) to have the total volume change in (m^3). After that, the volume change of each transect, $\Delta V_{profile}$ (m^3/y), over a period was estimated by fitting a least squares regression line to the yearly volume trends.

In Figure 4.6, the dune elevation (D_B) is shown as the highest point of the profile. The depth of closure (D_c) can be estimated using measurements of the active beach profiles if this data is available or by using the analytical method proposed by Hallermeier (1978). In this study at the Dutch coast, the closure depth parameter is taken from literature Hinton and Nicholls (1999). Therefore, a value of the closure depth of 8 m for the area of North-Holland is assumed. In case the measured profiles do not extend to the 8 m depth contour, the seaward limit is set to the most seaward measurements in that profile.

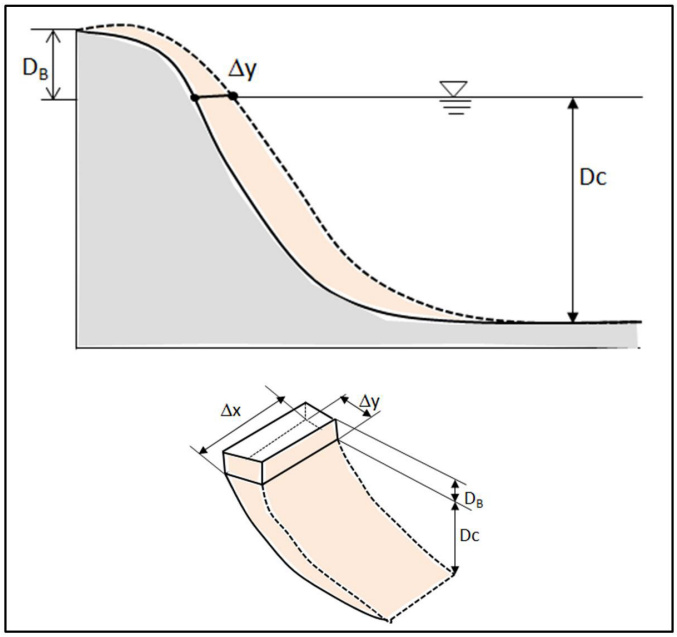

Figure 4.5: Assumption volume calculated from SDS

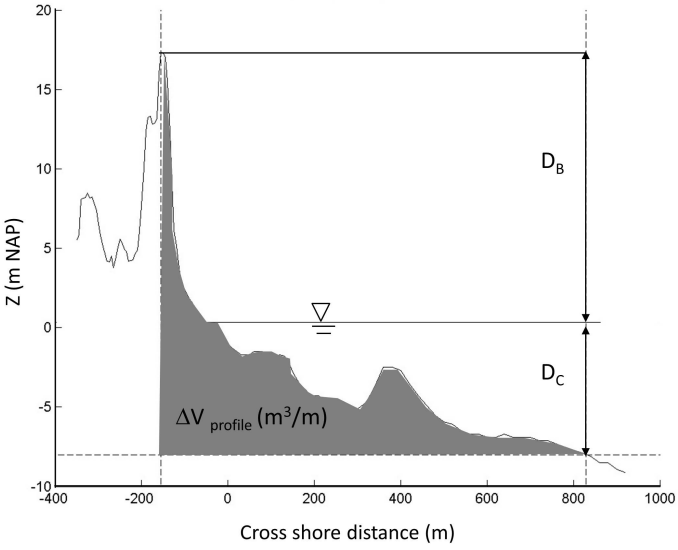

Figure 4.6: Volume derived from JARKUS profile (transect 7004025 in year 1985 and 2010)

To compare the volume changes, ΔV_{SDS} (m^3/y) and $\Delta V_{profile}$ (m^3/y) values were derived for different periods. A 5-year period, 1985-1990, a 10-year period (1990-2000, 2000-2010), a 20-year period (1990-2010), and a 25-year period (1985-2010) were considered.
Besides presenting the volume change per transect, the volume change in each coastal cell is also presented. These results provide a better description of sediment gains and/or losses within a cell and thus of the sediment budget of a larger coastal system. Volume changes are estimated for each coastal cell based on similarities in morphological behavior. We adopt the method of Van Rijn (1997) that divides the part of the North-Holland coast in this study into eight coastal cells (Figure 4.1). Zone I includes three cells, 1, 2 and 3 in which cell 1 (0 to 8.1 km) is located near the city of Den Helder; cell 2 (8.1 to 16.3 km) is located between Julianadorp and Callantsoog and cell 3 consist of the area between 16.3 and 20.5 km. Zone III includes five cells, 4, 5, 6, 7, and 8. Cell 4 consists of the area between 26 and 28 km. Cell 5 includes the area between 28 and 39 km. Cell 6 includes the area between 39 and 47 km. Then the last two cells located near IJmuiden harbor are 7 (47 to 50 km) and 8 (50 to 55 km). Volume changes for each coastal cell are estimated by summing the volume of all transects in each cell.

4.3.4 Deriving the accuracy of SDSs, SDSCRs and SDVCs

For assessing the accuracy of the satellite techniques we assume that the observed JARKUS shoreline provides the ground truth. The horizontal bias of the SDS relative to the JARKUS shoreline is taken as representative for the accuracy. This bias has a positive value if the SDS is found seaward of the JARKUS shoreline, or negative if found landward. The test was conducted on a set of 13 images divided into two segments, Zone I and Zone III. Statistical parameters such as maximum landward bias, maximum seaward bias, mean bias, standard deviation and root mean square error (RMSE) are used to analyze the accuracy in shoreline change rate of the SDS. A correlation coefficient (R^2) was used to assess the accuracy of SDSCR. Standard deviation and RMSE are also used to analyze the accuracy in SDVC.

4.4 Results

THIS section first presents the results of the quantitative evaluation of the satellite derived shorelines (SDS). Second, the results of the quantitative evaluation of the SDSCR are presented. Third, the results are presented of the quantitative evaluation of the satellite derived volume changes (SDVC).

4.4.1 Quantitative evaluation of the SDS

Tables 4.2 and 4.3 summarize the SDS error statistics (mean bias, standard deviation, maximum seaward bias, maximum landward bias, and RMSE) obtained for each period analyzed in Zones I and III. The mean bias is obtained by spatially averaging each transect's bias. For Zone I, the annual mean bias between SDS and JARKUS ranges from

Table 4.2: Summary of errors of all transects after the application the methodology to Landsat images in Zone I

Year	Maximum landward bias (m)	Maximum seaward bias (m)	Mean bias (m)	Standard deviation (m)	RMSE(m)	Total numer transects
1985	-63.02	25.52	1.86	13.85	13.98	94
1986	-35.39	32.38	6.96	11.23	13.21	94
1987	-38.35	68.02	8.73	10.98	14.03	112
1988	-59.39	27.50	2.31	12.09	12.31	112
1989	-61.26	26.65	2.75	13.33	13.61	112
1990	-27.22	39.01	17.50	10.01	20.16	112
1998	-30.15	36.24	8.46	8.63	12.09	112
1999	-76.91	35.57	-3.61	14.81	15.24	112
2000	-33.22	40.41	4.32	12.78	13.49	112
2005	-5.56	37.27	12.78	8.57	15.39	112
2006	-6.33	49.30	21.28	8.61	22.95	112
2009	-12.48	58.47	15.84	11.37	19.50	112
2010	-14.65	27.36	6.23	8.94	10.90	112
Mean	-35.69	38.75	8.11	11.17	15.14	109

Table 4.3: Summary of errors of all transects after the application the methodology to Landsat images in Zone III

Year	Maximum landward bias (m)	Maximum seaward bias (m)	Mean bias (m)	Standard deviation (m)	RMSE (m)	Total number transects
1985	-35.38	22.94	0.24	12.25	12.26	120
1986	-56.09	23.23	0.20	13.84	13.84	120
1987	-50.52	31.34	6.35	12.00	13.58	121
1988	-80.40	43.15	2.18	35.15	1.48	121
1989	-93.72	60.53	10.82	25.65	27.83	121
1990	0.95	63.01	24.52	10.84	26.81	121
1998	-14.88	67.96	18.51	17.03	25.16	121
1999	-68.69	72.20	1.92	26.68	26.75	121
2000	-114.47	13.53	-24.63	26.96	36.47	121
2005	-8.39	51.82	16.01	13.56	20.98	121
2006	-20.39	73.35	27.64	14.58	31.25	121
2009	-17.10	80.90	18.96	15.61	24.56	121
2010	-17.08	69.13	16.88	16.22	23.41	121
Mean	-44.32	51.77	9.20	18.49	21.88	121

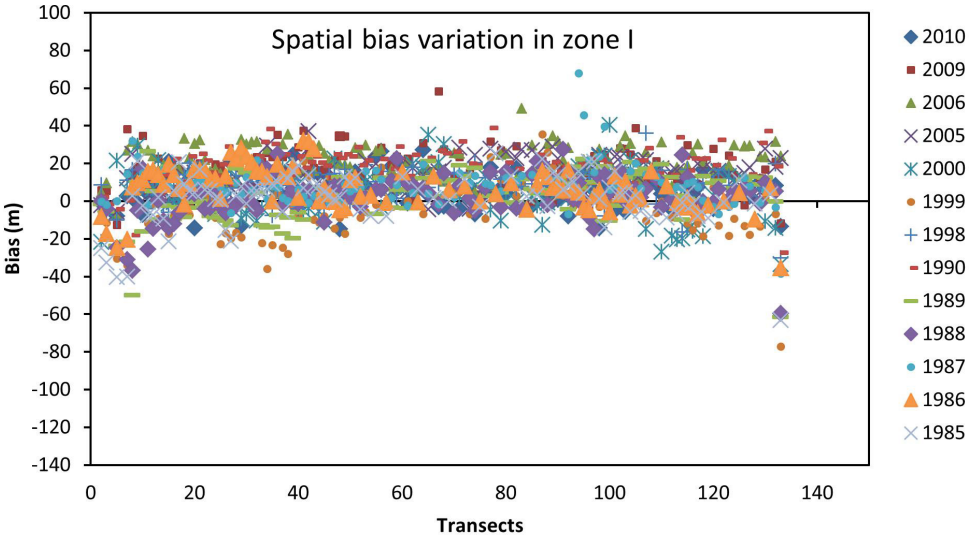

Figure 4.7: The bias along the shoreline through the years 1985 to 2010 in zone I.

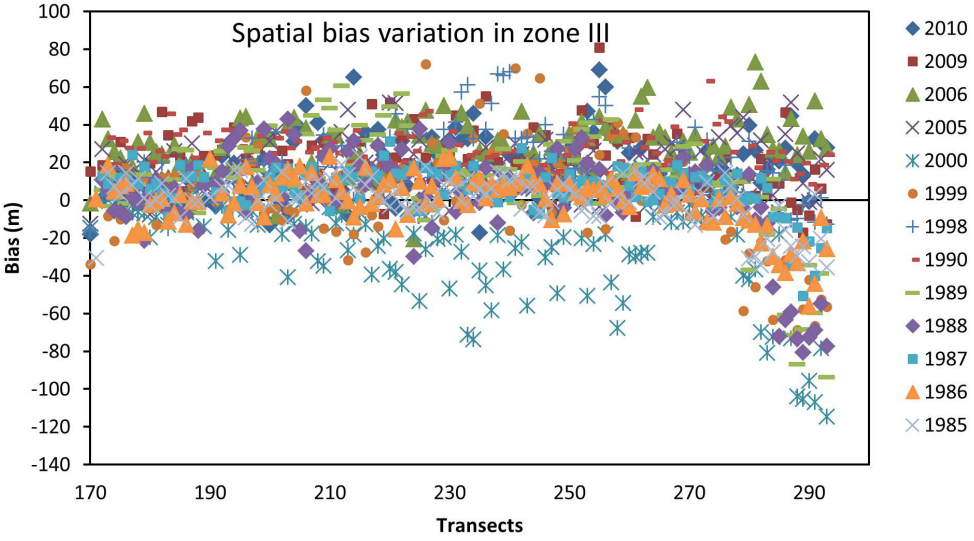

Figure 4.8: The bias along the shoreline through the years 1985 to 2010 in zone III

-3.6m to 21.3m approximately half to one pixel size (15m ÷ 30m) with a temporal average of 8.1m over the 25 year period. For Zone III, the annual mean bias ranges largely from -24.6m to 27.6m with an average of 9.2m over the 25-year period. In general, for the TM images, the mean bias is positive whereas the mean bias of the ETM+ images (1999 and 2000) is negative. It means that the SDS position of the TM images is generally found seaward of the JARKUS position while the position of Landsat ETM+ is generally found landward. The recent study of Pardo-Pascual et al. (2012, 2018),also mentioned different type of images (or different sensors) and different spectral resolutions to have significant effects on extracting the shoreline position.
The standard deviation is stable over time and has an average of 11.2m and 18.5m corresponding to Zone I and Zone III, respectively. The RMSE is stable over time and has an average of 15.1m and 21.9m corresponding to Zone I and Zone III, respectively.
The bias of SDS varies along the length of each zone (Figures 4.7 and 4.8). The greatest variation in bias along the shoreline was observed in Zone III, around transect 280 to transect 293 and was found in the years 1988, 1989, 1999 and 2000. Consequently, the standard deviation for these years is higher and ranges from 25.6m to 35.2m.

4.4.2 Quantitative evaluation of the SDSCR

Table 4.4: Summary of results of SDSCR over different periods (1985-1990, 1990-2000, 2000-2010, 1990-2010, and 1985-2010)

Zone	SDSCR	1985-1990		1990-2000		2000-2010		1990-2010		1985-2010	
	(m/y)	Jarkus	SDS	Jarkus	SDS	Jarkus	SDS	Jarkus	SDS	Jarkus	SDS
Zone I	Min	-2.17	-1.88	-2.77	-3.11	-4.36	-3.89	-1.14	-1.67	-0.25	-0.53
	Max	13.64	17.43	5.78	2.90	6.84	6.61	3.61	3.09	2.85	2.72
	Average	3.14	5.82	0.69	-0.91	1.15	0.52	0.94	0.51	1.20	1.06
Zone III	Min	-7.89	-0.53	-6.29	-7.20	-6.87	-4.14	-2.36	-2.60	-0.65	-0.35
	Max	13.12	18.03	12.26	5.20	6.39	8.08	6.09	5.15	6.51	6.11
	Average	3.15	8.80	1.67	-1.39	-0.04	2.29	0.80	0.51	1.57	1.67

Table 4.5: Summary of errors of SDSCR over different periods (1985-1990, 1990-2000, 2000-2010, 1990-2010, and 1985-2010)

Periods	Mean error (m/y)		Std(m/y)		RMSE (m/y)		R^2	
	Zone I	Zone III	Zone I	Zone III	Zone I	Zone III	Zone I	Zone III
1985-1990	2.69	5.59	2.35	2.69	3.57	6.20	0.56	0.57
1990-2000	-1.60	-3.06	1.27	2.32	2.05	3.84	0.38	0.56
2000-2010	-0.63	2.35	1.43	2.00	1.56	3.09	0.64	0.50
1990-2010	-0.43	-0.30	0.48	0.72	0.64	0.78	0.83	0.79
1985-2010	-0.14	0.10	0.32	0.46	0.35	0.47	0.77	0.89

The results of the SDSCR assessed at two different zones and over five different periods averaged over all transects are given in Figure 4.9 and Table 4.4 and 4.5. The calculations were divided into five different time spans (1985-1990, 1990-2000, 2000-2010,

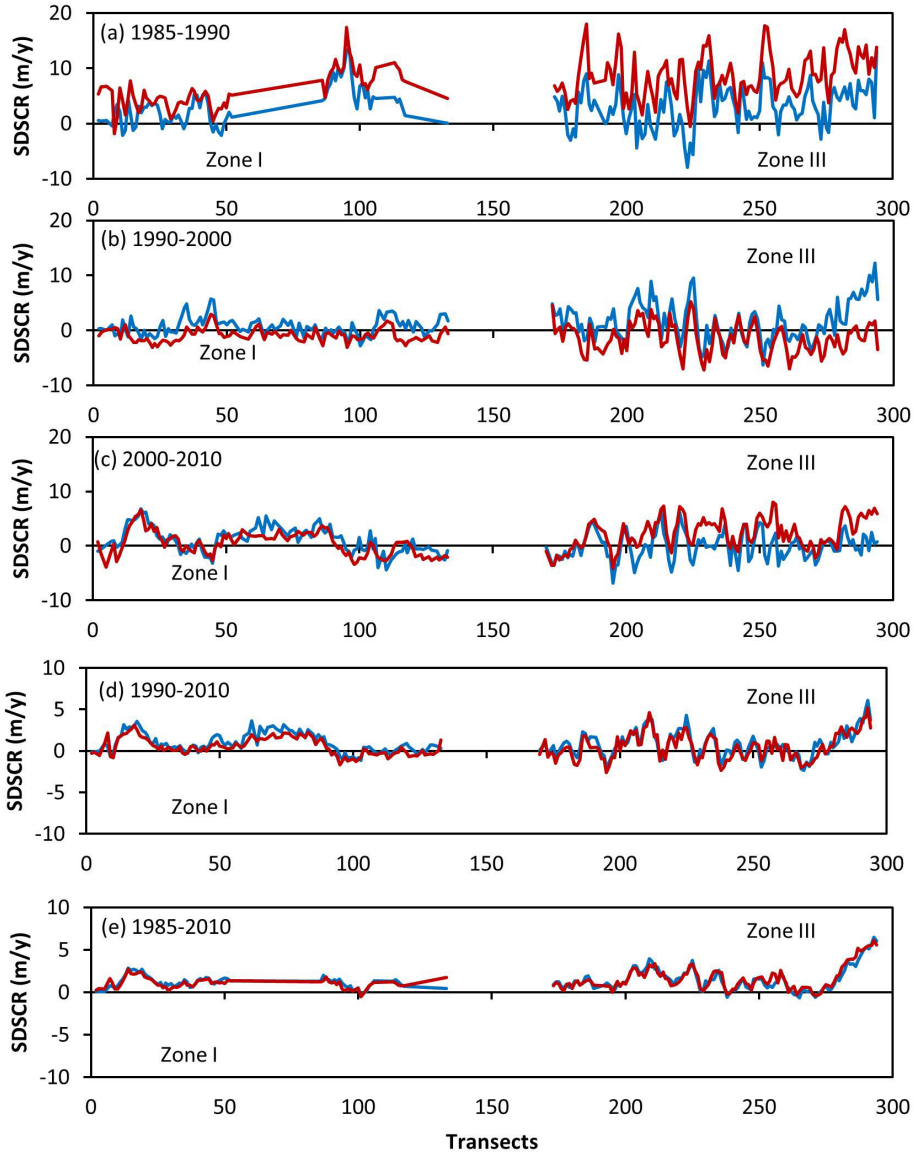

Figure 4.9: Results of calculated shoreline changes during (a) 1985-1989, (b)1990-2000, (c) 2000-2010, (d) 1990-2010 and (e) 1985-2010. The blue lines are shoreline changes from JARKUS and the red lines are shoreline changes from SDSCR.

1990-2010, and 1985-2010).
The results obtained for SDSCRs from JARKUS and SDS data are shown in Table 4.4 and Figure 4.9. In general, both JARKUS and SDS data also show much change in shoreline position between 1985 and 1990 with an average accretion rate of 3.1 m/y (JARKUS) and 5.8 m/y (SDS) in zone I and with an average accretion rate of 3.1 m/y (JARKUS) and 8.8 m/y (SDS) in zone III. For the other periods, 1990-2000, and 2000-2010 the shoreline trends in both JARKUS and SDS data indicate less regular changes in accretion and erosion. For the long term period, 25 years (1985-2010), the shoreline change shows accretion in both datasets, JARKUS and SDS with a similar average rate of 1.2 m/y (JARKUS) and 1.1 m/y (SDS) in zone I and of 1.6 m/y (JARKUS) and 1.7 m/y (SDS) in zone III. In general, the SDSCR show a better agreement in both zones I and III for the period of 25 years (1985-2010). This observation is supported by the derived standard deviations and RMSE that decrease with increasing time intervals (see Table 4.5). The highest standard deviation (Std) and RMSE are observed in a period of 5 years (1985-1990) while the lowest Std and RMSE are found in a period of 25 years (1985-2010). Moreover, the SDSCR within the period 1990-2010 and 1985-2010 show a higher correlation coefficient (R^2 >0.77) while a lower correlation coefficient (R^2 <0.69) is observed in the cross-correlation of the other periods (1985-1990, 1990-2000, and 2000-2010).

4.4.3 Quantitative evaluation of SDVCs

Table 4.6: Summary of results of SDVC over different periods (1985-1990, 1990-2000, 2000-2010, 1990-2010, and 1985-2010).

Zone	SDVC	1985-1990		1990-2000		2000-2010		1990-2010		1985-2010	
	(10^3m/y)	Jarkus	SDS	Jarkus	SDS	Jarkus	SDS	Jarkus	SDS	Jarkus	SDS
Zone I	Min	-64.38	-8.81	-5.63	-15.75	-2.23	-17.14	-0.37	-8.28	-0.88	-2.34
	Max	33.60	180.86	38.86	13.44	34.14	29.50	20.95	13.79	10.14	10.62
	Average	-5.45	29.12	5.27	-4.05	12.17	2.64	8.05	2.28	4.43	4.79
Zone III	Min	-25.67	-3.02	-53.45	-53.75	-16.09	-32.08	-6.85	-17.29	-6.22	-2.16
	Max	92.71	162.83	31.50	36.37	23.10	60.55	43.33	32.63	22.28	39.15
	Average	1.53	55.50	5.89	-8.92	3.68	15.61	5.86	3.38	4.55	10.38

Table 4.7: Summary of errors of SDVC over different periods (1985-1990, 1990-2000, 2000-2010, 1990-2010, and 1985-2010)

Periods	Mean error (10^3m^3/y)		Std(10^3m^3/y)		RMSE (10^3m^3/y)	
	Zone I	Zone III	Zone I	Zone III	Zone I	Zone III
1985-1990	34.57	53.97	21.73	30.56	40.84	62.02
1990-2000	-8.99	-14.81	6.51	14.90	11.11	21.01
2000-2010	-9.54	11.94	6.90	16.65	11.77	20.49
1990-2010	-5.77	-2.48	3.79	7.25	6.90	7.66
1985-2010	-0.37	5.84	2.44	5.03	2.47	7.71

The results of SDVC along the coast are shown in Figure 4.10 and Table 4.6 and 4.7. Overall, both JARKUS and SDVC show much change in volume over the period 1985 and

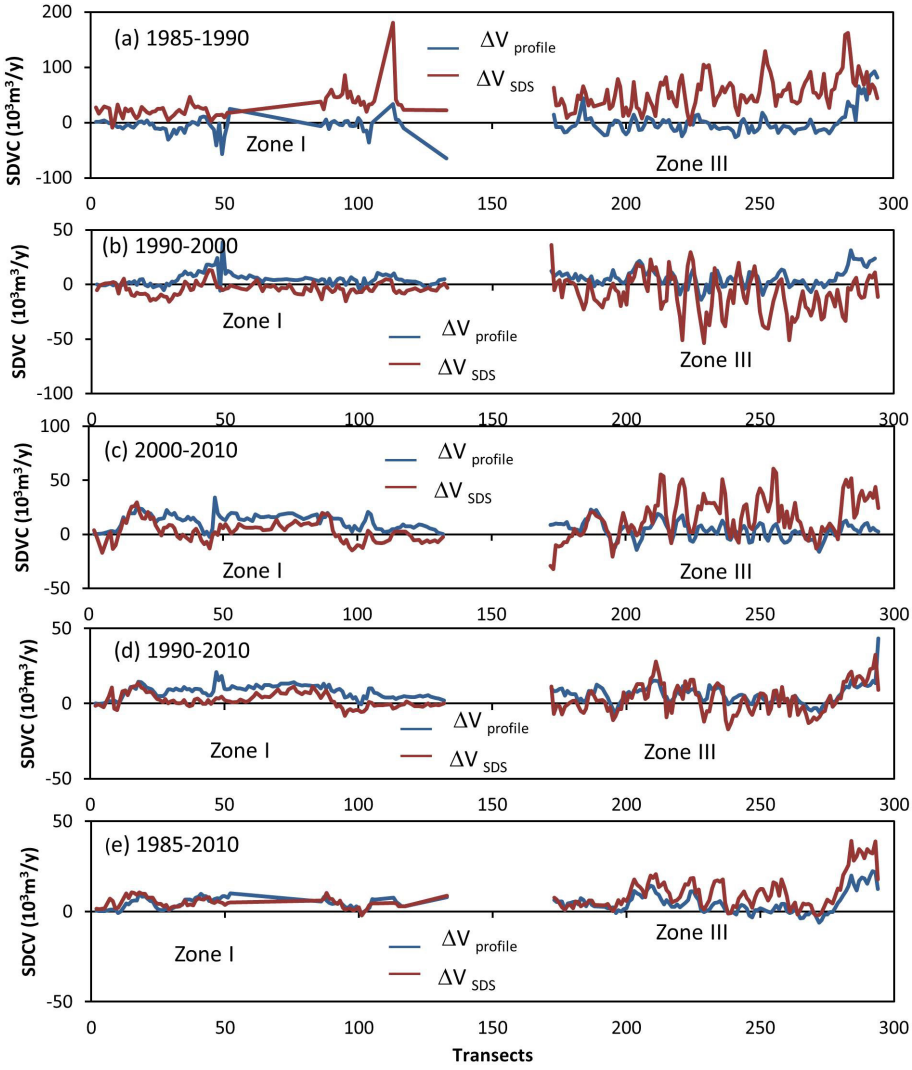

Figure 4.10: Results of calculated volume changes over different periods (a) 1985-1989, (b)1990-2000, (c) 2000-2010, (d) 1990-2010 and (e) 1985-2010. The blue lines are volumes from JARKUS and the red lines are volumes from SDVC

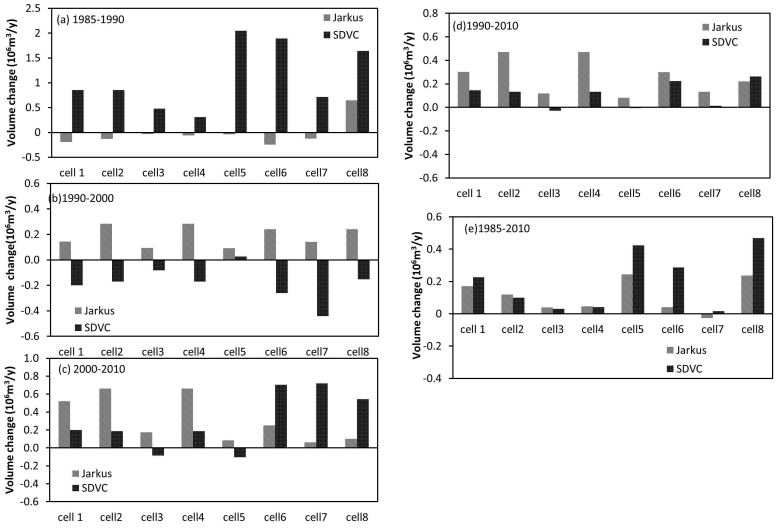

Figure 4.11: Volume changes through each cell over different periods

1990. During that period, the SDVC varies between -8.8 x10^3 m^3/y to 180.8 x10^3 m^3/y with an average of 29x10^3 m^3/y over zone I (Table 4.6). In the period 1990 to 2000 both JARKUS and SDVC also show irregular changes in volume along the coast in both zones. Mean volume changes of SDVC indicate negative values (-4.0 x10^3 m^3/y (zone I) and -8.9 x10^3 m^3/y (zone III) while mean values of JARKUS data show positive values (5.3x10^3 m^3/y (zone I) and 5.9 x10^3 m^3/y (zone III). In the other periods, 2000-2010, 1990-2010 and 1985-2010 the mean values of volume change in both data sets show positive values. Table 4.7 summarizes the SDVC error statistics (mean error, standard deviation, and RMSE) obtained for each period analyzed in Zones I and III. The largest differences in volume changes between the JARKUS and SDVC were found over the 5 y period 1985-1990 with highest mean errors varying from 35 x10^3 m^3/y (zone I) and 54 x10^3 m^3/y (zone III). The smallest difference in volume changes were found over the 25 year period 1985-2010 with mean errors varying from 0.4 x10^3 m^3/y (zone I) to 5.8 x10^3 m^3/y (zone III). This observation is supported by the derived standard deviations and RMSE presented in Table 4.7. The highest standard deviation and RMSE were found over a 5-year period (1985-1990). The smallest standard deviation and RMSE were observed over a 20-year period (1990-2010) and in a 25-year period (1985-2010). Over the 25-years period RMSE of SDVC are ranging from 2.5 x10^3 m^3/y (zone I) to 7.7 x10^3 m^3/y (zone III). Figure 4.11 shows the volume changes of each cell for both JARKUS and SDVC for different periods. The volumes of each cell are calculated by summing all transect values of each cell. The blue columns indicate the volume derived from JARKUS while the red column indicates the volume derived from SDVC. For the period 1985-1990 (Figure 4.11a) and the period 1990 -2000 (Figure 4.11b) the SDVCs show many differences in trends and magnitudes of the volume compared with the volume derived from JARKUS. For the other periods, 2000-2010 (Figure 4.11c) and 1990-2010 (Figure 4.11d) general trends SDVCs are quite similar compared with volume trends of JARKUS, both indicating that

almost all coastal cells are accreting. However, the magnitudes of the SDVC in some cells are underestimated or overestimated compared with JARKUS. For instance, in Figure 4.11c all cells in zone I the SDVC underestimate volumes while the other three cells (6, 7 and 8) in zone III overestimate the volumes. For the period 1985-2010 (a 25-year period) the SDVCs show a good agreement in both trends and magnitudes especially for the first four cells in zone I (Figure 4.11e). It seems the SDVCs show a better result over long-term periods (over 25 years) than the short term periods (5 years to 10 years).

4.5 Discussion

The comparison between Satellite data and JARKUS data over different periods provides a better understanding of the capabilities of using satellite images in shoreline identification and shoreline change rates as well as volume changes. The evaluation revealed that the extracted SDSs at the North-Holland coast have a seaward bias compared to JARKUS measurements of 8.1m and 9.2m for Zone I and Zone III. This is in line with current, be it very scarce, literature.
The seaward displacement of SDS relative to the JARKUS shoreline could be explained by light absorption by seawater and it might vary depending on water transparency (García-Rubio et al., 2015). For regions having higher turbidity, perhaps slightly higher wave conditions could increase the seaward displacement. However, the magnitude of these effects is still not known and needs further research. Very recently Pardo-Pascual et al., 2018 evaluate the accuracy of shoreline position obtained from Landsat 7, Landsat 8, and Sentinel-2 imagery on a natural beach and in a port in Valencia, Spain. The results indicate variability brightness in the terrestrial zone influences shoreline detection, brighter zones cause a small landward bias while darker zones move them seaward.
The results of shoreline change rates indicate a better agreement between the JARKUS and the SDS over longer periods (20-25 years) compared to shorter periods (5-10 years). The smallest standard deviation and RMSE were found over a 25-year period. (Table 4.4 and 4.5). The standard deviation and RMSE values increase with a decreasing period. Moreover, the highest RMSE values were found for zone III in the region near IJmuiden harbour having a large intertidal width. In terms of the correlation coefficient (R^2), the SDSCR shows a strong relationship ($R^2 > 0.78$) over the period 1990-2010 and 1985-2010 (Table 4.5). These high values mean that the SDSCR can be used better to quantify the beach change trends over a 25-years period than over shorter periods (5-10 years). The SDSCR methodology can be used to derive shoreline change rates comparable to those derived from JARKUS. On the other hand, lower regression coefficients values ($R^2 < 0.7$) are observed in the cross-validation of SDSCR over the shorter periods (a 5-year), indicating more uncertainty of SDSCR over the shorter periods. Probably, the longer periods rely on more data points and thereby averaging the short term variability in shoreline position leading to more reliable results. This could explain why the SDSCR has better results over periods of 20 years to 25 years than those results obtained over a 5 years period. Almonacid-Caballer et al. (2016) suggest using annual mean shoreline positions extracted from Landsat to avoid short term variability by averaging the instantaneous shoreline positions registered during the same year. Additionally, a larger time scale means larger absolute shoreline changes and a larger signal to noise ratio. This is

clearly indicated in transect 290 (corresponding to profile 7005400 in Figure 4.12a), the absolute shoreline change during a 20 year period (1990-2010) is larger than that during a 5 year period (1985-1990).
The results of SDVC also indicate better results over a 20 year to a 25 year period when compared to a 5 year period. This is reflected by the smallest mean error, standard deviation and RMSE. Since the volume changes have been calculated based on the results of the SDSCR similar results between SDVC and SDSCR are to be expected. Using satellite images to observe shoreline changes and volume changes seems to work better when considering longer periods (over 20 years) than shorter periods. The larger error in estimated volume change rates over shorter time periods could be explained by highly dynamic variations of the profile shape on the time scale of events (Bosboom and Stive, 2012). On timescales shorter than a year, dynamic variations of the upper shoreface profile may exist due to seasonal variations, cyclic behavior of bars and episodic changes (dune erosion). On longer timescales, Bosboom and Stive (2012) observed JARKUS profiles over period 1964 and 2008 where its measured profile variations remain in a steady envelope. This observation may explain why the results of SDVC over a long term period yield better results than over a short term period.
The different trends in calculating volume changes from satellite and from JARKUS occurring in some transects might be explained by changes in profile shape. The SDVC from Landsat assumes profiles are static and translated horizontally in seaward and landward direction with accretion and erosion respectively (Figure 4.5). Whereas the JARKUS profiles (Figure 4.6) do not exactly follow this assumption and changes in profile shape occur. That means that some JARKUS transects show a positive volume change while experiencing shoreline erosion and vice versa. See for example Figure 4.12b.
To test the validity of the stationary profile assumption, the volume estimated based on

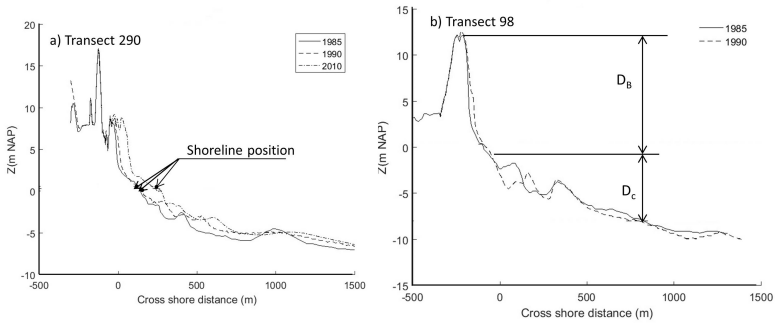

Figure 4.12: Profile 7005400 (transect 290) and profile 7004565 (transect 98) in year 1985, 1990 and 2010

shoreline change rates from the JARKUS data (ΔV_{jarkus} (m^3/y)), were compared with the volume changes that measured from profiles ($\Delta V_{profile}$ (m^3/y)). Figure 4.13 indicates the volume change rates along the coast and correlation between the JARKUS (ΔV_{jarkus}, blue line), the SDS (ΔV_{SDS}, red line), and the JARKUS profile ($\Delta V_{profile}$, green line) over the period 1985 and 2010. Figure 4.13d shows clearly the correlation between the volume changes from the same data but using a different methodology. One is estimated from the shoreline change rate using the assumption of a static profile. While the other is

estimated directly from the measured profile. The dash line indicates the 1:1 regression line while the continuous line indicates the actual regression line. The correlation analysis shows a significant positive correlation between the $\Delta V_{profile}$ and the ΔV_{jarkus} (R^2= 0.7). The $\Delta V_{profile}$ implies a general underestimation compared to the ΔV_{jarkus} with the bigger bias occurring at the higher volume changes. Although the results indicate the correlation is acceptable the cause of the bias could be subject of further research.

This study enables to make a quantitative assessment of intertidal zone properties that

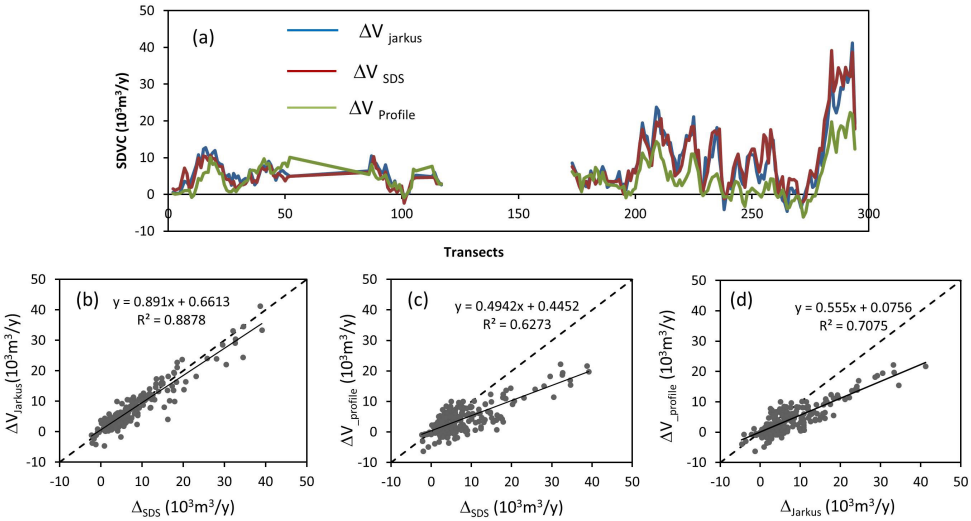

Figure 4.13: Comparision estimated volume changes and its correlation between derived from SDS, from JARKUS profiles and from shoreline change rates of JARKUS shorelines

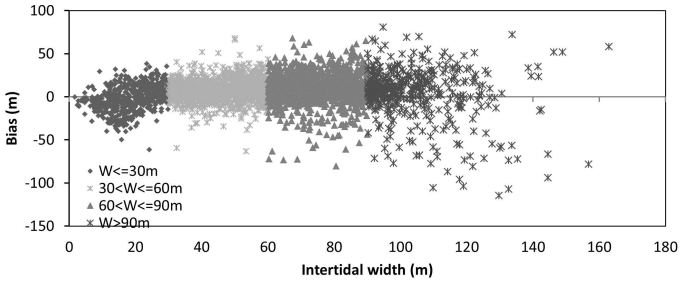

Figure 4.14: Relationship between intertidal width and bias

causes deviation of SDS from JARKUS data. The hypothesis is that the width of the intertidal zone (W) is an important factor in explaining displacement of SDS.

Figure 4.14 indicates the relationship between the bias (difference between Landsat shoreline position and JARKUS shoreline position) and W. The definition of W is the horizontal distance between the mean high water (MHW) and mean low water (MLW) and is estimated from JARKUS profiles. A relationship is investigated between W in terms of

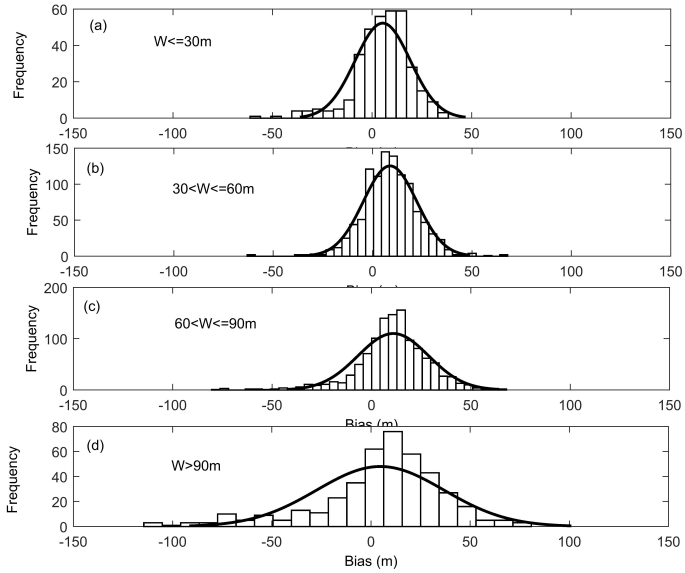

Figure 4.15: Histogram of errors on intertidal zone widths, with the normal adjusted curve superimposed in black

pixel size (30m) and the bias. Consequently, different classes are distinguished where W ranges between one pixel to two pixels (30<W<=60m); W ranges between two pixels to three pixels (60<W<=90m); and W is larger than three pixels (W>90m)). Figure 4.14 indicates that a gentle beach (W> 90m) and a steep beach (W<=30m) show more variation in bias. On wide beaches, this can be explained by the large horizontal range between wet and dry that makes it difficult to identify between land and sea. This observation is similar to the results of the study by Almonacid-Caballer et al. (2016). This study has shown that a relation exists between beach slope and the deviation between annual mean shorelines obtained from RTK-GPS and LiDAR surveys and Landsat. Their study indicates that shorelines in flatter beach segments are more variable during the year than in steeper segments. For a narrow/steep beach, the classification process between land and water is more sensitive to pixel size in relation to the definition of the shoreline. Steep beaches therefore have also more variation in bias.
Figure 4.15 also gives the distribution of the bias for different widths (W) of the intertidal zone. The distributions of the bias seem to follow a normal distribution, in which the smallest standard deviation is found in the range of W from one to two pixel sizes (Figure 4.15b). For W less than one pixel size (Figure 4.15a) and larger than two pixel sizes (Figure 4.15c,d) the distribution of the bias has a larger standard deviation as illustrated by the wider normal distribution curve (the curve in the Figure 4.15). Probably, the derivation of shoreline works best on beaches having intertidal width ranges between one pixel to two pixels (30<W<=60m).

4.6 Conclusions

THIS study used a combination of satellite remote sensing and GIS techniques for the extraction of satellite derived shorelines (SDS), satellite derived shoreline change rates (SDSCR) and satellite derived volume changes (SDVC) from Landsat images. The accuracy of shoreline extraction was assessed using 13 Landsat 5 TM and Landsat 7 ETM+ images acquired between 1985 to 2010 along two coastal segments of the North-Holland coast. Unsupervised classification was applied using the NDWI index to separate sea and land and extract the shoreline from the images. The observed JARKUS shoreline positions derived from the intersection between water level and cross-shore profile at each transect were used to evaluate the error of satellite derived shoreline (SDS) and change rates (SDSCR). The volumes from JARKUS profiles were used to evaluate the accuracy of satellite derived volume changes (SDVC).

The evaluation revealed that the extracted SDS at the North-Holland coast has a seaward bias compared to JARKUS measurements of 8.1m and 9.2m for Zone I and Zone III respectively. The mean standard deviation ranges from 11.1 m to 18.5m and RMSE varies from 15.1m to 21.8m. In all cases of Landsat 5 TM the mean errors tend to indicate a seaward bias whereas for two Landsat 7ETM images the mean errors are landward.

The results of shoreline change rates obtained using regression were applied to both datasets, SDS and JARKUS with five different time periods, a 5-year period, (e.g. 1985-1990), a 10-year period (e.g. 1990-2000, 2000-2010), a 20-year period (e.g. 1990-2010), and a 25-year period (e.g. 1985-2010). Cross-validation of shoreline change rate estimations have been carried out using statistical techniques, namely, the regression coefficient (R^2) and other statistical parameters such as mean error, standard deviation and RMSE.

The SDSCRs indicate a better agreement with JARKUS for longer periods (20-25 years) than for shorter periods (5-10 years). The smallest standard deviation and RMSE were found over a 25-year period. The results of the R^2 of the SDSCRs have higher values (R^2 >0.78) over the 20-year period and 25-year period. The lower correlation values ($R^2 < 0.7$) are observed in the cross-validation of SDSCR during the shorter periods (5-year). The finding of smallest mean error, standard deviation and RMSE and the highest R^2 over the longer period (20 to 25 years) leads to the conclusion that SDSCRs can be derived more successfully over long-term periods than over short term periods.

Similarly, volume changes obtained from shoreline change rates indicate less differences when derived from SDS and JARKUS profiles over long term periods (20 to 25 years) than over short period (5 to 10 years).

Finally, the current study has enabled to reveal that the intertidal width (W) influences the accuracy of SDS. The relationship between bias and intertidal beach width indicates that gentle beaches (W> 90m) and steep beaches (W <=30m) show more variation in the SDS bias. Interestingly, for beaches that have intertidal beach widths ranging from one to two pixel sizes (30-60m) results obtained are better than for wider or narrower beaches.

In summary, the results obtained suggest the possibility of using Landsat imagery as a source for monitoring shoreline change rates and volume change trends over decadal periods. For short term period, the results may be influenced by the signal to noise ratio and the short term variations in cross shore profiles.

References

Almonacid-Caballer, J., Sánchez-García, E., Pardo-Pascual, J. E., Balaguer-Beser, A. A., and Palomar-Vázquez, J. (2016). Evaluation of annual mean shoreline position deduced from landsat imagery as a mid-term coastal evolution indicator. *Marine Geology*, 372:79–88.

Blodget, H., Taylor, P., and Roark, J. (1991). Shoreline changes along the rosetta-nile promontory: Monitoring with satellite observations. *Marine Geology*, 99(1-2):67–77.

Bosboom, J. and Stive, M. J. (2012). *Coastal Dynamics I: Lectures Notes CIE4305*. VSSD.

Bouchahma, M. and Yan, W. (2012). Long-term coastal changes detection system based on remote sensing and image processing around an island. In *Geoinformatics (GEOINFORMATICS), 2012 20th International Conference on*, pages 1–5. IEEE.

Chander, G., Markham, B. L., and Helder, D. L. (2009). Summary of current radiometric calibration coefficients for landsat mss, tm, etm+, and eo-1 ali sensors. *Remote sensing of environment*, 113(5):893–903.

Chen, W.-W. and Chang, H.-K. (2009). Estimation of shoreline position and change from satellite images considering tidal variation. *Estuarine, Coastal and Shelf Science*, 84(1):54–60.

Do, A. T., de Vries, S., and Stive, M. J. (2019). The estimation and evaluation of shoreline locations, shoreline-change rates, and coastal volume changes derived from landsat images. *Journal of Coastal Research (JCR)*, 35(1):56–72.

Du, Z., Bin, L., Ling, F., Li, W., Tian, W., Wang, H., Gui, Y., Sun, B., and Zhang, X. (2012). Estimating surface water area changes using time-series landsat data in the qingjiang river basin, china. *Journal of Applied Remote Sensing*, 6(1):063609.

Ekercin, S. (2007). Coastline change assessment at the aegean sea coasts in turkey using multitemporal landsat imagery. *Journal of Coastal Research*, pages 691–698.

Feyisa, G. L., Meilby, H., Fensholt, R., and Proud, S. R. (2014). Automated water extraction index: A new technique for surface water mapping using landsat imagery. *Remote Sensing of Environment*, 140:23–35.

Foody, G. M., Muslim, A. M., and Atkinson, P. M. (2003). Super-resolution mapping of the shoreline through soft classification analyses. In *Geoscience and Remote Sensing Symposium, 2003. IGARSS'03. Proceedings. 2003 IEEE International*, volume 6, pages 3429–3431. IEEE.

Frazier, P. S., Page, K. J., et al. (2000). Water body detection and delineation with landsat tm data. *Photogrammetric engineering and remote sensing*, 66(12):1461–1468.

García-Rubio, G., Huntley, D., and Russell, P. (2015). Evaluating shoreline identification using optical satellite images. *Marine Geology*, 359:96–105.

Gens, R. (2010). Remote sensing of coastlines: detection, extraction and monitoring. *International Journal of Remote Sensing*, 31(7):1819–1836.

Grigio, A. M., Amaro, V. E., Vital, H., and Diodato, M. A. (2005). A method for coastline evolution analysis using gis and remote sensing—a case study from the guamaré city, northeast brazil. *Journal of Coastal Research*, pages 412–421.

Guariglia, A., Buonamassa, A., Losurdo, A., Saladino, R., Trivigno, M. L., Zaccagnino, A., and Colangelo, A. (2006). A multisource approach for coastline mapping and identification of shoreline changes. *Annals of geophysics*, 49(1).

Gutierres, F., Teodoro, A. C., Reis, E., Neto, C., and Costa, J. C. (2016). Remote sensing technologies for the assessment of marine and coastal ecosystems. In *Seafloor Mapping along Continental Shelves*, pages 69–104. Springer.

Hagenaars, G., de Vries, S., Luijendijk, A. P., de Boer, W. P., and Reniers, A. J. (2018). On the accuracy of automated shoreline detection derived from satellite imagery: A case study of the sand motor mega-scale nourishment. *Coastal Engineering*, 133:113–125.

Hallermeier, R. J. (1978). Uses for a calculated limit depth to beach erosion. In *Coastal Engineering 1978*, pages 1493–1512.

Hinton, C. and Nicholls, R. J. (1999). Spatial and temporal behaviour of depth of closure along the holland coast. In *Coastal Engineering 1998*, pages 2913–2925.

IPCC (2001). Ipcc third assessment report. *World Meteorological Organisation and UNEP http://www. ipcc*.

Karsli, F., Guneroglu, A., and Dihkan, M. (2011). Spatio-temporal shoreline changes along the southern black sea coastal zone. *Journal of Applied Remote Sensing*, 5(1):053545.

Kingston, K. S. (2003). Applications of complex adaptive systems approaches to coastal systems. Technical report, NASA.

Knoester, D. (1990). The morphology of the dutch coastal zone (analysis of the jarkus stock 1964-1986). *Note GWAO-90.010*.

Kuleli, T., Guneroglu, A., Karsli, F., and Dihkan, M. (2011). Automatic detection of shoreline change on coastal ramsar wetlands of turkey. *Ocean Engineering*, 38(10):1141–1149.

Kumar, A. and Jayappa, K. (2009). Long and short-term shoreline changes along mangalore coast, india. *International Journal of Environmental Research*, 3(2):177–188.

Kumar, P. D., Gopinath, G., Laluraj, C., Seralathan, P., and Mitra, D. (2007). Change detection studies of sagar island, india, using indian remote sensing satellite 1c linear imaging self-scan sensor iii data. *Journal of Coastal Research*, pages 1498–1502.

Lawrence, P. L. (1994). Natural hazards of shoreline bluff erosion: a case study of horizon view, lake huron. In *Geomorphology and Natural Hazards*, pages 65–81. Elsevier.

Liu, H. and Jezek, K. (2004). Automated extraction of coastline from satellite imagery by integrating canny edge detection and locally adaptive thresholding methods. *International Journal of remote sensing*, 25(5):937–958.

Liu, H., Wang, L., Sherman, D. J., Wu, Q., and Su, H. (2011). Algorithmic foundation and software tools for extracting shoreline features from remote sensing imagery and lidar data. *Journal of Geographic Information System*, 3(02):99.

L.Miller, T. and H.Flectcher, C. (2003). Waikiki: Historical analysis of an engineered shoreline. *Journal of Coas*, 19(4):1026–1043.

Lu, D. and Weng, Q. (2007). A survey of image classification methods and techniques for improving classification performance. *International journal of Remote sensing*, 28(5):823–870.

Maiti, S. and Bhattacharya, A. K. (2009). Shoreline change analysis and its application to prediction: a remote sensing and statistics based approach. *Marine Geology*, 257(1-4):11–23.

Mason, D., Davenport, I., and Flather, R. (1997). Interpolation of an intertidal digital elevation model from heighted shorelines: a case study in the western wash. *Estuarine, Coastal and Shelf Science*, 45(5):599–612.

McFeeters, S. K. (1996). The use of the normalized difference water index (ndwi) in the delineation of open water features. *International journal of remote sensing*, 17(7):1425–1432.

Minneboo, F. (1995). Jaarlijkse kustmetingen: Richtlijnen voor de inwinning, bewerking, en opslag van gegevens van jaarlijkse kustmetingen. Technical report, Rijkswaterstaat, RIKZ.

Muslim, A. M., Foody, G. M., and Atkinson, P. M. (2006). Localized soft classification for super-resolution mapping of the shoreline. *International Journal of Remote Sensing*, 27(11):2271–2285.

Noernberg, M. A. and Marone, E. (2003). Spatial-temporal monitoring of the paranagua bay inlet margins using multispectral landsat-tm images. *Journal of Coastal Research*, SI 35:221–231.

Ojeda, E. (2008). Shoreline and nearshore bar morphodynamics of beaches affected by artificial nourishment.

Pajak, M. J. and Leatherman, S. (2002). The high water line as shoreline indicator. *Journal of Coastal Research*, 18(2):329–337.

Pardo-Pascual, J. E., Almonacid-Caballer, J., Ruiz, L. A., and Palomar-Vázquez, J. (2012). Automatic extraction of shorelines from landsat tm and etm+ multi-temporal images with subpixel precision. *Remote Sensing of Environment*, 123:1–11.

Pardo-Pascual, J. E., Sánchez-García, E., Almonacid-Caballer, J., Palomar-Vázquez, J. M., Priego de los Santos, E., Fernández-Sarría, A., and Balaguer-Beser, Á. (2018). Assessing the accuracy of automatically extracted shorelines on microtidal beaches from landsat 7, landsat 8 and sentinel-2 imagery. *Remote Sensing*, 10(2):326.

Phinn, S. R., Menges, C., Hill, G. J., and Stanford, M. (2000). Optimizing remotely sensed solutions for monitoring, modeling, and managing coastal environments. *Remote Sensing of Environment*, 73(2):117–132.

Pianca, C., Holman, R., and Siegle, E. (2015). Shoreline variability from days to decades: Results of long-term video imaging. *Journal of Geophysical Research: Oceans*, 120(3):2159–2178.

Plant, N. G., Aarninkhof, S. G., Turner, I. L., and Kingston, K. S. (2007). The performance of shoreline detection models applied to video imagery. *Journal of Coastal Research*, pages 658–670.

Rokni, K., Ahmad, A., Selamat, A., and Hazini, S. (2014). Water feature extraction and change detection using multitemporal landsat imagery. *Remote Sensing*, 6(5):4173–4189.

Rosati, J. D. (2005). Concepts in sediment budgets. *Journal of Coastal Researchr*, 212:307–322.

Rosati, J. D., Gravens, M. B., and Smith, W. G. (1999). Regional sediment budget for fire island to montauk point, new york, usa. Technical report, ARMY ENGINEER WATERWAYS EXPERIMENT STATION VICKSBURG MS COASTAL AND HYDRAULICS LAB.

Rosati, J. D. and Kraus, N. C. (1999). Formulation of sediment budgets at inlets. Technical report, ENGINEER RESEARCH AND DEVELOPMENT CENTER VICKSBURG MS COASTAL AND HYDRAULICS LAB.

Rouse Jr, J., Haas, R., Schell, J., and Deering, D. (1974). Monitoring vegetation systems in the great plains with erts.

Ruggiero, P., Kaminsky, G. M., Gelfenbaum, G., and Voigt, B. (2005). Seasonal to interannual morphodynamics along a high-energy dissipative littoral cell. *Journal of Coastal Research*, pages 553–578.

Sánchez-García, E., Pardo-Pascual, J., Balaguer-Beser, A., and Almonacid-Caballer, J. (2015). Analysis of the shoreline position extracted from landsat tm and etm+ imagery. *The International Archives of Photogrammetry, Remote Sensing and Spatial Information Sciences*, 40(7):991.

Shen, L. and Li, C. (2010). Water body extraction from landsat etm+ imagery using adaboost algorithm. In *In Proceedings of 18th International Conference on Geoinformatics*, pages 1–4.

Sherman, D. J. and Bauer, B. O. (1993). Coastal geomorphology through the looking glass. *Geomorphology*, 7:225–249.

Stolk, A. (1989). Zandsysteem kust : een morfologische karakterisering. Technical report, Ministerie van Verkeer en Waterstaat, GEOPRO.

Teodoro, A. C. (2016). Optical satellite remote sensing of the coastal zone environment—an overview. In *Environmental Applications of Remote Sensing*. InTech.

Teodoro, A. C., Gutierres, F., Gomes, P., and Rocha, J. (2018). Remote sensing data and image classification algorithms in the identification of beach patterns. In *Beach Management Tools-Concepts, Methodologies and Case Studies*, pages 579–587. Springer.

Thieler, E. R., Himmelstoss, E. A., Zichichi, J. L., and Ergul, A. (2009). The digital shoreline analysis system (dsas) version 4.0-an arcgis extension for calculating shoreline change. Technical report, US Geological Survey.

Tyagi, P. and Bhosle, U. (2011). Atmospheric correction of remotely sensed images in spatial and transform domain. *International Journal of Image Processing*, 5(5):564–579.

van Rijn, L., Ruessink, B. G., and Mulder, J. (2002). *Coast3D-Egmond: The Behaviour of a Straight Sandy Coast on the Time Scale of Storms and Seasons: Process Knowledge and Guidelines for Coastal Management: End Document, March 2002*. Aqua Publications.

Van Rijn, L. C. (1997). Sediment transport and budget of the central coastal zone of holland. *Coastal Engineering*, 32(1):61–90.

Wang, C., Zhang, J., and Ma, Y. (2010). Coastline interpretation from multispectral remote sensing images using an association rule algorithm. *International Journal of Remote Sensing*, 31(24):6409–6423.

White, K. and Asmar, H. M. E. (1999). Monitoring changing position of coastlines using thematic mapper imagery, an example from the nile delta. *Geomorphology*, 29:93–105.

Wijnberg, K. M. (2002). Environmental controls on decadal morphologic behaviour of the holland coast. *Marine Geology*, 189(3-4):227–247.

Wilson, E. H. and Sader, S. A. (2002). Detection of forest harvest type using multiple dates of landsat tm imagery. *Remote Sensing of Environment*, 80(3):385–396.

W.Muttitanon and N.K.Tripathi (2005). Land use/land cover changes in the coastal zone of ban don bay, thailand using landsat 5 tm data. *International Journal of Remote Sensing*, 26(11):2311–2323.

Xu, H. (2006). Modification of normalised difference water index (ndwi) to enhance open water features in remotely sensed imagery. *International journal of remote sensing*, 27(14):3025–3033.

Zuzek, P. J., Nairn, R. B., and Thieme, S. J. (2003). Spatial and temporal considerations for calculating shoreline change rates in the great lakes basin. *Journal of Coastal Research*, pages 125–146.

Chapter 5

Planform Stability of A Complex Embayed Beach

The best way to have a good idea is
to have a lot of ideas.

Linus Pauling

This study presents an analysis of the planform stability of the complex embayed beach system of Da Nang Bay, Central Vietnam. As a result of the intensification of extreme weather conditions and human activities in this area (e.g. land reclamation, river damming, coastal structures), coastal safety as well as economic and ecological values are under pressure. In order to anticipate future changes in the system, it is important to understand the morphological stability of the beaches in Da Nang Bay. To obtain additional insight into planform stability of complex embayed beaches, we first applied the simple Parabolic Bay Shape Equation (PBSE) to 26 less complex embayed beaches on the central coast of Viet Nam to investigate its utility and interpretation. Shoreline change rates, derived from Landsat images, were used to evaluate the planform stability of the bay beaches with special attention to difficulties when determining the state of equilibrium due to multiple diffraction points. Subsequently , the PBSE and shoreline change rate were used to investigate the planform stability of the very complex headland of Da Nang Bay, also considering the influence of a seasonal wave climate. The PBSE and shoreline change rate analyses have successfully evaluated the planform stability of various headland bay beaches along the central coast of Viet Nam . We are therefore encouraged to use the PBSE equation to predict the development of the bay, which may be single bays bounded by two headlands, or one headland and the absence of rivers discharge . However, for a very complex headland, such as Da Nang Bay, uncertainty regarding the updrift control points continues to exist due to the complex shape of the updrift headland. The complexity of Da Nang Bay leads to uncertainties with respect to the selection of both down- and updrift control points associated with the PBSE. Especially the occurring bi-modal wave conditions in the

Parts of this chapter have been published in 36th IAHR World Congress Do et al. (2015).

East Sea and the seasonal availability of sediment from the two rivers discharging in Da Nang Bay might lead to a difficult interpretation of the PBSE. We have used the shallow water wave propagation model Delft3D WAVE to predict local wave conditions inside the bay and we have found that seasonality within the wave signal in the East Sea does not affect the local wave direction inside Da Nang Bay. Therefore, additional process based modelling might provide more information on the impact of sediment supply into the Da Nang Bay.

5.1 Introduction

HEADLAND bay beaches can be found in many countries over the world. In general, they occupy about 50% of the world's coastlines with different sizes, shapes and geometry (Hsu et al., 2010) . In most cases, these beaches are asymmetric in shape, characterized by a curved shadow zone, a gently curved middle transition zone, and distally by a relatively straight tangential end downcoast (Silvester and Hsu, 1997; Sivester and Hsu, 1993;Short, 1999). The distinguished curved shoreline planform has attracted researchers to define the equilibrium shoreline planform using different models. These models include the logarithmic spiral (Yasso (1950)), the parabolic bay shape (HSU and EVANS (1989); Silvester and Hsu (1997); Sivester and Hsu (1993)), and hyperbolic tangent (Moreno and Kraus (1999)). Among these models, the Parabolic Bay Shape Equation (PBSE) of HSU and EVANS (1989) is now the most accepted and commonly used to determine the static equilibrium shape of a Headland Bay Beach (HBB) along many locations around the world. The PBSE is used to predict planform stability at coasts worldwide, for example the coast of Santa Catarina State, Brazil (Silveira et al., 2010; Klein et al., 2010), the west and south coast of Portugal (Oliveira and Barreiro, 2010; andGama et al., 2011), beaches in northern Ireland (Jackson and Cooper, 2010), beaches on the Catalan Coast, Spain (Bowman et al., 2009), the coast in Thailand (Tasaduak et al., 2014), the East coast of Penisular Maylaysia (Razak et al., 2018) and the coast in China (Tong et al., 2014; Yu and Chen, 2011) and many others.

Da Nang Bay (Figure 5.1), a very complex headland in central Viet Nam with attached sea port, is located north of Da Nang city. It is bounded by the Hai Van Mountain to the north, bay beach Nam O to the west and the Son Tra Peninsula to the east. The Nam Chon cape is located at the foot of Hai Van pass, between the Nam O beach and Isabelle promontory. Nam Chon cape is known as the most natural sandy beach in Da Nang, partly due to the difficult access to this bay. There are two seasonal rivers discharging into Da Nang Bay, the Cu De River from the west and the Song Han River from the south. Due to its geographical location, Da Nang is one of the cities in Viet Nam that is most affected by natural disasters and extreme weather conditions (Dieu, 2012). During the last decades, several coastal structures were built in Da Nang Bay, such as seawalls, breakwaters, dams and bridges, as well as other human interventions, such as land reclamations for the construction of luxurious resorts. These human activities together with the effects of climate change potentially pose a threat to the coastal safety of Da Nang Bay.

The parabolic bay shape equation, developed by HSU and EVANS (1989) defines the static equilibrium planform of an embayment using a single representative wave direction, Down-coast Control Point (DCP) and wave diffraction point. It uses a second-order polynomial based on fitting 27 mixed cases of 14 prototype and 13 model bays that are believed to be in static equilibrium. Their equation for the parabolic shape of a headland-bay beach in static equilibrium has the general form of

$$\frac{R}{R_0} = C_0 + C_1(\frac{\beta}{\theta}) + C_2(\frac{\beta}{\theta})^2 \tag{5.1}$$

where there are two basic parameters, β and R_o (See also Figure 5.2). β is the reference wave obliquity angle, which is the angle between the incident wave crest (assumed linear) at the wave diffraction point and the control line R_o, joining the updrift diffraction

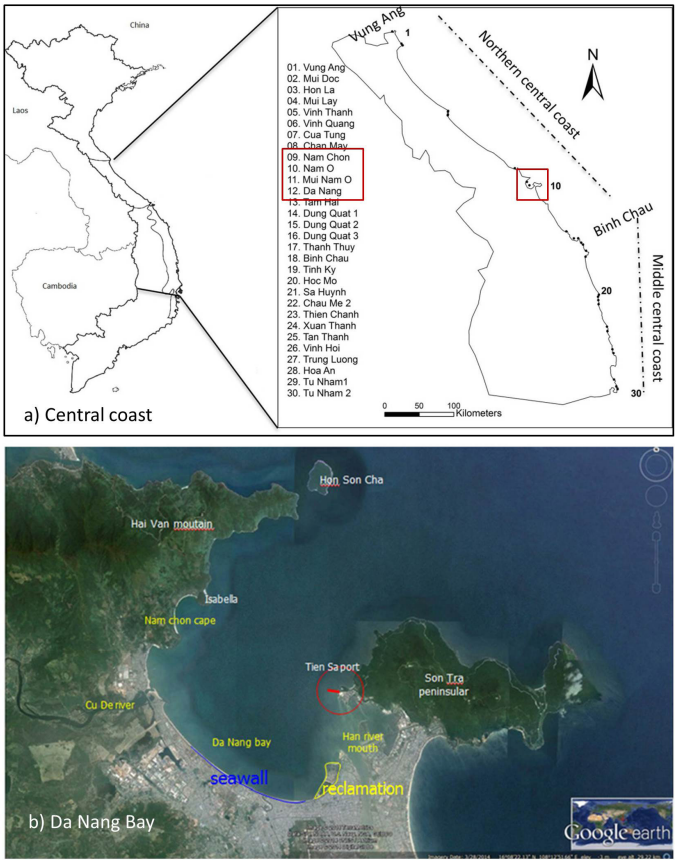

Figure 5.1: Central coast of Viet Nam (a) and Da Nang Bay (b)

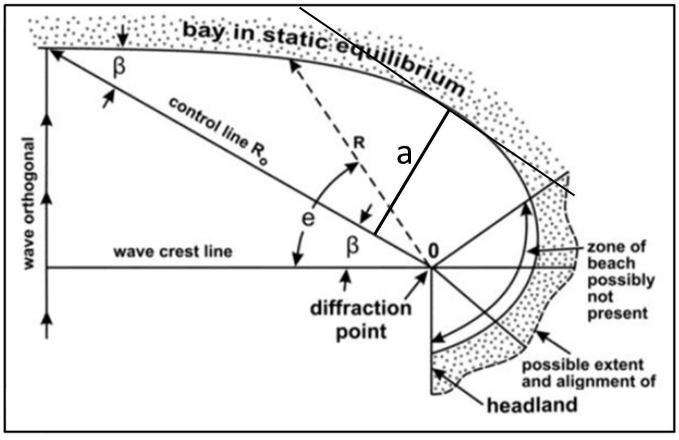

Figure 5.2: Definition sketch for the parabolic bay shape model (HSU and EVANS (1989), adapted by Lausman et al. (2010)

point to the near straight downdrift beach. The radius R to any point on the bay periphery in static equilibrium is at an angle θ from the same wave crest line radiating out from the wave diffraction point. The three constants (C_o, C_1 and C_2) differ with reference angle β (HSU and EVANS, 1989). These constants are bounded between -1.0 and 2.5 for the usual range of β from 10° to 80° applicable in most field conditions (Sivester and Hsu, 1993). The highest indentation, (a) is also measured normal from the control line (R_o) to the point of largest retreat of the shoreline (Silvester and Hsu, 1997).

In terms of planform stability Hsu et al. (2008) classified the headland bay beaches with three different stability conditions, e.g. static equilibrium, dynamic equilibrium and unstable or natural reshaping. If the existing embayed beach shoreline conforms well to the PBSE, the beach is said to be stable in Static Equilibrium Planform (SEP). It means that the shoreline of SEP is stable without long-term erosion or deposition. If the predicted SEP is landward of the existing shoreline, the bay beach is said to be in Dynamic Equilibrium Planform (DEP). This implies either a dynamic equilibrium, when the existing sediment balance is maintained, or an unstable situation if supply decreases and the beach retreats. If the predicted SEP is seawards of the existing periphery it implies a natural reshaping state. A state of natural beach reshaping occurs when the beach undergoes adjustment resulting from a newly installed structure, such as the extension of a harbour breakwater. In this case, downdrift erosion would occur accompanied by accretion in the lee of the structure (Hsu et al., 2008).

There are many factors that affect the stability of the headland bay beach, including the dimension of headlands, beach orientation, bathymetric configuration, as well as the presence of offshore obstacles, coastal structures, sediment supply and others (Benedet et al., 2005). Many studies that have currently applied the PBSE to cover complex bay shapes have pointed out problems regarding the uncertainties due to the choice of the control points and limitations of its application range (e.g. Martino et al., 2005; González and Medina, 2001; Jackson and Cooper, 2010; Lausman et al., 2010). Regarding the choice of the control points, several researches have been performed on the uncertainties of the application of the PBSE (Sivester and Hsu, 1993;Moreno and Kraus, 1999;Martino et al., 2005; Lausman et al., 2010).

Regarding complex bay beaches, the equilibrium plan shape cannot be determined from a single wave direction such as the empirical parabolic bay shape model (Daly et al., 2011, 2014). In the study of Daly et al. (2014), they found that a variable wave climate can have an influence on the equilibrium orientation and shoreline planform of the bay. Two other factors that have a potential effect on the equilibrium planform are the role of local bathymetry and the presence of other morphological structures capable of causing significant wave refraction/diffraction that influence planform stability. These factors are ignored when using the empirical PBSE. Illustrating these effects, Jackson and Cooper (2010) found the ebb tide delta as a diffraction point rather than the adjacent rocky headland. Moreover, Melo Ferraz (2013) demonstrated that the local morphology (delta) created significant wave refraction and used the position of the delta structure as the updrift control point instead of using the prominent headland as diffraction point in the PBSE model.

Due to the ambiguity of selecting a diffraction point amongst multiple potential points, difficulty exists in determining the state of the stability of head land bay beaches while

applying the empirical PBSE. Oliveira and Barreiro (2010) applied the PBSE for 42 beaches in Portugal and found that in some cases the planform was very close to the SEP although field data indicated that the beaches were in dynamic equilibrium due to a high-energy wave regime. Jackson and Cooper (2010) also stated the subjectivity in selecting the diffraction point that renders alternative explanations difficult and reduces the utility of the applications of the PBSE. Without adequate data, verifying the bay beach planform stability remains a challenging problem.

In order to gain indepth understanding about the possible discrepancies between observed and predicted behaviour using the PBSE of complex embayed beaches, this study applies the Parabolic Bay Shape Equation (PBSE) to 26 less complex embayed beaches on the central coast of Viet Nam to investigate its utility and interpretation. Comprising various headland bay beaches and having a strong influence of the tropical monsoon climate makes the central Viet Nam coast an ideal and interesting area for study. This chapter combines the empirical PBSE with shoreline change rates, derived from Landsat images, to evaluate planform stability of the less complex headland bay beaches along the central coast of Viet Nam. Followed, applying this approach to planform stability of a very complex headland, i.e. Da Nang Bay. The main objectives of this study are (1) to analyse the planform stability of headland bay beaches using the PBSE without prior knowledge of the wave conditions; (2) to interpret the planform stability by considering parameters such as planform characteristics, shoreline changes; and (3) applying the PBSE and shoreline change rate for a specific case with a very complex headland bay beach (Da Nang) as well taking the influence of the seasonal wave climate into consideration.

5.2 Environmental Settings

THE study area is located along the central coast of Viet Nam between 106° and 109° East longitude and between 13° and 18° North latitude (Figure 5.1a). That includes the northern central coast and the middle central coast according to the classification by Tung (2011). The coast at the northern part is straight and aligned in NW – SE direction, while the middle central coast has an orientation that slightly changes from SE to S. The entire coast is irregular and includes long sandy beaches from Vung Ang to Da Nang but also includes river mouths and many irregular small and large embayed sandy beaches. Figure 5.1a shows 30 embayed beaches along the central coast that comprises naturally developed beaches and artificially embayed beaches. The number of embayed beaches is geographically organized from north to south. Artificially embayed beaches indicate the presence of existing coastal structures on/along the coast. All of these bay beaches have one or two headlands or coastal defense structures. At several locations, a river discharges into the bay, such as at Tam Hai , Tinh Ky, Dung Quat 1 and Sa Huynh and Thien Chanh. Thirty embayed beaches were selected to execute stability analyses among the Da Nang Bay beach systems, including Nam Chon bay (11), Nam O bay (10), Mui Nam O bay (11) and Da Nang bay (12).

Meteorological conditions at the central coast of Viet Nam are characterised by a tropical monsoon climate with an average annual temperature of 24°C and an annual rainfall of

about 2700mm at the northern part of central coast. The monsoon climate in this region is characterised by a very long dry season and a short rain season with large storm and flood events. The region is subjected to winds varying with the seasons, which are dominated by the Northeast (NE) monsoon from September to March and by the Southwest (SW) monsoon from May to September. The wave data used in this study were extracted from the NOAA WAVEWATCH III hindcast reanalysis (http://polar.ncep.noaa.gov/waves/) at the grid point (16.5°N, 108.5°E) to define the wave climate at Da Nang coast. The data is based on the global wave (0.5°x 0.5°) from 1/02/2005 to 31/01/2014 at 3-hour intervals, at 00:00h, 03:00h, 06:00h, 09:00h, 12:00h, 15:00h, 18:00h and 21:00h every day.

Figure 5.3 shows the occurring variation in wave height, wave period and the direc-

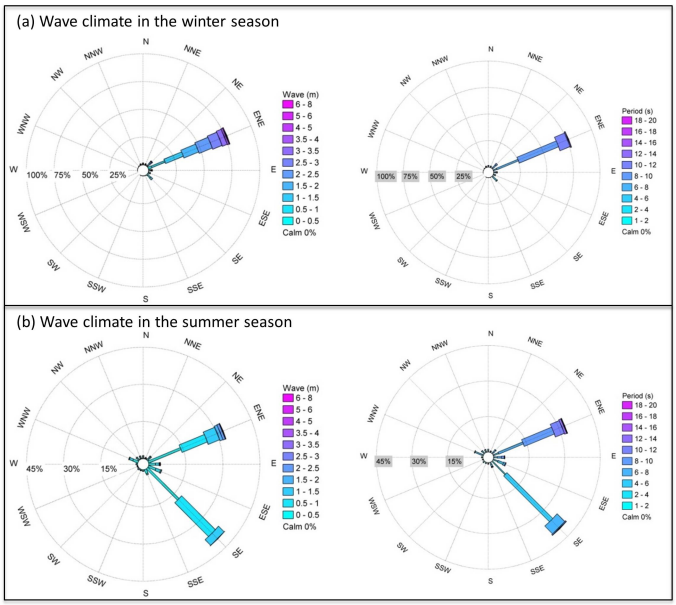

Figure 5.3: Seasonal wave direction in relation with wave height Hsig (left) and wave period Tm (right)

tional distribution of the waves. Due to the North East (NE) monsoon regimes, waves in the winter season (from September to March) were dominated by the Est North East ENE (76.74%) with wave heights ranging between 0.5 and 3.0 m and periods between 8 and 10 s. In the summer months (April to August), the waves were characterized by a bi-directional configuration. The waves were clearly influenced by the South East (SE) component and ENE directional component. The first dominant direction was from SE (40.45%) with wave heights of 0-1.0 m and periods of 4-6 s (27.40%). The second dominant wave direction was ENE (32.78%) with typical wave heights of 0.5-1.0 m and periods of 6-10 s. The highest wave heights normally occurred during the winter months due to typhoons or tropical storms and may reach up to 4-7 m in direction of N, NE, ENE, E and ESE. In general, the waves during the winter season had higher energy and longer periods than the waves in the summer season.

5.3 Methods

FIRSTLY the PBSE was applied to analyse the planform stability of 26 less complex embayed beaches without prior knowledge of the wave conditions. Secondly, the shoreline change rates derived from Landsat images were used to determine shoreline stability. After that, the PBSE and shoreline change rate were used to investigate planform stability of the very complex headland Da Nang Bay, also considering the influence of a seasonal wave climate. Delft3D WAVE is used to translate offshore wave conditions towards local wave conditions within the complex environment of Da Nang Bay, to address the local influence of a seasonal wave climate on the local planform stability analysis.

5.3.1 Planform stability analysis

There are two criterions determining the static equilibrium shape of headland bay beaches by applying the PBSE. The first criterion is based on the exiting curved shoreline comparing to the PBSE. The second criterion is based on the greatest indentation, (a), measured normal to the control line, as a ratio to its length (a/Ro). HSU and EVANS (1989)) applied the relationship between (a/Ro) and the angle of wave incidence (β) (Silvester and Ho, 1973) to examine planform stability. The information of indentation (a), in this study, was obtained by Google earth pro images. The highest indentation (a) is measured normal from the control line (Ro) to the point of largest retreat of the shoreline line (Silvester and Ho, 1973). This is obtained by drawing a tangent parallel to the control line as shown in Figure 5.4. Then the ratio (a/Ro) and obliquity (β) is compared to the curve in Figure 5.4. If it falls below the curve, then the bay can be considered unstable. If it falls close to the curve, then the bay is in static equilibrium.

The first criterion was performed using the MEPBAY software (Model of Equilibrium

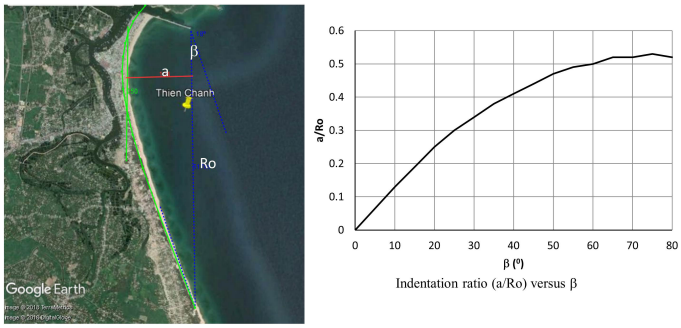

Figure 5.4: Determine the greatest indentation and the relationship between indentation ratios to obliquity wave for testing stability.

Planform of BAYed beaches) which had been developed to facilitate the model application (da Fontoura Klein et al., 2003). This is the most convenient tool for verifying the stability of a Headland Bay Beach (HBB) and for examining the effects of a new or existing

wave diffraction point on the downdrift beach, in addition to the design of a recreational bay beach. The Google earth images were loaded in MEPBAY to analyse the planform stability of the headland bay beaches. After loading the map of the planform of a bay into MEPBAY, the user has to identify control points on the image using the following general steps: (1) identify the updrift control point such as the point of wave diffraction or the tip of a headland or breakwater; (2) locate a downcoast control point that is any point on or near the straight downcoast section of the beach (da Fontoura Klein et al., 2003); (3) locate a downcoast tangent line. Then, comparing the results of applying the PBSE and existing shorelines to classify the planform equilibrium according to Hsu et al. (2008).

5.3.2 Shoreline change analysis

To detect the shoreline location, a total of four multispectral satellite images, acquired on different dates, were selected based on the lowest cloud cover and available data that cover the study areas (Table 5.1). The method to extract the shoreline positions are described in Chapter 4. Shoreline change rates are calculated following the End Point Rate (EPR) method using the Digital Shoreline Analysis System (DSAS) version 4.3, and the ArcGIS extension developed by the USGS (Thieler et al., 2009) for calculating shoreline changes. The EPR is calculated by dividing the distance of shoreline movement by the time elapsed between the earliest and latest measurements at each transect (Thieler et al., 2009). A baseline is constructed to serve as a starting point for all transects derived by the DSAS application. Using the EPR method shoreline change rates for the period between 1988 and 2018 are calculated. Shoreline change rates at every transect location are calculated by subtracting two derived shoreline locations at the beginning and at the end of each period.

Table 5.1: Landsat images that were used to detect shoreline change rates

Name	Acquisition date	Path/Row	Bay beaches
Landsat 5TM	03 September 1988	124/049	Nam Chon, Nam O, Da Nang, Tam Hai
Landsat 8 OLI-TIRS	17 May 2018	124/049	Dung Quat 2, Dung Quat 3, Binh Chau, Tinh Ky
Landsat 5 TM	10 July 1988	123/051	Hoa An, Tu Nham 1, Tu Nham 2
Landsat 8 OLI-TIRS	10 May 2018	123/051	

5.3.3 Wave modelling

The WAVE module of Delft3D was used to simulate wave propagation (refraction and diffraction) and dissipation (depth-induced breaking) inside Da Nang Bay. The wave

boundary conditions were modeled according to the main wave directions (ENE and SE) using the most frequent values of significant wave height and period in the derived data sets of the wave climate. The local bathymetry inside Da Nang Bay was obtained through the University of Da Nang and the bathymetry outside of Da Nang Bay was obtained from the Gebco08 bathymetry data set (http://www.gebco.net/data_and_products/gridded_bathymetry_data/), which has a grid resolution of 30 arc-second spacing. The wave conditions were used to relate the wave behavior to local bathymetry in order to characterize the overall wave propagation and specifically the near shore wave direction around the diffraction point.

5.4 Results and Discussion

THIS section first presents the results of the quantitative planform stability of the less complex headland bay beaches along the central coast using the PBSE. Secondly, the results of the shoreline change rates of some selected bay beaches are presented and discussed. Thirdly, the results of planform stability analysis with seasonal wave influences are represented for Da Nang Bay.

5.4.1 Planform headland bay beach stability along the central coast

Table 5.2 represents the results of the application of Equation (1) to 26 less complex embayed beaches along the central coast from Vung Ang to Tu Nham. About 58% (15 beaches) of the analyzed beaches are in dynamic equilibrium planform (DEP), 23% (6 beaches) in static equilibrium planform (SEP), and 19% (5 beaches) are categorized as mixed types between dynamic or reshaping and static or dynamic.

Almost all embayed beaches in static equilibrium are natural embayed beaches bounded by two headlands with no river supply into the bays. It seems that these beaches work as closed cells without sediment input or output and no littoral drift, as described by (Hsu et al., 2010, 2008). The results of the PBSE applied to these beaches show that the dominant wave direction is from ENE (dominant direction (red arrow in Figure 5.5) ranges from 56° to 67°) or coming from E direction (case of Chau Me 2). It seems that these beaches are exposed to the dominant waves during the winter season.

Headland bay beaches in dynamic equilibrium have been found at various beaches, with one headland or two headlands, having a significant river supply or no river supply, and at both natural and artificial beaches. Out of 15 embayed beaches in dynamic equilibrium, only 5 beaches are located near a river or have river flow into the bay, while the other 10 beaches indicate no river present. For the bays in dynamic equilibrium, sediment balance between input and output is the key factor that maintains the existing planform. The sediment supply may come from the rivers for those beaches with a river present or with a headland sediment bypass for the beaches where there is no river present. The latter phenomenon has been investigated by several authors (da Fontoura Klein et al., 2003; Bin Ab Razak, 2015; da Silva et al., 2016).

Table 5.2: Planform stability results (SEP indicates the static equilibrium planform, DEP indicates the dynamic equilibrium planform)

	Name	Characteristic	Planform stability
1	Vung Ang	harbour, near river	SEP/ reshaping
2	Mui Doc	two head land, no river	SEP
3	Hon La	two head land, no river	DEP
4	Mui Lay	two head land, rocky	DEP
5	Vinh Thanh	two head land	DEP
6	Vinh Quang	two head land	DEP
7	Cua Tung	two head land	DEP
8	Chan May	two head land, harbour, river	DEP
9	Tam Hai	one headland, river	DEP
10	Dung Quat 1	harbour, two headlands, river	DEP/reshaping
11	Dung Quat 2	two head land, no river	DEP
12	Dung Quat 3	two headland, no river	SEP
13	Thanh Thuy	two headland, no river	DEP
14	Binh Chau	two headland, no river	DEP
15	Tinh Ky	one headland, river	DEP
16	Hoc Mo	two head land, no river	SEP
17	Sa Huynh	harbour, river	SEP/DEP
18	Chau Me 2	two head land, no river	SEP
19	Thien Chanh	harbour, river	DEP
20	Xuan Thanh	one headland, no river	DEP
21	Tan Thanh	two headland, no river	DEP
22	Vinh Hoi	two head land, no river	SEP
23	Trung Luong	dual bay, two headlands, no river	SEP
24	Hoa An	two headland, no river	SEP/DEP
25	Tu Nham 1	dual bay, two headlands, no river	SEP/DEP
26	Tu Nham 2	two headland, no river	DEP

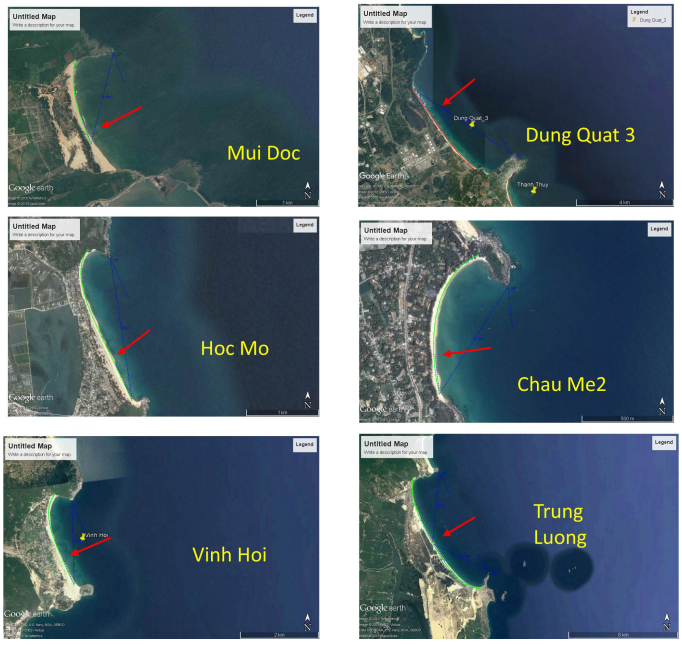

Figure 5.5: The headland bay beaches in static equilibrium planform.

For the mixed type of beaches, it proved very difficult to determine the state of equilibrium because multiple diffraction points lead to different predicted equilibrium planforms. For instance, at Hoa An beach there are two potential diffraction points; one on the natural headland (A) and a second one at a shoal (B) in Figure 5.6. The PBSE associated with diffraction point A (the green curve) is positioned landward of the existing shoreline, suggesting the beach is dynamic equilibrium. Whereas, when the diffraction point on the shoal was selected (point B) the PBSE shows very good agreement with the actual shoreline (the red curve) indicating that the beach is in static equilibrium. In case of data limited environments (without any information about beach profile, sediment characteristics and wave data), it remains difficult to confirm the validity of the results of the PBSE for this bay. We cannot confirm that the beach planform is in static equilibrium or in dynamic equilibrium. The other mixed type of beaches are found at complex headlands, which present artificial coastal structures with multiple potential diffraction points (e.g. harbors), such as Vung Ang, Dung Quat1 and Sa Huynh. Only Hoa An and Tu Nham are natural headland bay beaches.

The beach planform stability was also described by the relationship between the embayment indentation ratio (a/Ro) and the wave obliquity (β), according to Silvester and Hsu (1997). The obtained results are plotted in Figure 5.7. In which, Ro is the control line length; and the highest indentation (a) is the distance measured normal from the control line (Ro) to the point of the largest retreat of the shoreline (Silvester and Hsu, 1997).

Almost all SEP beaches are close to the static equilibrium conditions according to Silvester and Hsu (1997) except for two deep embayments with higher indentation ratios

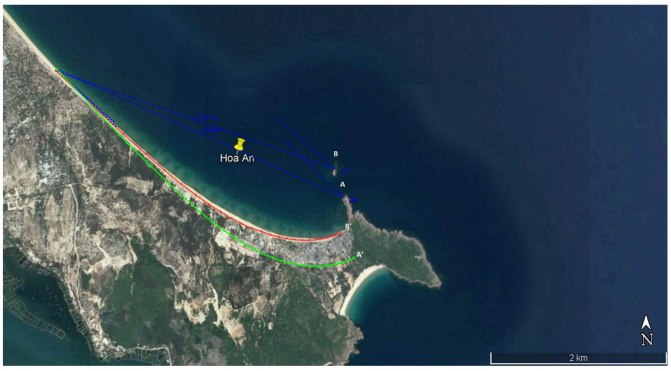

Figure 5.6: Model results for Hoa An bay beach showing the different diffraction points (the green curve is for tip of headland as diffraction point while the red curve is for shoal as diffraction point)

falling above the curve. These are Dung Quat 3 with indentation ratio of 0.36 and Tu Nham 1 with indentation ratio of 0.46. In which, Tu Nham 1 bay is categorized as mixed type between SEP/DEP. This result could contribute to confirming the static equilibrium planform of the beaches that fit the PBSE well (e.g. Mui Doc, Hoc Mo, Chau Me 2, Vinh Hoi and Trung Luong). The only beach for which the result of the PBSE indicates the planform is in static equilibrium, while this criterion indicates the beach is not in static equilibrium is Dung Quat 3. According to da Fontoura Klein and de Menezes (2001), almost all SEP beaches can be considered as exposed beaches (a/Ro = 0.28 - 0.39 and β <40°). Exception is Vinh Hoi beach that is semi-exposed with indentation ratio of 0.42.
Almost all dynamic planform beaches fall under the static equilibrium condition according to Silvester and Hsu (1997). The results demonstrate that most of the low indented beaches (or shallow embayment) fall below the stability curve, except for Tam Hai bay and Dung Quat 1 bay falling a bit above the curve. In which, Dung Quat 1 is categorized as a mixed type between DEP and reshaping. The observation of the shallow embayments falling under the stability curve is similar with Bowman et al. (2009) for the Catalan pocket beaches in Spain. It means that the dynamic beaches are shallow embayments and are not as indented as that of the SEP. Interestingly, there are some beaches that fall close to the static line (Tinh Ky, Thien Chanh and Tu Nham 1). Especially for the case of Sa Huynh, the results from applying the PSBE indicate the bay beach is in mixed SEP/Dynamic (Figure 5.8), but the relationship between the indentation ratio and the wave obliquity (β) show the embayed beach is in static equilibrium (Silvester and Hsu, 1997). On the other hand, reshaping beaches with high indention (0.41 and 0.55) are found above the static line (Figure 5.7c).
Results of the application of the PBSE and the indentation criterion indicate that beaches in either SEP or DEP can occur at various beaches. The majority of the embayed beaches in the central coast (58%) were found to tend toward dynamic equilibrium. The reason behind this is unknown and needs further research. Several beaches are categorized as mixed types between dynamic or reshaping and static or dynamic. It is difficult to determine the state of equilibrium of these beaches. Shoreline change rates analyses may contribute to explaining the planform stability in the next section.

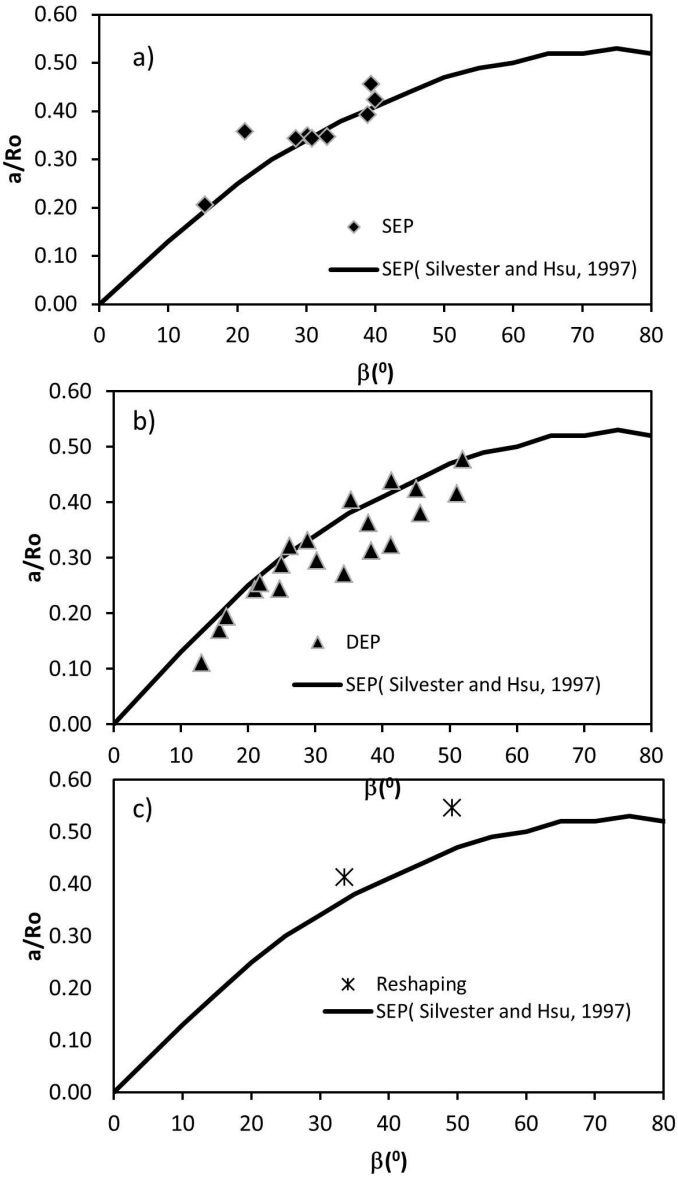

Figure 5.7: The relationship between the embayment indentation ratio (a/Ro) and the wave obliquity (β) with difference equilibrium statement. (a) Static Equilibrium Planform (SEP); (b) Dynamic Equilibrium Planform (DEP) and (c) reshaping conditions.

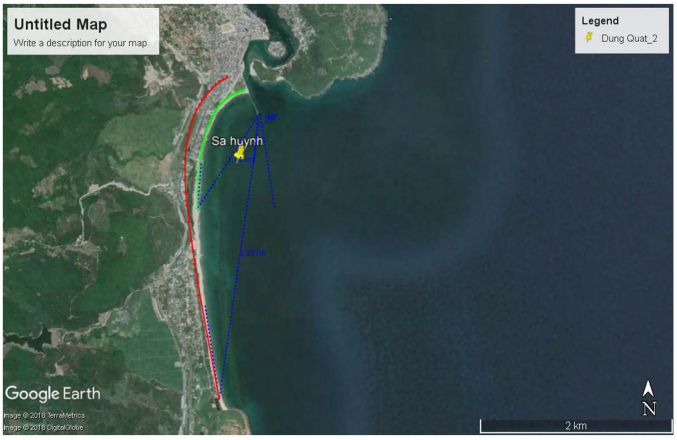

Figure 5.8: Result of parabolic bay shape for Sa Huynh

5.4.2 Shoreline change rate results

Nine embayed beaches, representing the SEP, DEP and mixed type beaches, were selected for further shoreline change rate analyses. The SEP beach that was selected is Dung Quat 3 due to the found discrepancies between observations, the PBSE and the relationship between the embayment indentation ratio (a/Ro) and the wave obliquity (β). The DEP beaches that were selected include Tam Hai, Dung Quat 2, Thanh Thuy, Binh Chau, Tinh Ky and Tu Nham 2. The mixed type beaches that were selected are Hoa An and Tu Nham 1. The dynamic beaches and the mixed beaches are selected based on available Landsat images.

Based on the concept of equilibrium planform, described by Hsu et al., 2010, 2008, the planform of a bay in static equilibrium exists where there is almost no littoral drift or no net movement of sediments. This implies that the shorelines of the bay are stable with no erosion/sedimentation occurring. The planform of a bay in dynamic equilibrium exists where there is a balance between sediment in and out of the bay to maintain the stability of the shoreline. If the sediment supply is interrupted or reduced, the shoreline of the bay will retreat. This suggests that the shoreline of a dynamic planform could be stable or retreating. The empirical PBSE can be used to estimate the bay beach stabilization state but it cannot give information about shoreline development. In some cases, such as the mixed type, we cannot confirm the results of the PBSE. The shoreline changes may contribute to more information to identify the state of the beach. In this study, shoreline stability is categorized in the 3 categories defined by Gutierrez et al. (2011): The stable shoreline (-1 m/y <rate <1m/y); the erosive shoreline (rate < -1m/y) and the accretive shoreline (rate > 1m/y).

The summary of the results of the shoreline change rates of the selected bays are presented in Table 5.3. In general, the rates of shoreline changes range from -3.5m/y to +3

m/y. Several beaches are categorized as stable shorelines, but have small sedimentation rates such as Hoa An (+0.4m/y), Tu Nham 1 (+0.3m/y) and Tu Nham 2 (+0.3m/y), while others show small erosion rates such as Dung Quat 2 (-0.2m/y) and Dung Quat 3 (-0.4m/y). Large erosion rates are found in the cases of Thanh Thuy (-3.5 m/y) and Binh Chau (-1.1 m/y). Moreover, results at Tam Hai and Tinh Ky indicate that there is a rotation of its shoreline. The shoreline of Tam Hai bay shows slight sedimentation on the sheltering segment (near the headland) and erosion on the transitional and tangential segments. The results of the measured shoreline changes in this bay also show clear influences of the shifting river mouth with high accretion and erosion at the sides of the river mouth. The shoreline change of Tinh Ky bay also show a rotation but its behavior is opposite. It shows erosion at the sheltering segment and accretion on the transitional and tangential segments. The location of the river supplying sediment to the bay might have an influence on this rotation behavior. For Tam Hai bay (Figure 5.9a), the river located near the shadow zone and the associated sediment supply to this area might result in accretion of the sheltering segment. Whereas, for Tinh Ky bay (Figure 5.9b) the river located at the tangential segment could contribute to the supply sediment of this area, resulting in the accretion on the tangential segment and erosion on the sheltering segment.

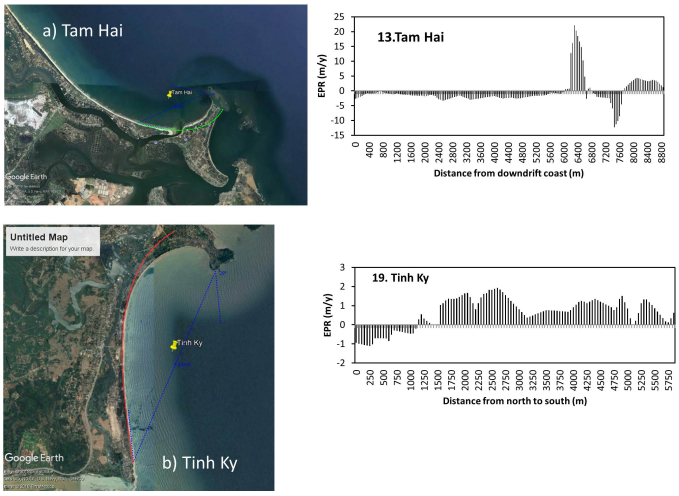

Figure 5.9: The results of PBSE and shoreline change rates (1988-2018): (a) Tam Hai bay; (b) Tinh Ky bay.

The information about the shoreline developments has significantly contributed to the identification of the planform stability of mixed type beaches. The results of shoreline change rates of Hoa An and Tu Nham 1 indicate their shorelines have been stable over a 30 year period with slight sedimentation rates of +0.4 m/y (Hoa An) and of + 0.3 m/y (Tu Nham 1), while the results from the PBSE show that these bays are considered as mixed types between SEP/DEP. The stable shoreline that is derived from shoreline change rates could contribute to determining the static equilibrium planform of these bay beaches. The results support the assumption that the ebb shoal, present at Hoa An

Table 5.3: Shoreline change of headland bay beaches in central coast during period 1988 and 2018.

Name	Planform stability	Shoreline change rates (1988-2018) (m/y)	Shoreline stability
Tam Hai	DEP	down coast erosion (-1.75m/y), river mouth shifting, sedimentation at shadow zone (+3 m/y)	rotation
Dung Quat 2	DEP	stable shoreline average erosion rate (-0.2 m/y)	stable shoreline
Dung Quat 3	SEP	average erosion rate (-0.4 m/y)	quite stable shoreline
Thanh Thuy	DEP	down coast erosion (-3.5 m/y), headland erosion	erosion
Binh Chau	DEP	erosion at shadow zone (head land) -1.1 m/y	erosion
Tinh Ky	DEP	erosion at shadow zone (head land) -0.45 m/y and sedimentation at downdrift beach +1.03m/y	rotation
Hoa An	SEP/DEP	sedimentation +0.42m/y	stable shoreline
Tu Nham 1	SEP/DEP	shoreline sedimentation +0.25m/y	stable shoreline
Tu Nham 2	DEP	slight erosion at shadow zone and sedimentation at down drift coast (+0.27m/y)	stable shoreline

bay, plays an important role as diffraction point instead of the tip of the headland.
Dung Quat 3 bay, representative of SEP, was selected for further shoreline change rate analysis. The result from PBSE indicate that the planform of Dung Quat 3 is in static equilibrium, meaning that the shoreline is stable, but the result from the shoreline change rate analysis show that the shoreline slightly eroded with an average of -0.4 m/y over the 30 year period. However, if we assume the stability of shoreline, as categorized by Gutierrez et al. (2011), the shoreline change rates of this beach are quite stable. Therefore, this result could contribute to confirm the static equilibrium planform from PBSE.

5.4.3 Planform stability analysis of Da Nang Bay

Da Nang Bay is a beach downdrift of the harbour breakwater and jetty river mouth. The southeast side of the bay contains a harbour breakwater and a jetty at the Han river mouth. The jetty nearly 1.9km (1), constructed in 1968 to protect the port of Da Nang, lies at the mouth of the Han River. The harbour breakwater (2) of 450m was constructed and completed in 2006 to protect Tien Sa port structures from high waves. The northwest of this bay comprises two natural rock headlands (one is Isabella, the other has no name) which are obvious diffraction points (point 3 and point 4). These four diffraction points (Figure 5.10) were selected for simulation of the shoreline position.
Applying MEPBAY and taking the tip of coastal structures (1 and 2) as the updrift control point together with a suitable downdrift control point, the results of static equilibrium planform are shown in Figure 5.10. With point 1 at the tip of the jetty as the updrift

Figure 5.10: . Predicted SEP of Da Nang bay (Google earth imagery 2014)

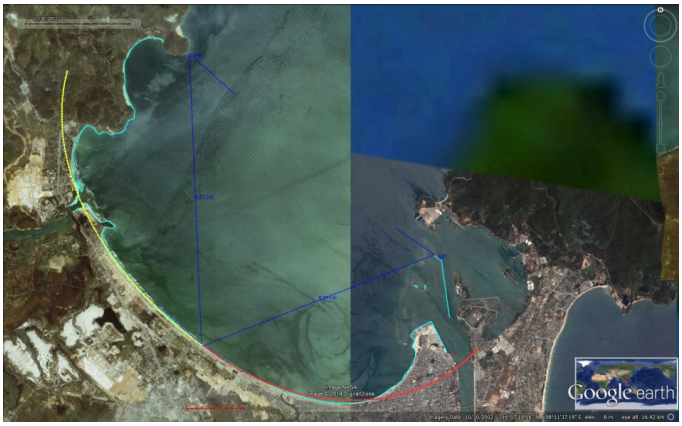

Figure 5.11: Predicted SEP of Da Nang bay (courtesy of Google earth imagery 2002)

control point, the predicted SEP is consistent with the actual shoreline at the downdrift beach, but it is found landward at the shadow area. Although the overall SEP fit quite well at the downdrift beach, there is one deviation from the SEP where the coast indented landward. This gap can be explained by erosion due to the impact of direct wave action during the NE monsoon, when the wave direction coming from the North will directly hit this region. Comparing the result with the 2002 shoreline planform (Figure 5.11), when the seawall and breakwater did not exist, the trend of the predicted shoreline was the same but the gap between the predicted SEP and coastal line in 2002 was larger than the present gap. This implicates that the seawall has contributed to control erosion in this area. Based on these results it can be seen that the planshape has remained in dynamic equilibrium during 2002 to 2014 under the control point of the tip of the jetty. Whereas using point 2 at the tip of harbour breakwater as the upcoast control point, the predicted SEP is found seaward of the actual shoreline (also Figure 5.10). According to

Hsu et al. (2010, 2008) the embayment would be classified as being in natural beach reshaping condition, when the northwest headland (point 3 and point 4) were selected as diffraction points. The result shows that both predicted shorelines are landwards to the existing shoreline; however, the SEP associated with diffraction point 4 is rather closer to the actual shoreline than the SEP associated with diffraction point 3. The existing shoreline in this region is being in dynamic condition according to classification of Hsu et al. (2008). One question however arises, if the current planform is still in dynamic equilibrium under the control of the tip of the jetty (point 1), or is there a natural reshaping under the control of the tip of the breakwater (point 2)? The PBSE with MEPBAY cannot answer this question, thus it is unknown how or what the state equilibrium of the current planform is. Therefore, shoreline change was suggested for further analysis to see how the beach development evolves.

Shoreline change rates at Da Nang Bay, which includes Nam Chon, Nam O and Da Nang

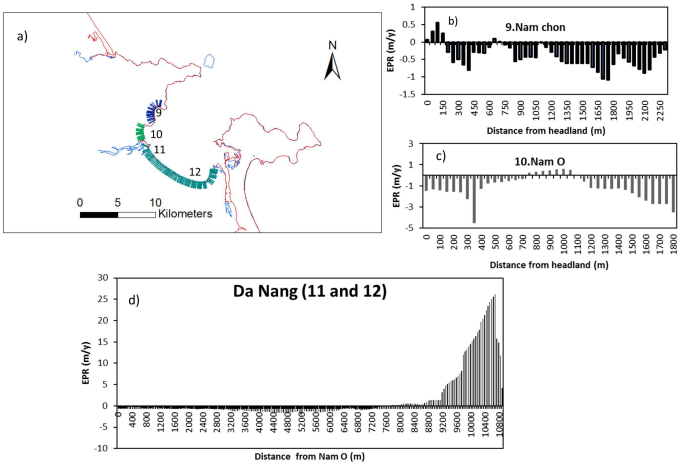

Figure 5.12: Shoreline change rates of Nam Chon, Nam O and Da Nang Bay from 1988 to 2018.

Bay for the period between 1988 and 2018, are calculated by the EPR method and shown in Figure 5.12. The shoreline of Nam O bay (Figure 5.12b) indicates erosion at the whole bay with an average rate of -1.2 (m/y). This result confirms the derived dynamic equilibrium from the PBSE. The shoreline retreat is likely caused by the decrease of sediment supply from the Cu De river.

The result of shoreline change at Da Nang Bay in Figure 5.11d shows slight erosion at the downdrift coast (-0.9 m/y) and significant accretion due to land reclamation (+7.6 m/y). The PBSE and shoreline change rates do not confirm the state of equilibrium of this bay. This is likely caused by a combination of a very complex and irregular headland bay beach in the presence of two rivers discharging into the bay and influences due to human interventions. Another explanation can be that PBSE for Da Nang Bay is influenced by seasonality in the wave climate, that might change the location of the point of diffraction and its planform stability. Daly et al. (2014) found that a variable wave climate can have an influence on the equilibrium orientation and shoreline planform of

the bay. Recently, El-Shinnawy et al. (2017) have also investigated the effect of the directional wave climate on the location of downdrift control points (Po), employing 44 headland bay beaches in Spain and Latin America. The study confirms dependence of the location of control points (Po) and directional variance of wave climate and offshore distance of the diffraction point from the straight segment of the shoreline. Consequently, they suggested that the implementation of the directional variability of the wave climate is critical in defining the location of Po and therefore the SEP of embayed beaches.
An interesting example is Nam Chon bay, located in Da Nang Bay, where the result of the PBSE indicates that the bay can be classified as unstable or natural reshaping for the southern area, whereas the northern area is in a dynamic condition (Hsu et al., 2008) as shown in Figure 5.13. The figure shows the results of the SEP position of Nam Chon bay using two different dominant wave directions. The static shoreline prediction, using the diffraction points at the tip of the headland, reveals that Nam Chon bay can be classified as unstable or natural reshaping for the southern area, whereas the northern area is in dynamic condition. However, the shoreline change rates at Nam Chon bay (Figure 5.12b) show a slight sedimentation at the shadow zone and show a slight erosion around the whole/total length of the bay with an average of -0.4m/y. Therefore, Nam Chon bay is considered to be a stable shoreline according to Gutierrez et al. (2011), suggesting that Nam Chon is in SEP or DEP.
It is interesting to note that the actual shoreline of Nam Chon beach fits the parabolic

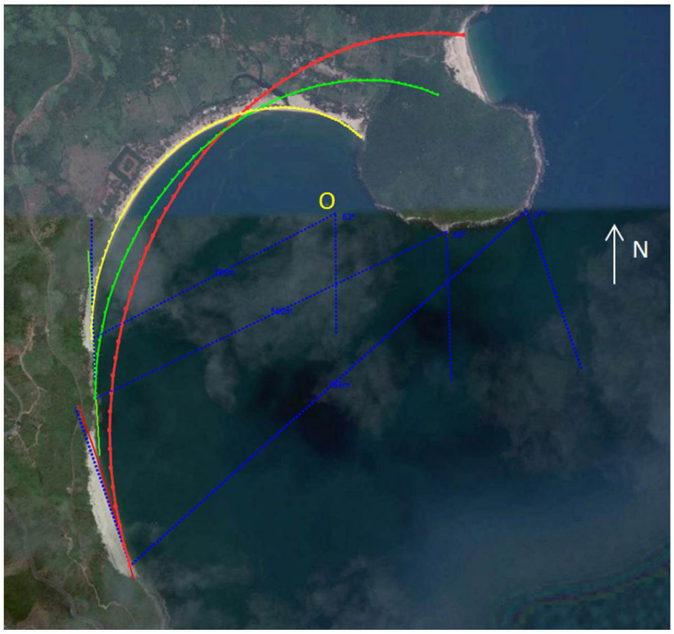

Figure 5.13: Parabolic bay shape approach for Nam Chon cape for different dominant wave angle approaches (red line (75°); green line and yellow line (89°))

curve rather well when the control point (O) is not located at the tip of the headland. De-

spite the fact that the shoreline is well represented by the parabolic curve, the meaning of point O is unclear. Point O can be interpreted as point of diffraction but it is not located at the tip of a headland. We hypothesise that seasonality in the wave climate might influence the location of the point of diffraction in case of a complex headland, Da Nang Bay.

To address the seasonal signal in the wave climate we have analysed the wave climate offshore (using NOAA WAVEWATCH III archives) in combination with Delft3D modelling software. The model was simulated with two dominant wave directions; ENE is the dominant wave in the winter and SE is the dominant wave in the summer.

The results of the wave modeling in ENE and SE direction are shown in Figure 5.14. To increase the detail inside the bay, the Nam Chon region (red rectangular region) was modeled at a higher grid resolution nested within the regional model. Model results show that refraction and diffraction occur both for ENE and SE wave direction resulting in a similar wave direction at the local Nam Chon region. The simulated wave directions at the tip of the Nam Chon headland are for offshore waves from ENE and SE, 85.45° and 83.7° respectively. The similar wave directions at the tip of the Nam Chon headland, due to waves propagating from ENE and SE direction from offshore into the bay, indicate that the dominant wave direction inside of the Da Nang bay is only slightly dependent on the seasonal wave climate measured offshore. In the case of Da Nang bay, the headland has an important role in wave diffraction, however, in order to assess stability of the planform we need to further account for more/additional factors that affect the stability, such as wave heights, wave periods and headland geometry.

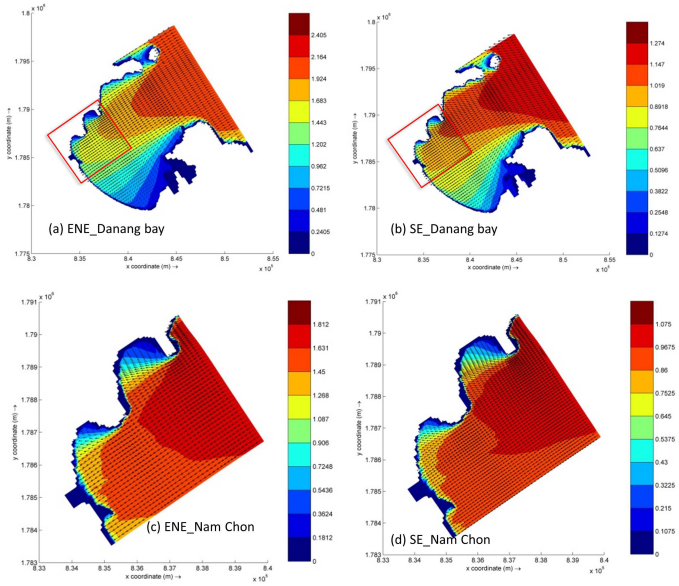

Figure 5.14: Model results for ENE direction (67.5°) on the left and SE direction (135°) on the right and color bar represent the wave heights.

5.5 Conclusions

IN order to investigate the utility of the empirical Parabolic Bay Shape Equation (PBSE) for testing stability of a very complex headland bay beach as Da Nang bay, this study has applied the PBSE combined with the shoreline change to assess the planform stability of 26 less complex bay beaches along the central coast of Viet Nam. Then, the PBSE and shoreline change rate were used to investigate planform stability of Da Nang bay, also considering the influence of a seasonal wave climate. Delft3D WAVE is used to translate offshore wave conditions towards local wave conditions within the complex environment of Da Nang bay to address the local influence of a seasonal wave climate on the local planform stability analysis.

We have applied the empirical Parabolic Bay Shape Equation (PBSE) to assess the planform stability of 26 less complex bay beaches located in central Viet Nam. The primary results from PBSE indicate that almost all bay beaches are in dynamic and static equilibrium planform. The majority of the embayed beaches in the central coast (58%) tend toward dynamic equilibrium. About 23% of the beaches are in static equilibrium planform and 19% are categorized as mixed types of beach.

The bay beaches in Static Equilibrium Planform (SEP) are found between two headlands, with no river present and a shoreline orientation exposed to the ENE wave dominant direction. The bay beaches in Dynamic Equilibrium Planform (DEP) are found in various morphodynamic settings. The planform of these beaches indicates shallower embayments than the SEP beaches. The results of the derived shoreline change rates of these beaches show various behaviours (e.g., stable shoreline, erosive shoreline and shoreline rotation). The rotation of shorelines has been measured at the beaches where a river was present. Bay beaches with no river could have stable shorelines or retreating shorelines, due to reduced sediment supply from headland bypassing.

The bay beaches in mixed types indicate a very difficult state of equilibrium due to multiple diffraction points leading to different predicted equilibrium planforms (mixed between SEP and Dynamic, or mixed between Dynamic and reshaping). The complexity of these bays can be explained by the irregular headlands with multiple potential updrift control points. For these kind of beaches, the results from shoreline change rates have significantly contributed to identify the planform stability of mixed type beaches. The stability criteria defined by Gutierrez et al. (2011) indicate that stable shorelines (-1 m/y <rate <1m/y) or erosion (rate < -1m/y) and accretion (rate > 1m/y) can successfully explain the planform stability by applying the PBSE.

Da Nang bay falls in the mixed type, but the PBSE and shoreline change show an unsuccessful application for testing stability in Da Nang bay. We have applied the PBSE to explain the shape of a particular bay located inside /within Da Nang bay. The complexity of this bay leads to uncertainties with respect to the selection of both downdrift and updrift control points associated with the PBSE. Especially the occurring bi-modal wave conditions in the East Sea might lead to a difficult interpretation of the PBSE. We have used the shallow water wave propagation model Delft3D WAVE to predict local wave conditions inside the bay and we have found that seasonality within the wave signal in the East Sea does not affect the local wave direction inside Da Nang Bay.

Although the PBSE and shoreline change rates analysis have successfully evaluated the

planform stability of various less complex headland bay beaches along the central coast of Viet Nam. We are therefore encouraged to use the PBSE equation to predict the development of the bay, which is that single bays may be bounded by two headlands, or by one headland and in the absence of a river's discharge. However, for a very complex headland, such as Da Nang bay, uncertainty regarding the updrift control points continues to exist due to the complex shape of the updrift headland. The additional presence of two seasonal river discharges could be also considered by process based modelling and might provide more information on the stability of Da Nang bay.

References

Benedet, L., Klein, A. H., and Hsu, J. R. (2005). Practical insights and applicability of empirical bay shape equations. In *Coastal Engineering 2004: (In 4 Volumes)*, pages 2181–2193. World Scientific.

Bin Ab Razak, M. (2015). Natural headland sand bypassing; towards identifying and modelling the mechanisms and processes.

Bowman, D., Guillén, J., Lopez, L., and Pellegrino, V. (2009). Planview geometry and morphological characteristics of pocket beaches on the catalan coast (spain). *Geomorphology*, 108(3-4):191–199.

da Fontoura Klein, A. H. and de Menezes, J. T. (2001). Beach morphodynamics and profile sequence for a headland bay coast. *Journal of Coastal Research*, pages 812–835.

da Fontoura Klein, A. H., Vargas, A., Raabe, A. L. A., and Hsu, J. R. (2003). Visual assessment of bayed beach stability with computer software. *Computers and Geosciences*, 29(10):1249–1257.

da Silva, G. V., Toldo Jr, E. E., Klein, A. H. d. F., Short, A. D., and Woodroffe, C. D. (2016). Headland sand bypassing—quantification of net sediment transport in embayed beaches, santa catarina island north shore, southern brazil. *Marine Geology*, 379:13–27.

Daly, C. J., Bryan, K. R., Roelvink, J. A., Klein, A. H. F., Hebbeln, D., and Winter, C. (2011). Morphodynamics of embayed beaches: The effect of wave conditions. *Journal of Coastal Research SI*, 64(64):1003–1007.

Daly, C. J., Bryan, K. R., and Winter, C. (2014). Wave energy distribution and morphological development in and around the shadow zone of an embayed beach. *Coastal Engineering*, 93:40–54.

Dieu, N. (2012). Sustainable development, climate change adaptation and disaster risk reduction: A case study in danang, vietnam. *Sustainable Development*.

Do, T., Stive, M., Brouwer, R., and De Vries, S. (2015). Analysis of embayed beach planform stability in danang, vietnam. In *E-proceedings of the 36th IAHR World Congress, The Hague, the Netherlands, 28 June-3 July 2015*. IAHR.

El-Shinnawy, A., Medina, R., and González, M. (2017). Equilibrium planform of headland bay beaches: Effect of directional wave climate. *Coastal Dynamics 2017*.

Gama, C., Coelho, C., Baptista, P., and Albardeiro, L. (2011). Equilibrium configuration of sandy embayed beaches from the southwest portuguese rocky coast. *Journal of Coastal Research*, 64:2037–2041.

González, M. and Medina, R. (2001). On the application of static equilibrium bay formulations to natural and man-made beaches. *Coastal Engineering*, 43(3-4):209–225.

Gutierrez, B. T., Plant, N. G., and Thieler, E. R. (2011). A bayesian network to predict coastal vulnerability to sea level rise. *Journal of Geophysical Research: Earth Surface*, 116(F2).

Hsu, J. R., Yu, M. J., Lee, F. C., and Benedet, L. (2010). Static bay beach concept for scientists and engineers: A review. *Coastal Engineering*, 57(2):76–91.

Hsu, J. R.-C., Benedet, L., Klein, A. H. F., Raabe, A. L. A., C.-P.Tsai, and T.-W.Hsu (2008). Appreciation of static bay beach concept for coastal management and protection. *Journal of Coastal Research*, 241(241):198–215.

HSU, J. R. C. and EVANS, C. (1989). Parabolic bay shapes and applications. *Proceedings of the Institution of Civil Engineers*, 87(4):557–570.

Jackson, D. W. and Cooper, J. A. G. (2010). Application of the equilibrium planform concept to natural beaches in northern ireland. *Coastal Engineering*, 57(2):112–123.

Klein, A. H., Ferreira, Ó., Dias, J. M., Tessler, M. G., Silveira, L. F., Benedet, L., de Menezes, J. T., and de Abreu, J. G. (2010). Morphodynamics of structurally controlled headland-bay beaches in southeastern brazil: A review. *Coastal Engineering*, 57(2):98–111.

Lausman, R., Klein, A. H. F., and Stive, M. J. F. (2010). Uncertainty in the application of the parabolic bay shape equation: Part 1. *Coastal Engineering*, 57(2):132–141.

Martino, E., Moreno, L., and Kraus, N. C. (2005). Uncertainties in design guidance for headland-bay beaches. *Coastal Dynamics*, pages 1–14.

Melo Ferraz, M. (2013). *Influence of Delta Morphodynamics on Coastal Response to Climate Change*. PhD thesis, University of Sydney.

Moreno, L. J. and Kraus, N. C. (1999). Equilibrium shape of headland-bay beaches for engineering design. *Proceedings Coastal Sediments '99*, 860:860–875.

Oliveira, F. S. and Barreiro, O. M. (2010). Application of empirical models to bay-shaped beaches in portugal. *Coastal Engineering*, 57(2):124–131.

Razak, M. S. A., Suryadi, F. X., Jamaluddin, N., and Nor, N. A. Z. M. (2018). Shoreline planform stability of embayed beaches along the malaysian peninsular coast. *Journal of Coastal Research*, 85(sp1):631–635.

Short, A. D. (1999). *Handbook of beach and shoreface morphodynamics*. Number 551.468 HAN.

Silveira, L. F., Klein, A. H. d. F., and Tessler, M. G. (2010). Headland-bay beach planform stability of santa catarina state and of the northern coast of são paulo state. *Brazilian Journal of Oceanography*, 58(2):101–122.

Silvester, R. and Ho, S.-K. (1973). Use of crenulate shaped bays to stabilize coasts. In *Coastal Engineering 1972*, pages 1347–1365.

Silvester, R. and Hsu, J. R. (1997). *Coastal stabilization*, volume 14. World Scientific Singapore.

Sivester, R. and Hsu, J. (1993). Coastal stabilization: innovative concepts.

Tasaduak, S., Weesakul, S., Babel, M. S., Clemente, R. S., and Phien-Wej, N. (2014). Equilibrium of crenulated bays in thailand. *Coastal Engineering Journal*, 56(4):1450019–1.

Thieler, E. R., Himmelstoss, E. A., Zichichi, J. L., and Ergul, A. (2009). The digital shoreline analysis system (dsas) version 4.0-an arcgis extension for calculating shoreline change. Technical report, US Geological Survey.

Tong, X., Shi, L., Xia, X., et al. (2014). Shoreline evolution and stability analysis of headland-bay beach of huangcheng. In *The Twenty-fourth International Ocean and Polar Engineering Conference*. International Society of Offshore and Polar Engineers.

Tung, T. T. (2011). *Morphodynamics of seasonally Closed Coastal IInlet at the Central coast of Vietnam*. PhD thesis, Delft University of Technology.

Yasso, W. E. (1950). Plan geometry of headland-bay beaches. *Journal of geology*, 73(5):702–714.

Yu, J.-t. and Chen, Z.-s. (2011). Study on headland-bay sandy coast stability in south china coasts. *China Ocean Engineering*, 25(1):1.

Chapter 6

Conclusions

I didn't get there by wishing for it or hoping for it,
but by working for it.

Estee Lauder

The main objective of this study is the unravelling of the main processes controlling typical coastal systems in Central Vietnam (Cua Dai inlet and Da Nang Bay in particular) while accepting the challenge that it is a data limited environment. This chapter first provides an overview of the highlight characteristics of Cua Dai inlet and Da Nang Bay. Second, the conclusions are by answering the research questions as formulated in chapter 1. Finally, besides these conclusions, this chapter also offers an outlook for future research.

6.1 Cua Dai Inlet and Da Nang Bay

In Central Vietnam, one finds many seasonally varying tidal inlets and many headland bay beaches. According to Tung (2011) there are 32 inlets of wave dominated estuaries and there are about 740 rivers with lengths of more than 10 km each along the 1500km of the central coastline. These inlets that formed at the mouth of wave dominated estuaries. Almost all rivers originate from the Truong Son mountain range and are characterized by very steep slopes in the upstream part and by very low-lying coastal plains. Besides coastal inlets, more than 30 embayed headlands are observed by the author. The seasonal inlets and the headland bay beaches are formed in a microtidal, wave dominated, coastal environment and experience a strong seasonal variation in river discharge and wave climate (Tung, 2011).

The climate in Central Vietnam is strongly governed by tropical monsoons. The mon-

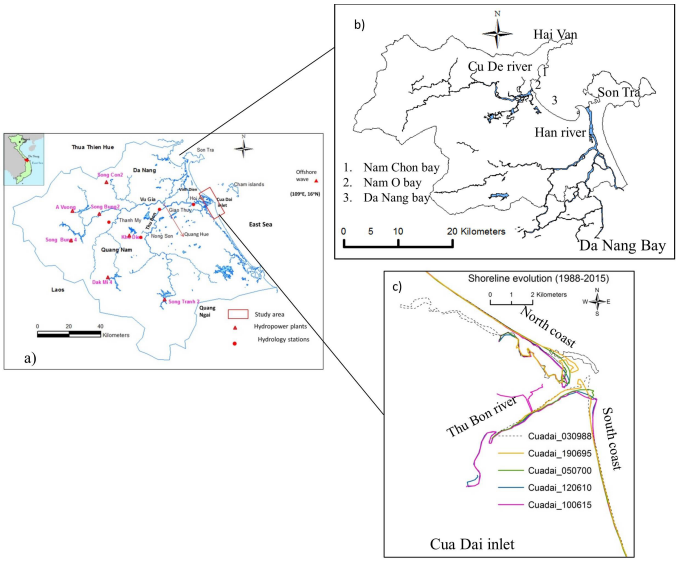

Figure 6.1: Location of Da Nang Bay and Cua Dai inlet

soon influences both the wave conditions and the river flow. During the NE monsoon regime, waves in the winter season (from September to March) are mainly from ENE direction. In the summer months (from April to August) when the SW monsoon is active waves come from SE and ENE directions. In terms of river discharge, two main seasons can be distinguished, the dry- or summer season and rain- or winter season. Distinctive geomorphologic features and forcing such as seasonality in wave climate and river flow regime, narrow coastal plains, short steep rivers make the central Vietnam coast, one of the most vulnerable to natural disaster such as floods and tropical storms. Next to the coastal erosion in the region, coastal threats have been increasing due to human pressure. The pressure of increasing population and economic activities (e.g. fisheries, tourist hotels and associated tourism activities, hydropower plants and land reclamation) have contributed to unwanted changes in the coastal system.

Cua Dai Inlet and Da Nang Bay, two typical deltaic coastal formations on the central coast of Vietnam, are under pressure due to coastal erosion. These two coastal systems are associated with the biggest river system in Central Vietnam, The Vu Gia-Thu Bon river system. This study has focused on these two cases studies in order to unravel the main process controlling such typical coastal systems.
Cua Dai estuary is a typical, seasonally varying inlet connected to the catchment area of the Vu Gia and Thu Bon Rivers. Figure 6.1 shows a map of The Vu Gia-Thu Bon river network (Figure 6.1a) and of the dynamic shoreline behavior of Cua Dai inlet (Figure 6.1c), the right riverbank and the channel shifting from north to south and new ebb shoal development into the south. Cua Dai beach has experienced erosion since 1995 after the welding of bars to the beach. Whereas, the southern coast shows signs of a typical downdrift coast that has historically benefited from bypassing of sediment because of tidal currents and wave action. The big erosion that occurred at the riverbank over the period from 1990 to 2000 might be related to two extreme floods in 1998 and 1999. These floods may have scoured the riverbank and flushed sediment into the ebb tidal delta and the later feeding to the northern coast. This phenomenon has been observed clearly in simulations of the effect of seasonal river discharge and seasonal waves on alongshore sediment transport. Figure 6.2 indicates that the seasonal variation in wave climate and river discharge have a strong influence on sediment transport patterns around the inlet and its adjacent coasts. A long dry season combines a lower wave energy condition with a lower river discharge whereas a higher wave energy is associated with a higher flood discharge during the winter season. During the winter, waves also induce the alongshore transport and bypass sand to the southern shores. Another distinctive feature in this system is the Cham islands group, which is comprised of a group of 8 islands, located about 16 km in Northeast direction from the Cua Dai inlet. The Cham Islands have an important impact on the offshore wave propagation to the nearshore, increasing the complexity of the seasonal wave climate of Cua Dai Beach. Especially the area around Cua Dai Inlet, waves from the SE direction during the summer (Figure 6.2b) induces alongshore sediment transport to the north, whereas the waves from ENE (Figure 6.2a) create longshore sediment transport to the south. The influence of the river discharge is presented clearly in the sediment transport through the inlet and at the northward side of th ebb tidal delta during the winter season that is associated with a higher river discharge. During this period, the river flow carried out sediment thought the inlet to the ebb tidal delta and partly toward the northward side to later feed the northern coast.
Da Nang Bay (Figure 6.1), a very complex headland in central Vietnam with attached

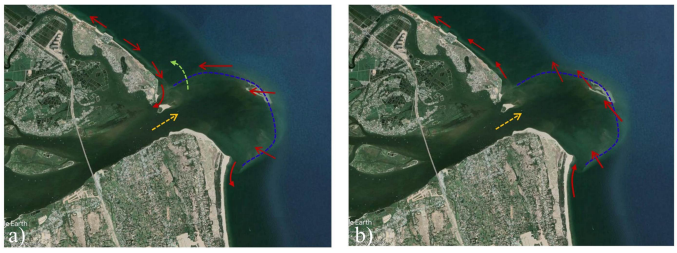

Figure 6.2: Variation in sediment transport pattern; a) for the winter season; b) for the summer season.

sea port, is located north of Da Nang city. It is bounded by the Hai Van Mountain to the north, bay beach Nam O to the west and the Son Tra Peninsula to the east. In particular, Da Nang Bay includes other small embayed beaches such as Nam Chon bay, Nam O bay and Da Nang Bay as presented in Figure .6.1a. The Nam Chon bay is located at the foot of Hai Van pass, between the Nam O beach and Isabelle promontory. The Nam O bay is located at the river mouth of Cu De river. There are two seasonal rivers discharging into Da Nang Bay, the Cu De River from the west and the Song Han River from the south. Due to its geographical location, Da Nang is one of the cities in Viet Nam that is most affected by natural disasters and extreme weather conditions (Dieu, 2012). During the last decades, several coastal structures were built in Da Nang Bay, such as seawalls, breakwaters, dams and bridges, as well as other human interventions, such as land reclamations for the construction of luxurious resorts. These human activities together with the effects of climate change potentially pose a threat to the coastal safety of Da Nang Bay.
The planform configuration of headland bay beaches generally tend to adopt an equilibrium planform that fits commonly used empirical Parabolic Bay Shape Equation (PBSE). This equation has been applied to evaluate the planform stability of other less complex embayed beaches along the central coast of Vietnam. The PBSE performs well for those natural embayed beaches bounded by two headlands with no river supply into the bays that are in static equilibrium. It seems that these beaches work as closed cells without sediment input or output and no littoral drift, as described by Hsu et al. (2010, 2008). Although these beaches are located along the central Vietnam coast which is characterized by a seasonal wave climate, all these beaches are exposed to dominant East North East (ENE) waves during the winter season.
Headland bay beaches in dynamic equilibrium have been found at various beaches along the central Vietnam coast, with one headland or two headlands, having a significant river supply or no river supply, and at both natural and artificial beaches. For the bays in dynamic equilibrium, sediment supply may come from the rivers when a river is present or with a headland sediment bypass where there is no river present. Furthermore, the results of derived shoreline change rates of these beaches show various behavior. The bays with a river present show a rotation in their shoreline change. The location of the river supplying sediment to the bay might have an influence on this rotation behavior. The bays with no river could have stable shorelines or retreating shorelines, due to reduced sediment supply from headland bypassing.
Besides static equilibrium and dynamic equilibrium planform, several beaches are categorized as mixed types between dynamic or reshaping and static or dynamic. The bay beaches in mixed types indicate a state of equilibrium that is difficult to interpret due to multiple diffraction points leading to different predicted equilibrium planforms. Da Nang bay falls in the mixed type.

6.2 Response to research questions

Research Question 1: What are the processes that govern morphological changes and extreme erosion at Cua Dai beach during recent decades?
In order to derive a better understanding of recent and present processes governing the

evolution of Cua Dai Beach, we have reconstructed the historical shoreline positions and we have estimated volume changes derived from Landsat imageries. Moreover, we have applied a process-based model to investigate the influence of waves, tides, and river discharge on sediment transport and morphological changes.
The results of this study indicate that the erosion of Cua Dai beach since 1995 was the result of a long-term geomorphological inlet development reflecting a non-periodic cyclic process that takes place over several decades. It appears that channel shifting from North to South, triggered by typhoon Cecil in 1987, dictated the geomorphological development of Cua Dai Beach. The decrease of sediment supply from the river, estuary and squeeze by coastal developments may have contributed to the erosion. Before 1995, Cua Dai inlet was a sediment rich system with a sub-areal beach barrier being part of the ebb-tidal delta in 1988. During this time, the system did not experience any impact of human activities but only experienced natural processes. It is our hypothesis that the river system provided a large amount of sediment to the inlet gorge and/or to the ebb tidal delta, depending on the dry or wet season respectively. Hence, the wave driven alongshore sediment transport on the northern beaches caused by the ENE waves was available to not only build a shoal such as present in 1988, preventing erosion of the Cua Dai near inlet shore, but also to feed the more northern shore, annihilating the effect of divergence in transport. This hypothesis has been supported by the simulation results. Since 1995, after the welding of the ebb-tidal beach barrier, Cua Dai beach has retreated with significant erosion occurred during the period from 2000 to 2010. The estimated volume changes indicate that the system has lost a considerable sediment volume; approximately 243,000 m^3/y to 310,000 ^{3}/y. The reduced sediment supply from the river, sand mining and land reclamation could have contributed to the reduction of sediment supply from the river to Cua Dai inlet. Consequently, Cua Dai beach has eroded.

Research Question 2: What is the estimated combined effect of seasonal varying waves and river discharges on the sediment transport and morphological feedbacks of Cua Dai inlet?
Process-based models are used to investigate the seasonal varying sediment transport and morphological feedback due to the seasonal varying river discharge and seasonal wave climate. Sediment transport patterns at adjacent coasts show significant variations. During the winter, when ENE events dominate, the longshore sediment transport (LST) close to the inlet is generally directed to the South. However, there is a transport divergence point at approximately 3 km to the north at the northern coast. Whereas, a transport convergence point exists at approximately 4 km to the south, at the southern coast where the direction of LST is toward the north. During the summer months, despite the bidirectional occurrence of ENE and SE, the net LST is directed towards the north. At the northern coast, the LST increases from the inlet to the north. At the southern coast, the LSTR decreases from the south in the direction of the inlet. The simulation results of longshore sediment transport patterns at the adjacent coast agreed well with the results of earlier estimations based on theory of longshore sediment transport induced by waves only.
The combined effect of river flows and waves show clear variations in sediment transport through the river mouth and the northern coast especially during the simulated

flood event. Waves coming from the ENE at the northern coast induce longshore sediment toward the inlet and supply sediment to the inlet. The river flow induced ebb flow capacity to carry out sediment from the estuary and to supply sediment to the ebb tidal delta. The inlet experiences sediment import or export depending on the interaction between waves and river flows. The increasing river discharge leads to less sediment import into estuary. Especially, when the river flow is large during the flood season, river processes are dominant leading to the system to flush out sediment through the estuary and even over the ebb tidal delta. Moreover, the waves approaching from both SE and ENE directions cause different magnitudes of sediment import into the estuary. Waves coming from the ENE contribute to larger sediment import than waves coming from the SE.

Research Question 3: How can shoreline locations and sediment volumes be evaluated using satellite techniques in data limited and data rich environments?
It is generally not possible to validate a method without observed data such as in data limited environments. However, data rich environments could provide the necessary information for validation of the methodology to be applied in data limited environments. Chapter 4 of this thesis is an intermezzo step that illustrates the application of remote sensing techniques to derive shoreline positions and derived volume changes that was evaluated for a data-rich region the North-Holland coast in The Netherlands. This coast is globally unique for its long in-situ monitoring record and provides a perfect case to evaluate the potential of shoreline mapping techniques.
The results of chapter 4 show that the use of Landsat images for deriving shorelines, shoreline change rates and volume changes have accuracies that vary with different timescales. Accuracies are limited when compared to relatively small annual timescales but are comparable to observed in-situ measurements when considering (larger) decadal scale measurements. This shows the potential of applying Landsat images to monitor shoreline change and coastal volume change over decades. For the short term period, the results may be influenced by the signal to noise ratio, the short term variations in shorelines and the highly dynamic variations in cross shore profiles. Therefore, satellite imagery based on freely available high quality images such as Landsat might offer a good alternative and a low cost method for coastal monitoring of especially the larger decadal scales. Especially where there is concern about shoreline erosion and financial budgets for coastal monitoring and shoreline changes are scare. This method has successfully been applied to the case of Cua Dai beach where no available observed data was available.

Research Question 4: Can morphological or planform stability of the complex embayed beach of Danang Bay be explained by seasonal variability in wave conditions?
The commonly used empirical parabolic bay shape equation (PBSE) and shoreline change rates analyses have successfully evaluated the planform stability of various (less complex) embayed beaches along the central coast Vietnam. We have applied the PBSE and shoreline change rates to explain the shape of a particular complex bay located in Da Nang, Vietnam. The results from the PBSE depends on its elementary assumptions being the updrift control point selection and single dominant wave direction. According to the PBSE the Da Nang plan shape is in dynamic equilibrium if the up drift control

point is at the tip of the river jetty whereas the plan shape is in natural reshaping if the control point is at the tip of Tien Sa breakwater. The shoreline change results show slight erosion at the downdrift coast and significant accretion due to land reclamation. The PBSE and shoreline change rates could not explain the state of equilibrium of the very complex headland at Da Nang bay. These results indicate that the complexity of this bay leads to uncertainties with respect to the selection of both down drift and up drift control points associated and therefore the application of the PBSE. This is likely caused by a combination of a very complex irregular headland bay beach with the presence of two rivers discharging into the bay and influences due to human interventions. Another aspect that can explain the unsuccessful application the PBSE for Da Nang bay is the seasonality in the wave climate that might influence the location of the point of diffraction. We have used the shallow water wave propagation model Delft3D WAVE to predict local wave conditions inside the bay and we have found that seasonality within the wave signal in the East Sea does not affect the local wave direction inside Da Nang Bay.
The application of the PBSE and shoreline change rates to explain the planform stability of the complex bay beach Da Nang bay has its limitations. The limitations might result from the single dominant wave direction assumption where the uncertainty remains in selecting control points and from the complex shape of Da Nang Bay. This study is however encouraged to use the PBSE equation to predict the development of less complex bays, which are single bays bounded by two headlands, or one headland and have a well defined location of the updrift diffraction point. For the single headlands with presence of river discharge, this study is encouraged to use to the PBSE combining shoreline change rate analysis to determine their planform stability.

6.3 Perspective

There are possible further works that can develop base on this thesis.
Regarding the stability of a complex bay beach headland, the effect of sediment supply from rivers is an unadressed and possibly an important parameter that affects the dynamic equilibrium plan shape of the bay. Therefore it is necessary to investigate how sediment input and redistribution along the bay develops in a time dependent manner. Open research questions exist regarding temporal trends in bay beach development and if the seasonal monsoon can influence a dynamic equilibrium? If so, which dominant mechanisms exist behind this trend?
Regarding the processes controlling extreme erosion at adjacent coasts of Cua Dai inlet, the reconstructed historical shoreline change rates and volume changes and alongshore sediment transport have successfully explained the main mechanism behind the past and current morphological changes. However, the cross-shore sediment transport induced by storms should be further investigated. Beside the effect of the resorts that were built close to the coasts and other hard structures need to be included in process-based modeling to evaluate these effects on the longshore sediment transport at the adjacent coasts. This study we did not include these effects because of limitations in observed data to validate our model.
Satellite images have proved to be a tool with tremendous potential in shoreline change

monitoring in this thesis particularly in ungauged or data limited areas. Recently, satellite imagery provides a wide range of applications to many research themes in coastal monitoring such as suspended sediment, water quality and even using satellite imagery to retrieval of nearshore bathymetry. Consequently, it would be interesting to use higher resolution satellite images as a source of observed data to validate numerical models in cases of limited data availability. For instance, some high spatial resolution satellite images can be used to resolve detail of suspended sediment such as IKONOS, WordView-2 (WV2), Système Pour l'Observation de la Terra (SPOT), Sentinel and MODerate resolution Imaging Spectroradiometer (MODIS).
In this study, it is shown that a combination between satellite imagery and a process-based model has proved as successful approach to understand a complex coastal system as Cua Dai inlet in case of limited data. The general approach derived from this study can be used to apply for similar areas.

- **Step 1**: collect as much as possible the free available data concerning the study area/study objectives (e.g. free available satellite imagery, free available bathymetry, global waves, river flow)

- **Step 2**: reconstruct historical shoreline changes from satellite imagery and estimate volume changes based on shoreline change rates and assume closure depth. This step gives the insight in sediment budget changes over each period. These sediment budgets are a fundamental element of coastal sediment processes. This information contributes to determine if the system is experiencing sediment abundance of scarcity. Historical shoreline changes give the insight in erosion/sedimentation of the coast.

- **Step 3**: apply process-based models to derive longshore sediment transport and simulate potential morphological changes. The results of this step contribute to explain the results from step 2 and investigate the mechanism behind that. Especially the effects of waves, tides, and river discharge on the sediment transport and morphological changes of coastal system .

These 3 basic steps could be applied to understand other similar areas and especially other coastal erosion regions in the central Vietnam coast.
The most important finding in this study indicates that Cua Dai beach is in need of sediment. The recommendations to mitigating the erosion is suggested to a soft, sand strategy for example beach nourishment. Because other hard structures do not create or add the sediment needed which can diminish the volume of sand that has been lost in the past.

References

Dieu, N. (2012). Sustainable development, climate change adaptation and disaster risk reduction: A case study in danang, vietnam. *Sustainable Development*.

Hsu, J. R., Yu, M. J., Lee, F. C., and Benedet, L. (2010). Static bay beach concept for scientists and engineers: A review. *Coastal Engineering*, 57(2):76–91.

Hsu, J. R.-C., Benedet, L., Klein, A. H. F., Raabe, A. L. A., C.-P.Tsai, and T.-W.Hsu (2008). Appreciation of static bay beach concept for coastal management and protection. *Journal of Coastal Research*, 241(241):198–215.

Tung, T. T. (2011). *Morphodynamics of seasonally Closed Coastal IInlet at the Central coast of Vietnam*. PhD thesis, Delft University of Technology.

Acknowledgements

Time flies, I still can't believe that at the moment I am writing this acknowledgment. Doing a PhD is a long journey which brought me not just an improvement of my knowledge, but also personal enrichment. This thesis would not have been possible to complete without the help and support of many people whom I wish to acknowledge at this time.
First of all, I would like to express deep gratitude to Professor Marcel Stive and Dr. Sierd de Vries for their guidance, unconditional support and encouragement. I consider it an honour to have both of you as supervisor.
Marcel Stive, thank you so much for giving me the great opportunity to undertake interesting research and to know how beautiful the Netherlands and the Dutch people are. I still remember the first period of my PhD: it was the summer time in 2014 but you were still there at the TU Delft working the whole holiday and I was just a beginner in coastal engineering, who did not know how face the challenge that was ahead. You have taught me how to approach a new thing from the beginning and provided me with an incredible freedom to work. You always gave me the impression that it would work out in the end, especially when I was worrying about my research. Thank you for being my promotor and being a model that I will try to follow.
A special appreciation to Sierd de Vries who spent the most time working with me during my PhD. You made me realize that I am a result oriented person and that I would work better with a deadline setting. During periods of slow progress you always pushed me by setting deadlines and regular meetings, things that helped me a lot to overcome the difficult times. I have found that some of my ideas were only coming out at the end of a meeting with you, when you would ask me:"what do you think, Anh?" Even when before that I did not have any ideas, in the end I did have ideas. You have encouraged me to explore my ideas, but also taught me to make good decisions, focusing on the priority of things. Later in time, you were not just my supervisor, but you are also a friend. I do not know how to express it, but I just want to express that I highly appreciate spending your time with me and sharing life experiences that we are facing. Thanks a lot for being my supervisor, Sierd.
My great acknowledgement is extended to my colleagues and my friends from TU Delft and the University of Da Nang, and to my Vietnamese friends in Delft. Thanks, Qing Hua for guiding me in Delft 3D from the beginning of using it and giving me efficient suggestions/comments whenever I asked you. Thanks to my PhD colleagues, Phan Hung, Dao Tung, Truong Son, Phan Linh, Thu Ha, Sien Liu and Rong Zhang for sharing research topics, great discussions and enjoying our lunch time. Thanks for the help from Anh Ngan,

when I first came to Delft, showing me how to survive in the Netherlands with the Jumbo supermarket and buying a very good second hand bicycle.
Additionally, I am so grateful to Veronique for a very warm welcome at the first day I arrived in Delft and the valuable financial support for my last period. Besides, I would like to express my appreciation to Mariette, who always supported me and helped me to check the English for my thesis and having warm dinners with her. A group of friends, who are not in Delft but they are very close to me, "XNL" I am very grateful to have you as good friends in my life. Thank you for chatting and sharing almost everything outside of our research interests.
My acknowledgements are also dedicated to Chi Lan and her family, Maya, Caroline and Katerina, for making my life in Delft become more meaningful and cheerful. Chi LAN, to know you and your family seems a big honour. I have learned many valuable things from you and you have helped me and my family a lot. I am always thinking of you as my big sister. Maya, thank you so much for being my friend with whom I can share my thoughts and my emotions. Thanks to Caroline and Katerina for nice talks and sharing different cultural and political issues.
I would like to acknowledge my sponsor the Erasmus Mundus Mobility with Asia 2014 (EMMAsia2014) and the Lamminga Fund for providing a full financial support for these four years of my PhD.
Last but not least, thanks to my parents, sisters and brother for always believing in me and always offering support and encouraging me to freely discover my life. Finally, to my beloved husband, Minh Canh and my lovely son BEN, words cannot describe how grateful I am to have both of you in my life. Minh Canh, thank you so much for your sacrifice and your love, as well as your taking care our son during the busy and difficult time of my PhD. Ben, I am so honoured and proud to be your mother. You have brought a lot of positive energy and happy moments for our family.

Do Thi Kim Anh
Delft, October 2018

Curriculum Vitæ

Do Thi Kim Anh was born on February 20th 1984 in Quang Binh, Viet Nam. She started her undergraduated in the University of Da Nang- University of Science and Technology (UD-UST) in 2002. She obtained B.Sc. degree in Water Resource Engineering in June, 2007. After graduation, she was employ as assistant lecture at the faculty of Water Resource Engineering (UD-UST) in October, 2007. In February 2010 she obtained a scholarship from Ministry of Education and Training of Vietnam and from Distinguished International Student Scholarship of National Cheng Kung University (NCKU), Taiwan to pursue her master degree in NCKU. During her master she specialised in hydrological modelling within the Hydraulic and Ocean Engineering Department at NCKU. She obtained MSc in February, 2012.
In June 2014, she was granted a scholarship from Erasmus Mundus Mobility with Asia (EMMAsia2014) to pursue her Ph.D. in coastal hydrodynamics and morphodynamics at Delft University of Technology (TU Delft) under the supervision of Prof.dr.ir. M.J.F. Stive and dr.ir. Sierd de Vries.
Currently she is working as a post-doc researcher at Cerema (Centre d'études et d'expertise sur les risques, l'environnement, la mobilité et l'aménagement), France with a research project related to hydrodynamic and sediment transport model of Mahury estury (French Guiana).